Final report POLESat

The Pole Oriented Laser Elevations Satellite

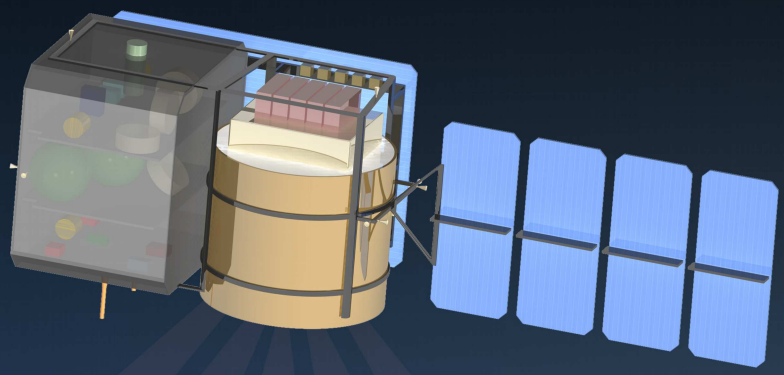

Design Synthesis Exercise 2008 - Group 13

Date: 11 June 2008

TU Delft

Delft University of Technology

Final report POLESAT

The Pole Oriented Laser Elevations Satellite

Design Synthesis Exercise 2007-2008 - Group 13

Date: 11 June 2008
Version: 1.1

Dick Allewelt
Mohammed Tayyab Babar
David Bekaert
Koen Duijnmayer
Huibert van Horssen
Rick Koole
Robin Landzaat
Rob Mulders
Ilhan Sen

Preface

In this report, the results of group 13 of the Design Synthesis Exercise (DSE) 2008 are presented. The Design Synthesis Exercise is a major part of the curriculum at the Faculty of Aerospace Engineering of the Delft University of Technology. The educational goal of the DSE is to gain experience with a design process having strict deadlines, and working full-time with a project team.

In our specific case, we have worked together with nine students on the design of POLESat: the Pole Oriented Laser Elevations Satellite. The design of this satellite is described in this report, for which we assume that the reader has a technical background and is familiar with the field of aerospace engineering.

We would like to thank everyone who helped us with writing this report. Special thanks go to Dr. R.C. Lindenbergh, Ir. W.A.A.M. Bierbooms and Ir. J. Bouwmeester for assisting and coaching our team. We also want to thank Dr. C. de Haan for her guidance and training during the oral presentations course. Next to this, the assistance of P. Drok, sales specialist Laser Systems from BFi OPTiLAS was much appreciated.

For questions about this report, you are encouraged to contact the authors or the principal tutor, Dr. R.C. Lindenbergh.

Delft, 11 June 2008,

The POLESat team

Contents

List of abbreviations

3D	Three dimensional
A/D	Analog-to-digital
AD&C	Attitude determination and control
APD	Avalanche photodiode
BOL	Beginning of life
C&DH	Command and data handling
CCD	Charge-coupled device
CHAMP	CHAllenging Minisatellite Payload
ClF_5	Chlorine pentafluoride (spacecraft fuel)
CMG	Control moment gyro
DEM	Digital elevation model
DET	Direct energy transfer
DOD	Depth-of-discharge
DOT	Design options tree
DOE	Diffractive optical element
DSE	Design Synthesis Exercise
EADS	European Aeronautic Defence and Space company
ERS	European Remote-Sensing satellite
ESA	European Space Agency
FEL	Free electron laser
GLAS	Geoscience Laser Altimeter System
G&N	Guidance and navigation
GNSS	Global Navigation Satellite System
GOCE	Gravity field and steady-state Ocean Circulation Explorer
GPS	Global Positioning System
GRACE	Gravity Recovery And Climate Experiment
ICBM	Inter-continental ballistic missile
ICESat	Ice, Cloud, and land Elevation Satellite
IPCC	International Panel on Climate Change
KSAT	Kongsberg Satellite Services
LASER	Light amplification by stimulated emission of radiation
LEO	Low Earth orbit
LIDAR	Light detection and ranging
LOLA	Lunar Orbiter Laser Altimeter
MOC	Mission operations control
MOLA	Mars Orbiter Laser Altimeter
NASA	National Aeronautics and Space Administration
N_2H_4	Hydrazine (spacecraft fuel)
PLSV	Polar Satellite Launch Vehicle
PNG	Portable network graphics
POLESat	Pole Oriented Laser Elevations Satellite
PPT	Peak power tracking
PREMIER	PRocess Exploration through Measurements of Infrared and millimeter-wave Emitted Radiation

QSL	Quasi-static load
S&M	Structures and mechanisms
SNR	Signal-to-noise ratio
STK	Satellite Tool Kit
SWOT	Strengths, weaknesses, opportunities, threats
TT&C	Telemetry, tracking and command
TRAQ	TRopospheric composition and Air Quality
TRW	Thompson Ramo Woolridge, Inc.
USAF	United States Air Force
YAG	Yttrium aluminium garnet

List of symbols

Symbol	*Description*	*Unit*
a	Albedo	[–]
a	Semi-major axis	[m]
$\bar{a}_{emp}$	Empirical forces acting on the satellite	[N]
$\bar{a}_{ng}$	Gravitational forces acting on the satellite	[N]
c	Speed of light	[m/s]
d_{al}	Along track resolution/distance	[m]
e	Eccentricity	[–]
e	Elongation	[–]
f	Focal length	[m]
f_{nat_ax}	Natural axial frequency	[Hz]
f_{nat_lat}	Natural lateral frequency	[Hz]
g_0	Gravitational constant of the Earth	[m/s^2]
h	Planck's constant	[m^{2}kg/s]
i	Inclination	[°]
l	Aerodynamic force moment arm	[m]
m, M	Mass	[kg]
n	Average angular velocity of the satellite	[rad/s]
n	Index of refraction	[–]
n_{ax}	Axial load factor	[–]
n_{cycles}	Number of cycles	[–]
n_{lasers}	Number of lasers	[–]
n_{lat}	Lateral load factor	[–]
n_{rep}	Pulse repetition rate	[Hz]
q	Reflectance factor	[–]
q_i	Earth infrared radiation	[W/m^2]
r	Distance between the center of the Earth and the satellite	[m]
$\bar{r}$	Position vector of the center of mass of the satellite	[m]
r_e	Earth radius	[m]
r_r	Distance between the satellite and ground station	[m]
t	Time	[s]
t	Thickness	[m]
t_{ax}	Wall thickness in axial direction	[m]
t_{burn}	Burning time	[s]
t_{lat}	Wall thickness in lateral direction	[m]
t_{life}	Expected lifetime	[s]
t_{orbit}	Orbital period	[s]
Δt	Time-interval-unit resolution	[s]
A	Cross sectional area	[m^2]
A_b	Area of the satellite bus	[m^2]

Symbol	*Description*	*Unit*
A_c	Area of the equivalent cylinder	[m^2]
A_{earth_i}	Surface area of the satellite directed towards the Earth	[m^2]
A_R	Receiver area	[m^2]
A_{sa}	Solar array area	[m^2]
A_{sat_side}	Surface area of a side of the satellite	[m^2]
A_{sun_i}	Surface area of the satellite directed towards the sun	[m^2]
B	Detector bandwidth	[Hz]
C_D	Drag coefficient	[–]
C_g	Center of gravity	[m]
C_{sp}	Center of solar pressure	[m]
D	Detector diameter	[m]
D	Drag	[N]
D	Residual dipole of the satellite	[Am^2]
D	Laser beam divergence angle	[rad]
Div	Divergence laser beam after leaving the laser	[rad]
E	Detector received energy	[J]
E	Young's modulus	[N/m^2]
E_0	Eccentric anomaly	[rad]
E_0	Laser transmitted energy	[J]
E_{pp}	Power per pulse	[W]
F	Avalanche photodiode excess noise factor	[–]
F	Force	[N]
F_{tu}	Allowable stress	[N/m^2]
F_{tu}	Ultimate tensile strength	[N/m^2]
F_{ty}	Yield tensile strength	[N/m^2]
G_s	Solar constant	[W/m^2]
H, $h_{satellite}$	Satellite altitude	[km]
I	Moment of inertia	[kgm^2]
I	Area moment of inertia	[m^4]
I_d	Inherent degradation	[–]
$I_{mission}$	Total impulse	[Ns]
I_{sp}	Specific impulse	[s]
K_s	Speckle signal-to-noise ratio	[–]
L	Satellite lifetime	[year]
L_d	Degradation factor	[–]
M	Bending moment	[Nm]
M	Earth's magnetic moment	[T/m^3]
M_0	Initial mean anomaly	[rad]
MS	Margin of safety	[–]
N_b	Mean solar background photoelectrons	[–]
N_D	Mean detector dark counts	[–]
N_{pulses}	Number of pulses	[–]
N_s	Mean signal photoelectrons	[–]

Symbol	*Description*	*Unit*
P_{axial}	Axial load	[N]
P_{BOL}	Power generated at beginning of life	[W/m^2]
P_{cr}	Critical buckling load	[N]
P_D	Power required during daylight	[W]
$\bar{P}_{drag}$	Perturbations due to the atmospheric drag	[N]
P_e	Power required during eclipse	[W]
$\bar{P}_{earth}$	Perturbations due to the Earth radiation pressure	[N]
P_{EOL}	Power generated per square meter at end of life	[W/m^2]
P_{eq}	Equivalent axial load	[N]
$P_{eq\_ultimate}$	Ultimate axial load	[N]
$\bar{P}_{lasers}$	Total power used by the lasers	[W]
$\bar{P}_{sun}$	Perturbations due to the sun	[N]
$\bar{P}_{ot}$	Perturbations due to the ocean tides	[N]
$\bar{P}_{rd}$	Perturbations due to the rotational deformation	[N]
$\bar{P}_{rel}$	Perturbations due to the general relativity	[N]
P_{sa}	Power generated by the solar panels	[W]
$\bar{P}_{solar}$	Perturbations due to the solar radiation pressure	[N]
$\bar{P}_{st}$	Perturbations due to the solid Earth tides	[N]
$\bar{P}_{thermal}$	Perturbations due to the thermal radiation	[N]
Q_{in}	Heat absorbed by the satellite	[W]
Q_{in_heat}	Internal heat generation	[W]
Q_{in_IR}	Absorbed Earth infrared radiation	[W]
$Q_{in\_reflected}$	Absobed solar radiation reflected by the Earth	[W]
Q_{in_solar}	Absorbed solar radiation	[W]
Q_{out}	Heat dissipated by the satellite	[W]
$Q_{out\_radiation}$	Heat radiated into space by the satellite	[W]
R	Radius of the cylinder with area and wall thickness equal to the space bus	[m]
R_1, R_2	Lens radius	[m]
R_{fp}	Radius of the footprint size due to the beam divergence of the laser	[m]
S	Signal-to-noise ratio	[–]
S_{cap}	Cap area	[km^2]
$S_{frontal}$	Frontal area of the satellite	[m^2]
S_x	Surface slope along track	[rad]
S_y	Surface slope across track	[rad]
T	Average temperature of the satellite	[K]
T	Laser pulse duration	[s]
T	Torque	[Nm]
T	Detector integration time	[s]
$T_{current}$	Temperature of the louvers	[K]
T_d, t_{sun}	Time spent in daylight	[s]
T_e, $t_{eclipse}$	Time spent in eclipse	[s]

Symbol	*Description*	*Unit*
T_G	Gravity gradient	[m/s^2]
T_{max}	Temperature of the louvers when they are fully closed	[K]
T_{min}	Temperature of the louvers when they are fully open	[K]
T_S	Pulse waveform centroid time	[s]
U_{FS}	Ultimate factor of safety	[–]
V	Velocity	[m/s]
X_d	Path efficiency solar array -> electronics	[–]
X_e	Path efficiency solar array -> battery -> electronics	[–]
Y_{fs}	Yield factor of safety	[–]
Z	Range to the surface	[m]
α	Coefficient of thermal expansion	[–]
α	Absorption ratio	[–]
B, θ	Sun incidence angle	[°]
γ	Reduction factor	[–]
δ	Latitude	
δ_x	Latitude of the sub-satellite point	[°]
ϵ	Elevation angle	[°]
ϵ	Measurement error	[m]
ϵ	Emissivity ratio	[–]
ϵ	Effective emissivity	[–]
ϵ_{max}	Maximum effective emissivity	[–]
η	Optical efficiency	[–]
η	Solar cell efficiency	[–]
η_{lasers}	Laser energy efficiency	[–]
θ	Laser pointing angle	[rad]
λ	Earth's center angle	[°]
λ	Laser wavelength	[m]
λ_s	Longitude of the sub-satellite point	[°]
μ	Solar cell mass	[kg/m^2]
μ	Universal constant of gravitation multiplied with the Earth's mass	[m^3/s^2]
ν	True anomaly	[rad]
ρ	Density	[kg/m^3]
ρ	Earth angular radius	[rad]
ρ	True outer horizontal angle	[°]
σ	Stefan-Boltzmann constant	[W/m^{2}K^{-4}]
σ_{cr}	Buckling stress	[N/m^2]
τ	Atmospheric transmittance	[–]
ϕ	Laser pointing angle off-nadir	[rad]
$\Delta\phi_x$	Laser pointing angle uncertainty along track	[rad]
$\Delta\phi_y$	Laser pointing angle uncertainty across track	[rad]
ω	Argument of perigee	[rad]
Ω	Right ascension of ascending node	[rad]

List of Figures

List of Tables

Abstract

This report is about the design of POLESat, a satellite for measuring the effects of global warming on the polar ice sheets. Currently, a satellite with a similar purpose is operational (ICESat), but this satellite is near the end of its lifetime. Because a continuation of the measurement time series is necessary, this report gives detailed information on the feasibility of a follow up mission, with the aim to improve both coverage and measurement accuracy.

First, the requirements for the satellite will be explained. This is followed by a presentation of the different design options that satisfy these requirements. One of the design options is worked out in detail and a motivation is given why this option is most suitable for the follow-up mission. After the details of the design, information is provided on what still needs to be done to get POLESat in space.

In the end, it was found that it is feasible to take 40 times more measurements than ICESat for only a 10% increase in cost. Next to this, a longer lifetime is achievable and a follow-up mission can be launched as soon as mid-2012.

1 Introduction

To obtain information about the actual influence of climate change on the polar ice sheets, accurate elevation measurements over the poles are necessary. In the past, several missions have been performed to determine elevations of land ice; these include ERS-1 and ERS-2, Envisat and ICESat. However, ERS-1, ERS-2 and Envisat did not have measurements of land ice elevations as their primary goal. ICESat was the first satellite mission specifically designed for measuring ice sheet elevations with relatively high accuracy.

Now, ICESat is almost at the end of its lifetime, and its measurement campaigns need to be continued. For this purpose POLESat, the Pole Oriented Laser Elevations Satellite, has been designed, of which the details are discussed in this report. It will be shown that POLESat improves the ICESat measurements in various ways.

First, the background of the POLESat mission is given in chapter 2. This chapter is followed by a review of the top-level requirements (chapter 3) and a short overview of the general design options (chapter 4). The market for POLESat is analyzed and discussed in chapter 5. The risks of the final concept are evaluated in chapter 6, after which a function analysis is performed in chapter 7. The reliability, availability, maintainability and safety characteristics of the POLESat mission are investigated in chapter 8, followed by a technical resource allocation in chapter 9. The design of all subsystems of POLESat is discussed in chapter 10. Next, the interface chart of the subsystems will be presented in chapter 11, after which chapter 12 deals with the operation of POLESat and the distribution of the data products. The estimated costs of the total POLESat mission are given in chapter 13. In chapter 14, it will be discussed whether the requirements for POLESat are met or not. Finally, a schedule for after the DSE project is given (figure 15.3), followed by the conclusions in chapter 16.

2 Background

The Earth's climate is changing. In the past years, awareness has grown that human activities have an impact on the climate change. Current research about this topic is done by the Intergovernmental Panel on Climate Change (IPCC), a scientific body with the task of evaluating the risk of climate change caused by human activity.

A change in Earth's climate can have severe consequences for human life in several areas. To illustrate the need for research in this area, some findings are summarized below (confidence levels in these quotes are very high: $> 90\%$, high: $> 80\%$ and medium: $> 50\%$).

From [7]:

> In both polar regions, there is strong evidence of the ongoing impacts of climate change on terrestrial and freshwater species, communities and ecosystems (very high confidence). Recent studies project that such changes will continue (high confidence), with implications for biological resources and globally important feedbacks to climate (medium confidence).
>
> In both polar regions, components of the terrestrial cryosphere and hydrology are increasingly being affected by climate change (very high confidence). These changes will have cascading effects on key regional bio-physical systems and cause global climatic feedbacks, and in the north will affect socio-economic systems (high confidence).
>
> Continued changes in sea-ice extent, warming and acidification of the polar oceans are likely to further impact the biomass and community composition of marine biota as well as Arctic human activities (high confidence).

From [41]:

> The large uncertainties reflect the difficulties in estimating the global ice mass and its variability, because global monitoring of ice thickness is impossible (even the total area of glaciers is not exactly known) and extrapolation from local measurements is therefore necessary. A regional extension of the monitored ice masses and an improvement of measurement and extrapolation techniques are urgently required. In spite of the large uncertainties, the data that are available portray a rather consistent picture of a cryosphere in decline over the 20th century, increasingly so during 1993 to 2003.

Although there is high confidence about the relation between global warming and melting of polar land ice, there is a lack of sufficient scientific data to give a clear insight in what

Cryospheric component	Sea level equivalent (mm/year)	
	1963–2003	1993–2003
Glaciers and ice caps	$+0,32$ to $+0,68$	$+0,55$ to $+0,99$
Greenland	$-0,07$ to $+0,17$	$+0,14$ to $+0,28$
Antarctica	$-0,28$ to $+0,55$	$-0,14$ to $+0,55$
Total (adding ranges)	$-0,03$ to $+1,40$	$+0,55$ to $+1,82$
Total (Gaussian error summation)	$+0,22$ to $+1,15$	$+0,77$ to $+1,60$

Table 2.1: Estimates of cryospheric contributions to sea level change.

is actually happening in the polar regions. Of main interest is the ice sheet mass balance, which is the net increase or decrease in total stored water in the polar ice caps. Figure 2.1 gives an overview of processes influencing this mass balance.

There are three ways to measure the mass balance of ice sheets (from [61]):

- Mass budget method, which compares losses by melting and ice discharge with total net input from snow accumulation. Net accumulation is inferred primarily from icecore measurements, and melt rates are commonly estimated from positive degree-day models.
- Measurements of elevation change over time, which are translated into measurements of volume change by including estimates of the vertical motion of underlying ground associated with isostatic rebound or tectonics.
- Measurements of gravity changes, done with space based gravimetry platforms. This measures the mass balance directly from changes in the gravitational field of the Earth.

The method of interest for POLESat is measuring elevation change over time, which roughly works as explained in [71]:

> Elevation changes corrected for isostatic rebound reflect thickness changes due to changes in ice flow, bottom melting, snow accumulation, [*ed*: compaction] and ablation. In the interior, bottom melting is small and few places experience net ablation. If we assume that in the interior, ice is flowing by internal shear over a frozen or rough bed, the flow is unlikely to have altered on century to millennial time scales. Accumulation since the middle of the 19th century has fluctuated in the interior about a constant mean accumulation rate. A change in elevation should result from either a century-scale mass imbalance or a contemporary fluctuation in accumulation rate. (We assume a century scale because there are few records of accumulation before 1850.)

The actual measuring of the mass balance due to climate change is a rather complicated procedure. One of the most pertinent climate parameters, the accumulation rate, has an uncertainty leading to an equivalent error in global sea level change of more than $\pm$0.6mm per year. Nevertheless, it is very important to get quality data about the changes in mass balance, to assess the impact of climate change on the ice sheets and global sea level.

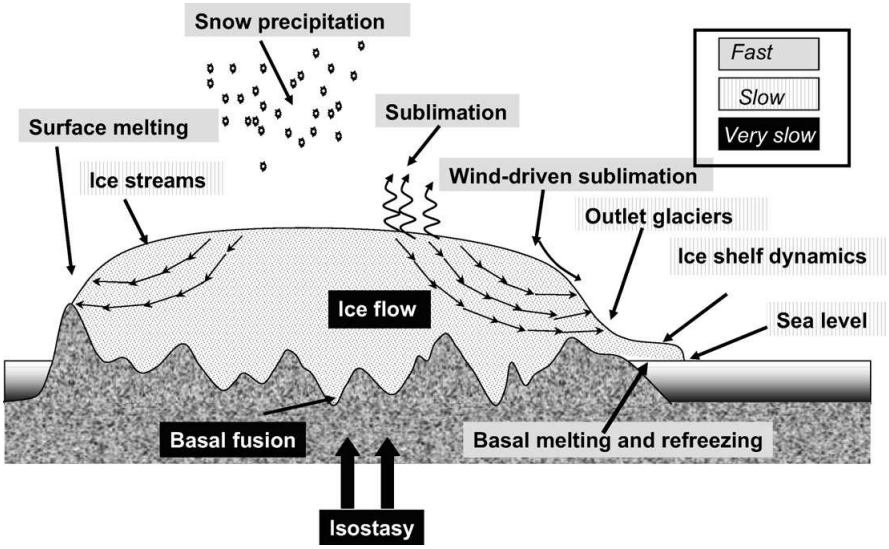

Figure 2.1: Ice-sheet mechanism and time-scale outline (taken from [59]).
Surface melting, snow precipitation, sublimation, wind-driven sublimation, and basal melting or refreezing are assumed to instantaneously react to climate change. Ice streams, outlet glaciers and ice-shelf dynamics are assumed to react slowly to climate change, meaning between 100 and 1000 years. On the contrary, ice flow, basal temperature and fusion isostasy take a very long time to react, meaning that the time lag is between 10 000 to 100 000 years.

3 Requirements review

For the design of POLESat, top-level requirements have been suggested [44]. To evaluate the feasibility of these requirements, they will now all be discussed. This discussion includes possibilities and difficulties in achieving the requirements. If any requirements are set which are impossible to achieve, it will become apparent in this way.

3.1 Space based platforms

For deriving the mass balance of the polar ice sheets, four space based platforms have been identified. These are radar altimetry, gravimetry, spectrometry and laser altimetry.

In an earlier stage of the design process, a pulse based laser altimetry system was selected to be the best option for POLESat. This is mainly because of the attainable spatial resolution in combination with the accuracy of a laser system. For further details, see the mid-term report.

3.2 Digital elevation model

A top-level requirement of the POLESat mission is to take measurements that allow the construction of an accurate digital elevation model (DEM) of the ice sheets on Greenland and Antarctica. For a high resolution DEM, the distance between footprints over the land ice sheets in both across-track and along-track direction needs to be small. A small along-track distance can be achieved by choosing an appropriate number of laser pulses per second. For ICESat, the along-track spacing of the footprints is 170 m. For POLESat, the aim is to decrease the along-track spacing to approximately 100 m. To create a better across-track distance with respect to ICESat, the ground tracks need to be close to each other. This is difficult to achieve for the southern part of Greenland and at the edges of Antarctica. Unfortunately these are also the parts most interesting to have an accurate DEM for. To get an acceptable across-track distance further away from the poles, a long repeat cycle, the time before the satellite will follow the same ground track again, is needed.

3.3 Mission start in 2010

To have a mission start in 2010, the whole satellite, including the payload, should be designed, built and tested in two years. Using off-the-shelf technology is thus important. Using new technology poses a larger risk though, because it will need more time for development and testing, which can cause a delay of the mission start.

The main bottleneck for POLESat is the payload itself. Especially a multi-beam laser needs a lot of development time, since it is untested for space applications. The design

and testing of the payload will take approximately 1.5 years (see chapter 15). After the payload is tested, the satellite has to be tested as well. This means that a mission start in 2010 is unlikely to be achieved. A mission start in 2012 is more realistic.

The launch is an important factor for the start of the mission as well, because if the launch fails, it will be impossible for the mission to start in time. Moreover, the availability of launchers should be checked to find a launcher that is available in 2012.

3.4 Minimum lifetime expectancy of 5 years

The minimum lifetime of POLESat should be 5 years and the estimated lifetime should be 10 years. To meet the minimum and estimated lifetimes of the mission, many technical factors have to be considered. For example, all of the subsystems on board should have an expected life span of at least 10 years.

Next to this, the lasers on board of the satellite should be able to operate for at least 5 years, with an expected lifetime of 10 years. Because comparisons need to be made between elevations measured at the beginning of the mission and at a later time, it is important to have the lasers working as long as possible. When a laser lifetime of 10 years is not possible to achieve in space, it might be necessary to include more lasers (not counting redundancy) to keep the mission operational for 10 years.

Furthermore, the cost of the mission should be taken into account. If the minimum lifetime of 5 years can be achieved with reasonable cost, but an expected lifetime of 10 years cannot, a trade-off has to be made. This trade-off will be influenced by the amount of interest in the mission and the level of funding available.

In conclusion, the lifetime requirements for the satellite are not impossible. But it will require a close look into all the subsystems and the payload, especially the laser.

3.5 Ranging accuracies

To measure elevations of ice and snow, one or more lasers will be used by POLESat. The accuracy that needs to be obtained is 5 cm vertical and 5 m horizontal, under clear sky and over flat terrain. To see if this accuracy is attainable, a closer look needs to be taken at the contributions to the measurement errors.

The vertical accuracy depends on instrumental parameters and on the surface that needs to be measured. Estimates for these contributions can be calculated using [32]. For the design parameters, optimal values are chosen in order to obtain an optimal accuracy. In chapter 10, this will be elaborated on in detail.

For a perfectly flat, horizontal surface, ranging errors due to slope, off-nadir angle, pointing jitter and surface roughness become zero. The error of orbit determination, system effects on range measurements and the atmospheric conditions then become the largest contributions to the measurement error. These errors are estimated and discussed in section 10.7.

4 Design options & final concept

At an early stage in the design, several ideas are proposed as potential design for the mission. Proposals can contain several characteristics for the configuration of the design. These characteristics are called design options. Options can be visualized in a tree, where the top level of the tree indicates what requirements should be met. The lower levels contain options that will satisfy the requirement. For every set of options, only one can be chosen. Hence, a design can only use one branch of the tree as configuration.

Several design options are not feasible with the available resources or are otherwise unqualified for the mission. While these options are recorded in the design options tree (DOT) at an early design phase, these options are left out in this stage of the design for a better overview of the realistic configurations. Several options can be listed as a design choice for any of the lowest level configurations. Of these options, the ones that are considered relevant for what the satellite will do are listed in a separate tree, while others are left out for a better overview.

4.1 Design options tree

Shown in the design options tree for the laser system (figure 4.1) are the primary design choices that influence many of the other design choices for the satellite. The first branch of the tree involves a choice between single and multi-beam laser systems. This is an important factor, because the total ground coverage of the POLESat mission depends on this design option. The multi-beam laser system can be created with a split beam or with multiple lasers. The split beam can be created with beam splitters and mirrors or with a diffractive optical element (see section 10.1). If only one laser beam is used, the option for multiple satellites is considered to increase the total coverage. Likewise, the orbit selection is dependent on the previous design choices.

For the actual data that is obtained during the mission, there is a choice between single elevation or full waveform measurements, see figure 4.2. The single elevation measurements are relatively easy to obtain, but lack information about the type of terrain, slope, surface roughness and vegetation characteristics. This information can be obtained with full waveform measurements, but then considerably more data is generated with every laser pulse and more on-board data processing is necessary.

In the design process, all other satellite subsystems are chosen to support POLESat's payload, the laser altimetry system, in the most optimal way.

4.2 Investigated design options

In an initial trade-off, three different concepts were chosen. To make the concepts as diverse as possible, three different branches of the DOT are chosen. The main difference between

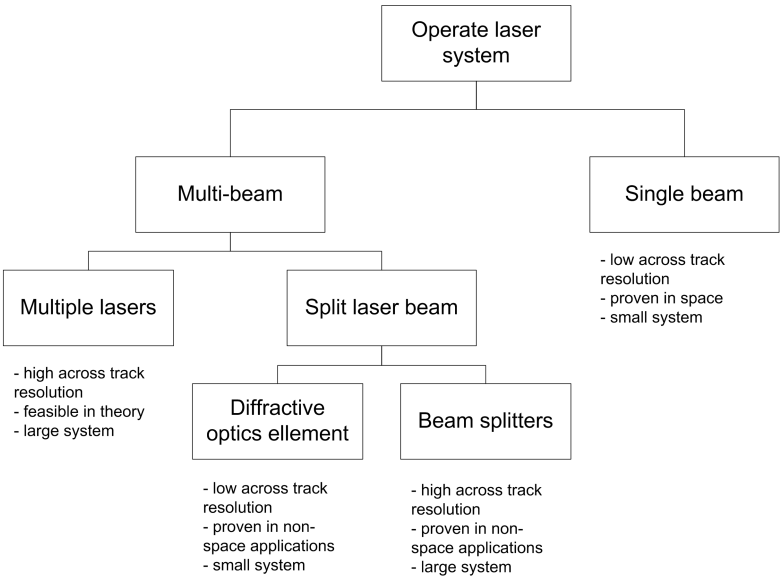

Figure 4.1: Design options tree for the laser system.

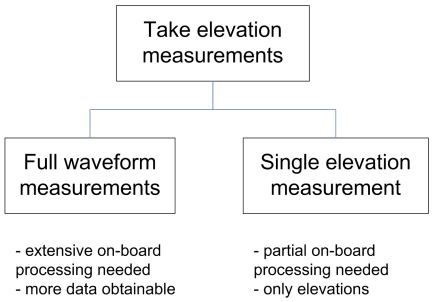

Figure 4.2: Design options tree for the types of measurements.

the concepts is the laser configuration. One concept will look at the single beam laser configuration combined with multiple satellites (to increase the amount of data collected with respect to the ICESat mission). The two other concepts will look into the multiple lasers and split beam options, respectively. Further differences are chosen during the concept design phase itself. These choices include full waveform versus single elevation measurements and different orbits.

For the concept design phase, the DSE group was split in three subgroups. Each subgroup looked into one of the design options, which were defined as:

- Concept A: laser with split beam.
- Concept B: multiple lasers.
- Concept C: multiple satellites with single beam laser.

The strong and weak aspects of all of these concepts have been identified and compared, leading to a final concept which was elaborated during the second half of the project.

In the rest of this section, the differences between the three design concepts will be discussed, to explain the choices made for the final concept. For the exact details of the concept designs, please refer to the mid-term report for POLESat.

The main characteristics of concept A are:

- Laser with beam splitter (5 footprints per pulse).
- Full waveform measurements.
- Sun-synchronous orbit without eclipse at 400 km.
- 75×5 measurements per second.
- Slant range accuracy ≤ 8 cm over ice (clear sky and flat terrain).
- Detector diameter of 1.5 m.
- 0.5 km spacing between footprints for each single measurement.

Concept A uses one laser at a time, meaning that if this laser fails, another laser should be switched on. As a consequence, it is important that the laser subsystem for this concept is sufficiently redundant. The main advantage of concept A is the high amount of measurements. The main disadvantages are a high power consumption and a high value for the propellant mass.

The main characteristics of concept B are:

- Five operating lasers.
- Single elevation measurements.
- Sun-synchronous orbit with eclipse at 500 km altitude.
- 40×5 measurements per second.
- Slant range accuracy ≤ 8 cm over ice (clear sky and flat terrain).
- Detector diameter of 1.5 m.
- 2.2 km spacing between footprints for each single measurement.

The configuration of concept B uses five lasers at a time; additional lasers are carried for redundancy. If more lasers fail than there are redundant lasers on-board, less lasers will be operational, but the mission can still continue. The main advantage of concept B is the across-track distance between footprints. This distance is such that footprints are evenly distributed at 70° latitude. The main disadvantage of this concept is the quality of the data, as the full waveform of the returned signal is not stored.

The main characteristics of concept C are:

- Single operating laser, two satellites.
- Full waveform measurements.
- Sun-synchronous orbit with eclipse at 500 km altitude.
- 60×2 measurements per second.

- Slant range accuracy ≤ 5 cm over ice (clear sky and flat terrain).
- Detector diameter of 2.0 m.
- Only one footprint for each single measurement.

Like concept A, both satellites of concept C will have a sufficient amount of redundant lasers on board. The main advantages of the concept with multiple satellites are the high measurement accuracy and the reliability of the satellite components. A notable disadvantage of the satellites is the high dry mass. Both the high value for the dry mass and the high slant range accuracy are a result of the detector size. Additionally, the satellites are launched separately to reduce risk, which increases the cost.

4.3 The final concept

After looking into the various concept designs, another trade-off was done. In this trade-off, a final concept was selected, which combines the advantages of concepts A through C. The final concept is basically a derivation from the concept with multiple lasers. Many characteristics are similar, but some properties are changed or improved, based on the other concepts. The multiple laser concept was chosen, because some improvements could easily be applied, while the concept was already an attractive choice. The final concept is further elaborated on in the remaining parts of this report.

The main characteristics of the final concept are the:

- 5 operating lasers with 5 redundant lasers.
- Full waveform measurements, both with near-infrared (1064 nm) and green (532 nm) light.
- Sun-synchronous orbit without eclipse at 477 km altitude.
- Repeating orbit every 91 days.
- Up to 75 measurements per second.
- Slant range accuracy ≤ 5 cm over ice (clear sky, flat terrain).
- Effective detector diameter of 1.5 m.
- 2.5 km spacing between footprints for each single measurement.

The increase in slant range accuracy with respect to concept B is obtained by increasing the pulse energy of the laser. The extra power required is in turn obtained by changing the orbit in such way that the satellite experiences no eclipse period. Extra fuel will be needed for attitude control though, as the configuration of the chosen concept is less stable (see 10.5). The main consequence of taking full waveform measurements is an increase in required downlink data rate, but during the final design phase this was proven to cause no problems.

5 Market analysis

Now the final concept has been discussed, a short market analysis will be done in this chapter. The supply/demand chain for POLESat has already been discussed in the mid-term report. Therefore, only an analysis of the strengths, weaknesses, opportunities and threats is given.

5.1 SWOT analysis

Strengths

POLESat will be a follow-up mission of ICESat and is able to continue the unique time series of measurements taken by this satellite. A longer time series is essential to distinguish between random (annual) variations and systematic trends in the ice sheets mass balances.

Next to this, climate change is a very hot topic at the moment, and therefore a mission to measure the height of the polar ice sheets will be quite popular.

Finally, POLESat will take full waveform measurements with a higher accuracy than ICESat, which will eventually lead to the construction of a better DEM of Greenland and Antarctica.

Weaknesses

It is expected that in the POLESat mission some new technology will be used. This will likely result in an increase of performance of the satellite, but it also means that the chance of failure will increase.

The objective is to keep the costs of this mission as low as possible, which in combination with the short amount of time to develop and test the satellite, can be considered a weakness.

Opportunities

The POLESat mission is an opportunity to apply and test new laser technology.

Another opportunity is the possibility to acquire data of for example vegetation or sea level heights with the multiple laser system taking full waveform measurements.

Next to this, it might be possible to combine data from other satellite missions or aerial surveys to improve the accuracy of the DEMs.

Threats

POLESat will not be the only satellite delivering data from which ice sheet mass balances can be derived. For example, data from Crysat-2, ASTER, GRACE, GOCE or any combination of these can in principle also be used for this purpose (likely with less accuracy though).

Another threat could be a shift in the budget of potential customers, resulting in the budget for this mission to be scrapped.

A summary of the SWOT analysis is shown in table 5.1.

Strengths	**Weaknesses**
Continuation of ICESat time series	New laser technology
Popular subject, market demand	Low budget mission
Full waveform measurements	Short time for development
High accuracy	
Opportunities	**Threats**
Application of new technology	Competition of other platforms
Use the laser for secondary purposes	Shift of client budget/focus
Combining data from other sources	

Table 5.1: SWOT analysis.

6 Technical risk assessment

In this chapter an assessment is made of the technical risks for POLESat. For this assessment, risk is defined as the probability an event occurs, multiplied by the severity of its consequences on the POLESat mission. Risk drivers that are associated with the mission are [35]:

- The state of technology.
- The complexity of the system.
- The dependency on other factors like resources and schedules.
- Other risk categories.

6.1 Spacecraft subsystems & mission segments

For a spacecraft mission, it makes sense to split the risk assessment into all space system segments and satellite subsystems. Some of the subsystems discussed are proven in other space missions, which gives a reliable insight of the performance and the probability of failure. However, for some subsystems new technologies are used, which implies a higher risk. Precautions need to be taken in cases of high risks.

Payload

The main payload of POLESat consists of a laser altimeter, i.e. multiple lasers and a detector. The lasers have not been tested extensively in space. The effects of the space environment on lasers are therefore not yet known. The impact of failure of a laser is not critical; because there are redundant lasers available, failure of a laser will not end the mission. It will influence the lifetime, the collection of data and number of campaigns performed by POLESat though. The other part of the payload is the detector. This detector has a lower probability of failure, since telescopes and optical detectors have been flown during previous space missions. The detector is not a redundant system; therefore failure will have a catastrophic impact.

Attitude determination & control

The AD&C subsystem is necessary for pointing the laser in the right direction. When the pointing fails to a certain extent, operating the laser altimeter might still be possible, but with a lower accuracy. Attitude determination is done with a star tracker, which has a design proven in space. The probability of failure is therefore small. The attitude control is done with momentum wheels and thrusters. One redundant wheel is present and the thrusters have been used and tested in space. Overall, the chance of failure of the AD&C subsystem is small, but impact of its failure on POLESat's performance is critical.

Telemetry, tracking & command

The link to the ground segment for sending data and receiving commands is important for every mission. Telemetry failures can range from very small interruptions to failure of the mission objective. Communications is present in every satellite mission and is therefore a proven part of the mission design (i.e. low probability of failure).

Command & data handling

For POLESat, the data handling is important, because its data is the end-product of the mission. If any computer failure occurs, data might be lost and commands no longer processed. In the worst case, this means the satellite is no longer able to operate. Failure of the CD&H subsystem is not likely however, since it has been used many times in space. However, any custom electronics need to be tested extensively.

Power

Power is needed to operate all satellite subsystems, including the laser and detector, which forms the payload of POLESat. If the power system fails, the mission goal will be impossible to accomplish. It is also important to realize that over time the power subsystem will deteriorate. For this reason, POLESat is equipped with enough solar cells to provide the required power till mission end-of-life. For the hardware of the power subsystem, many designs are available that are already space-proven, and therefore have low probability of failure.

Thermal control

Every space mission needs thermal control to provide suitable conditions for the payload and other subsystems. Since there is extensive experience available in this field, the probability of failure of the thermal control system is very small. However, when the thermal control system fails on POLESat, this could lead to damaging temperature peaks due to the high power consumption of the lasers.

Structures & mechanisms

The structures & mechanisms for this mission will consist of proven technology. During launch the supporting structure should withstand high loads, and during the mission it should protect the payload and other systems from small space debris. Failure of the structure is highly unlikely, but will have a large impact on the mission if it occurs.

Guidance & navigation

The guidance and navigation subsystem is mainly concerned with station keeping (i.e. localization of the satellite) and orbit maintenance. Like AD&C, this subsystem is important for the correct position and orientation of the satellite. If it does not work correctly, the result can be anywhere from a somewhat lower accuracy to the impossibility of taking measurements. For locating the satellite, GPS and laser ranging are used. These systems are quite commonly used and experience with these systems is readily available, so the probability for failure is considered to be low.

Launch segment

The launch of the system is its transport from Earth to an orbit from which it will start its operations. If the launch fails, the mission is lost. This means that failure of the launch has

a large impact on the mission. The probability of the failure is dependent on the selected launcher.

Ground segment

The ground segment is responsible for data handling, processing and distribution on the ground. Since an existing ground segment will be used, failure probability is very low. Moreover, failure of the ground system is considered to be quickly recoverable, which means that the impact of failure on the mission is only marginal. An overview of the risks associated with the various subsystems is shown in the risk map (table 6.1).

Feasible in theory				
Working laboratory model				
Based on existing non-space engineering			1 (laser)	
Extrapolated from existing space design				1 (detector)
Proven space design		10	2,3,4,5,6,7,8	9
	Negligible	Marginal	Critical	Catastrophic

Probability of failure →

Performance consequence →

1. Payload
2. Attitude determination & control
3. Telemetry, tracking & command
4. Command & data handling
5. Power
6. Thermal control
7. Structures & mechanisms
8. Guidance & navigation
9. Launch segment
10. Ground segment

Table 6.1: Risk map.

6.2 Cost risk assessment

During the design process, there is a risk that the available budget will be exceeded. Therefore, also cost risks have to be considered in the technical risk assessment.

There are two possibilities for the budget to be exceeded. First, it is possible that resources need to be added when planning is not met for whatever reason. Secondly, there is the possibility more resources than planned have to be allocated to fulfill the technical requirements within the planned time. The total cost risk is the sum of both of these risks.

In case of POLESat, the main risks are the development of the laser subsystem and the data handling & processing methods. These are rather unique systems for this mission, which means no cost estimates from previous experience are available. The supporting subsystems (power, thermal control, etc.) have a considerably lower cost risk, because many satellites have been designed with similar systems. Estimates of the amount of resources needed for the development of these subsystems are therefore readily available (see also chapter 13) .

The cost risk of delays in the schedule can be reduced by closely monitoring the design progress. An early recognition of bottlenecks in the work schedule is vital, so actions can be taken before serious problems occur. It is very important to structure the project using flowcharts to lower the cost risk. Identifying the base cost and well-organizing the schedule will also lower the cost risk.

7 Functional analysis

7.1 Functional breakdown

The functional breakdown (figure 7.1) gives an overview of all the functions POLESat has to perform during its mission. The mission operations are subdivided in three categories: payload, satellite bus and ground segment. The operation of the payload consists of emitting a laser pulse, measuring the backscattered signal, pre-processing the received signal and transmitting the data to the ground segment. The operation of the satellite bus is needed to support the payload. The usual functions are listed here to make a functional satellite. The operation of the ground segment takes care of the command of the satellite and the further processing and storing of the acquired data.

7.2 Functional flow diagram

The functional flow diagram gives a clear insight in the functions of the mission process. In the case of the POLESat mission two flow diagrams have been made. The lifetime functional flow diagram (figure 7.2) describes the lifetime of the mission from mission need statement to decommissioning of the satellite and further data use. All functions in the total lifetime of the mission are indicated and linked to the follow-up function.

The data functional flow diagram (figure 7.3), describes the operational phase. When a command is received to start the measurements, the location and attitude of the satellite are determined and they are combined with the measurements of the lasers to create a data package. This data package is pre-processed to some extent, depending on the design choices, and transmitted to the ground station. The measuring is a continuous process. Only the data transfer is bound to the time frames when there is contact with a ground station.

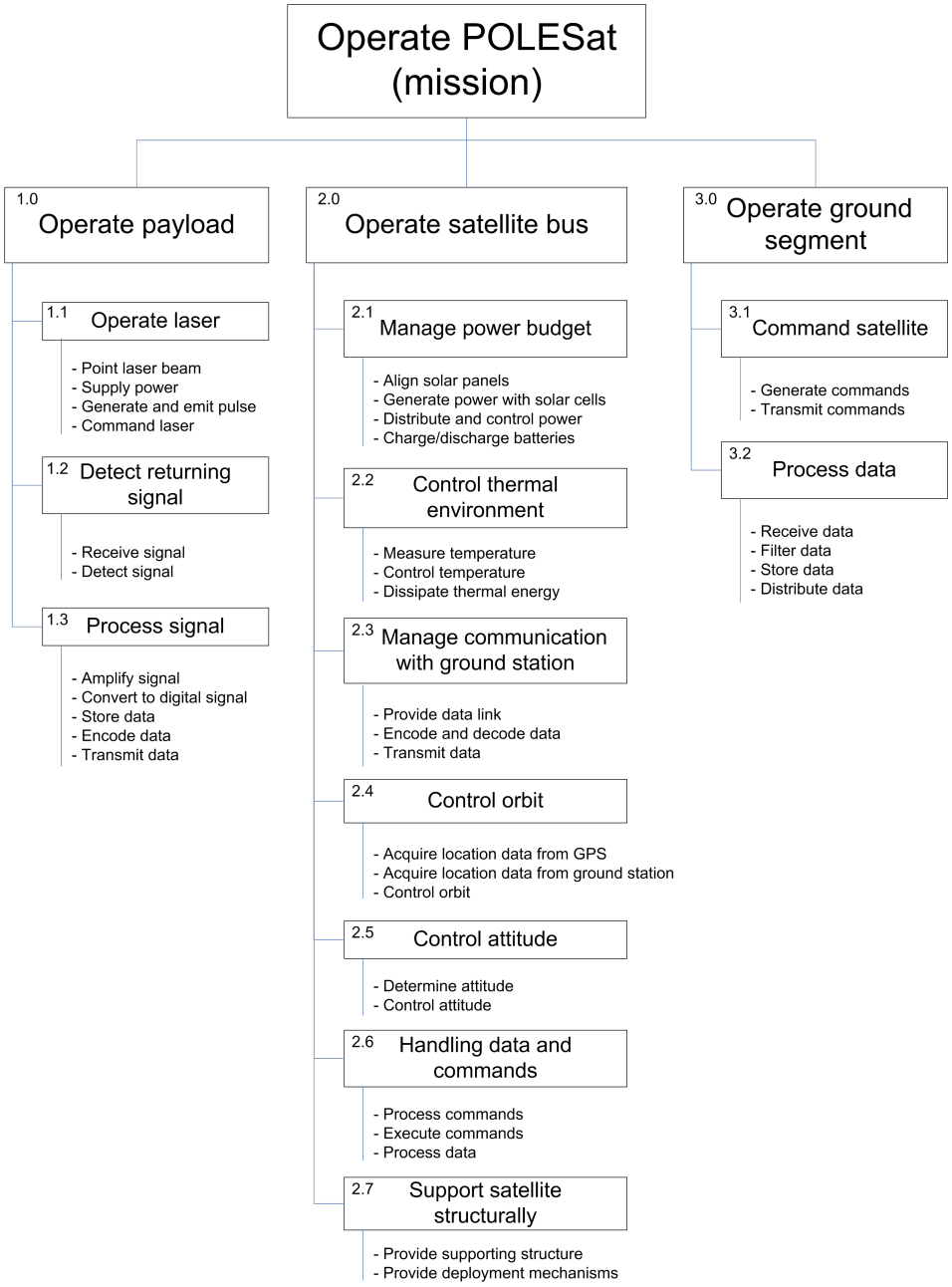

Figure 7.1: Functional breakdown.

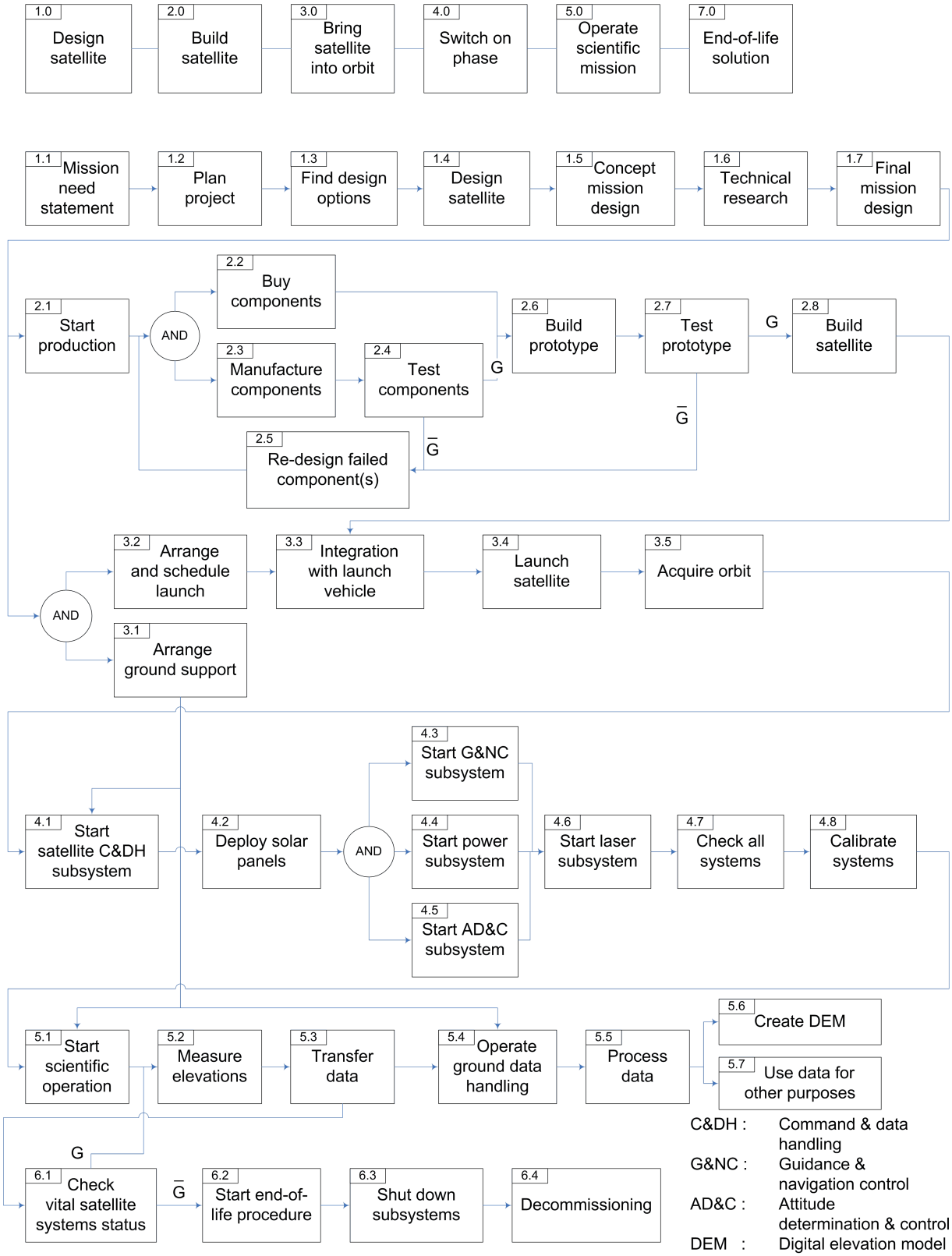

Figure 7.2: Lifetime functional flow diagram.

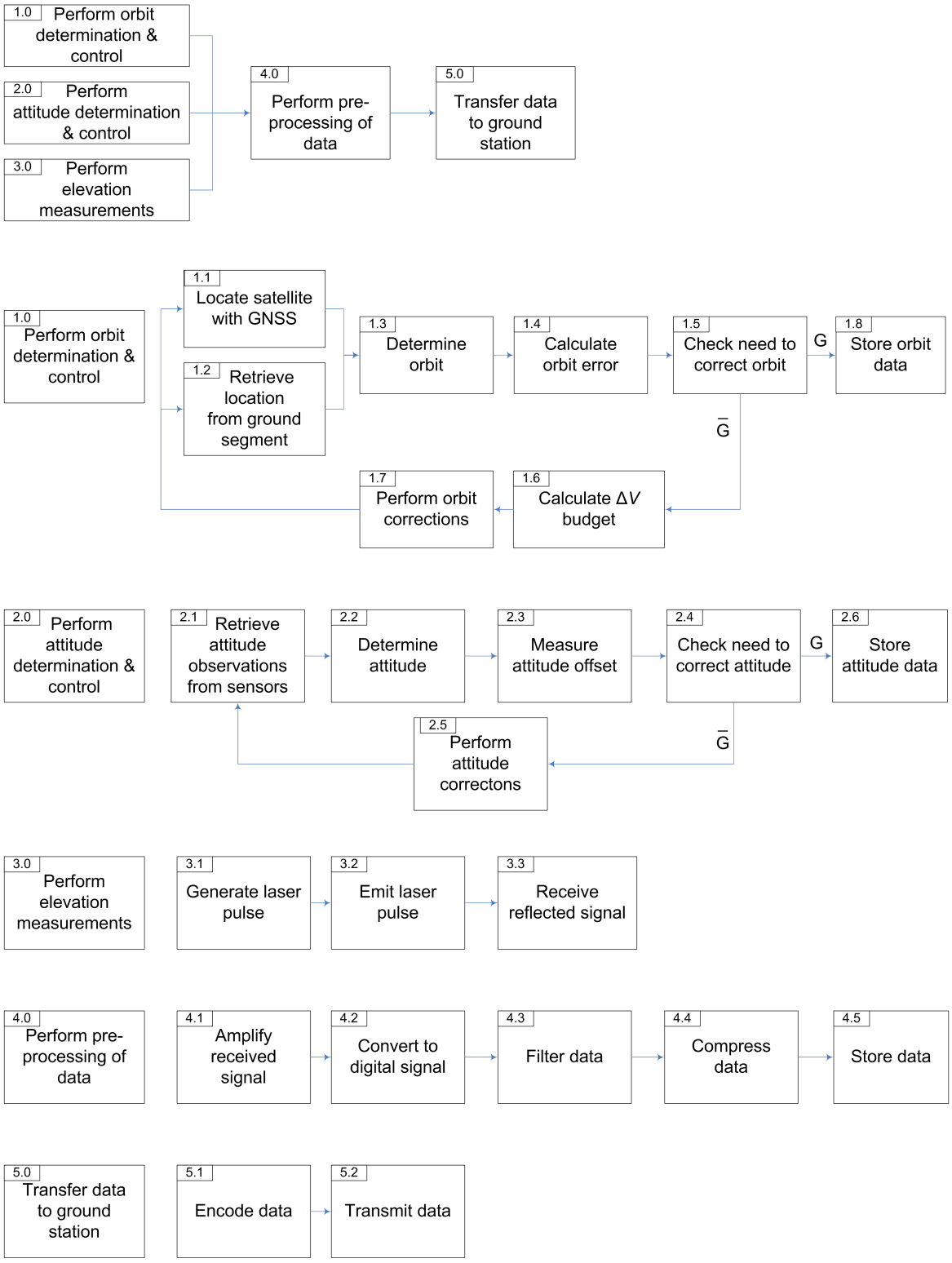

Figure 7.3: Data functional flow diagram.

8 Reliability, availability, maintainability and safety

8.1 Reliability

Most of the subsystems of POLESat have a high expected lifetime and thus, a high reliability. Except for the laser subsytem, which is a special case, the reliability of the subsystems is well above the expected lifetime of the satellite. The lifetime of the satellite is therefore determined for the most part by lifetime of the laser. As discussed in the section about the expected lifetime of the laser system (section 10.1), the operating time of the laser can be adjusted to increase the lifetime of the laser system, if necessary. As a result, it is very likely that the satellite will be operational for 10 years, although the amount of measurement campaigns may be decreased depending on the performance of the laser.

8.2 Availability/maintainability

The availability of the satellite for measurements is determined by the amount of time required for orbit and attitude maintenance. Maintenance is controlled from the ground segment. When the satellite is found to deviate from the intended orbit or attitude, commands for correction are sent to the satellite from the ground. Orbit and attitude maintenance can be done from the ground, but the satellite is autonomous in other maintenance respects. This means that in case a satellite component fails, the component can not be replaced or repaired. As a result, the satellite is designed to be able to handle failure of certain components by itself. This is done either with redundant components or by using components that are unlikely to fail. The consequence for the availability is that no time is spent on maintenance. In some cases, however, the satellite will require new commands for maximum performance after failure of a component. For example, the operational status of lasers may need to be adjusted. The time component involved with this type of maintenance is negligible with respect to the satellite lifetime, however.

The attitude maintenance consists of the desaturation of the momentum wheels. This is discussed in section 10.1 to be 100 seconds per 60 hours. The orbit maintenance consists of weekly orbit corrections. This requires an engine burning time of 16.5 minutes every 7 days, or 168 hours. Assuming both operations are not performed simultaneously, the percentage of time satellite is unavailable can be calculated with the following equation:

$$T_{unavailable} = (T_{md,\,time}/T_{md,\,period} + T_{oc,\,time}/T_{oc,\,period}) \cdot 100\%$$

Where the subscripts $_{md}$ and $_{oc}$ indicate the time in seconds for momentum wheel desaturation and orbit correction, respectively. The subscripts $_{time}$ and $_{period}$ indicate the required time and the period in seconds in which the corrections and desaturation are performed, respectively. Inserting the above numbers results in a value of 0.2% for the unavailability

of the satellite. The availability of the satellite for measurements is the remaining time, or 99.8% of the time.

The corrections and desaturation can be performed while the satellite is not flying over Greenland or Antarctica, meaning that the most important measurements will not decrease in amount as a result of maintenance. However, if required, the corrections and desaturation can be done at any time.

Next to this, there is the possibility that the number of campaigns is reduced to extend the lifetime of the lasers. In that case, the availability of the satellite for takng measurements is reduced as well.

8.3 Safety

Before and during the launch, the satellite itself has no factors compromising the safety of equipment or personnel. During the lifetime of the satellite, the satellite is not a threat to equipment or personnel either. The laser beams are not hazardous to living beings. The only factor that should be considered is the possibility of a collision in space. A collision with another spacecraft will cause direct damage to equipment, while a collision with space debris may indirectly result in damage to other systems, in addition to the possibility of contributing to more space debris.

9 Technical resource budget

The technical resource budget is made to set certain boundary values with respect to the (future) design of POLESat. The technical resource budget is split in two parts. The technical budget breakdown will be discussed in 9.1, followed by a brief discussion of contingency management in 9.2.

9.1 Technical budget breakdown

In order to control the performance risks of the POLESat design, a technical budget breakdown is performed. This means that a certain limit is ascribed to technical parameters, to constrain the domain of the design solution. Because experience shows that the margin between the required and achieved values tends to decrease during a project, contingencies are set for each design phase. An estimate for the technical budgets of POLESat is derived from three worked out concepts (see the POLESat midt-erm review).

An important requirement is to improve the accuracy of the POLESat mission with respect to ICESat. The total weight of the satellite and the envelope of the satellite are limited to this number in order to fit in the fairing of most launchers. The maximal diameter of the payload fairing of an average launcher capable of injecting POLESat in polar orbit is 3 meters (source [13, 50]). Table 9.1 clearly shows the differences between ICESat and POLESat with respect to mass and payload.

For POLESat, the aim is to have a better accuracy, for which a larger detector is needed. This increases the payload mass and therefore the dry mass of the satellite. The electrical power budget of 2500 W is higher than the ICESat mission (650 W), which is a result of the multiple lasers, all with a higher intensity and a higher pulse rate than the type of laser on board of ICESat. The data storage budget of 500 Gb is much higher compared with ICESat (56 Gb), to be able to store all data from the multiple lasers. The envelope size of 2.5 m $\times$ 2.5 m $\times$ 3 m is in the same range as ICESat. For the pointing (error) and communication link, the budget is set the same as for the ICESat mission. One of the design goals is, of course, to improve the performance with respect to these parameters. The ΔV budget (excluding launch, so for the satellite only) and the propellant mass are estimated values for a sun-synchronous orbit with an altitude of 500 km for an Earth observation satellite with a lifetime of about 10 years.

The production costs are an estimated value for the satellite to be still a competitive Earth observation mission. This means that budgets of similar projects were considered and with this data an estimate has been made. Although the values in the table 9.1 look like hard numbers that may never be exceeded, it is important to realize that for a performance driven design like POLESat, the budgets are often tight and it might happen that not all subsystems can be designed within the allocated budget. Therefore, a reallocation of the budgets or a redefinition of requirements is likely necessary during the design process.

	ICESat	POLESat
Dry mass	882 kg	1300 kg
Payload mass	300 kg	425 kg
Electrical power	640 W (350 W orbit avg.)	2500 W
Data storage	56 Gb	500 Gb
Envelope size	1.9 m × 1.9 m × 3.1 m	2.5 m × 2.5 m × 3 m
Pointing (error)	30″ roll, 60″ pitch, 1° yaw (3σ)	30″ roll, 60″ pitch, 1° yaw (3σ)
Communication link	40 Mbps X-band	600 Mbps X-band
ΔV	unknown	400 m/s
Propellant mass	77 kg	300 kg
Production cost	$\sim$ 900 million USD	$\sim 1,000$ million USD

Table 9.1: Technical budget breakdown.

9.2 Contingency management

Contingency management is a tool for risk management. Its purpose is to mitigate the risk and to preserve the baseline performance of the project. The contingencies of the mass and the power budget for the subsystems are derived from experience [35]. These contingencies are taken into account during the conceptual design phase and are given in table 9.2.

High Contingency Both the laser and the detector are experimental and have never been built for this purpose. This implies that the weight estimation needs a larger contingency. For the payload, a contingency of about 30% is used to give a more reliable power consumption and weight estimation.

Medium Contingency Propulsion, structures & mechanisms, propellant mass and thermal control are highly dependent on the other subsystems. Although estimations can be done very accurately because of all the experience along the years ,their power consumption and mass will change because of the so-called snowball effect. Therefore a contingency of 20% is given to these parts of POLESat.

Low Contingency A lower contingency is given to parts which are bought and are off-the-shelf. Their weight and power consumption will not change too much, since they are fixed and well known. These systems are attitude determination & control, command & data handling and telemetry, tracking & command. A contingency of 10% is implied for these sybsystems.

Overall Contingency The weights of all subsystems are added and a total weight including the contingency can be calculated. From this (table 9.2) an average contingency of about 20% can be derived. There are no values given in table 9.2 for the power consumption for propulsion, power, structures & mechanisms and propellant mass, because they do not consume any power.

	Contingency (%)	
	Mass	Power
Payload	30	30
Thermal	20	20
Attitude determination & control	10	10
Propulsion	20	–
Power	20	–
Command & data handling	10	10
Telemetry, tracking & command	10	10
Structures & mechanisms	20	–
Propellant mass	20	–

Table 9.2: Mass and power contingencies for the conceptual design phase.

10 Final design

In the initial design phase, several concepts have been considered as a solution to meet the mission requirements. One of these concepts was chosen to be worked out in more detail, which is done during the final design phase. A summary of the trade-off performed between the considered concepts can be found in chapter 4. Section 4.3 also contains a quick summary of the concept used for the final design

This section contains the results of the final design of the various subsystems and satellite characteristics. First of all, the subsystems are described for which the parameters are initially selected. The subsystems that require information of other subsystems are listed later. It should be noted, however, that the design is an iterative approach, which means that the selected parameters will often change during the design, until an optimal solution is obtained. The calculations involved with the selection of the parameters are explained in each section, while elaborate calculations are included in appendices. In addition to the technical parameters, each subsection also contains descriptions of the components used for the subsystem. Design choices are motivated using the above mentioned presented information.

10.1 Payload (laser)

The payload of the POLESat mission is the laser altimetry system. This system consists of the laser subsystem and the detector subsystem. This section will look into the details of the laser subsystem. The name laser is an acronym of "Light Amplification by Stimulated Emission of Radiation". A laser emits light in a narrow, low-divergence beam with a well-defined wavelength. First the working principles and the terminology of a laser will be explained. All the functions that are needed in the POLESat laser will be discussed. Secondly several types of lasers will be evaluated. To obtain useful measurements several requirements need to be fulfilled. The third part will look into these requirements. From these top-level requirements parameters can be derived. After that the best option for the POLESat laser will be described. The last paragraph will look into the problems yet to solve and the research that needs to be done on the POLESat laser before launch.

10.1.1 The working principles of a laser

A laser consists of several components; all determining certain parameters. To create an appropriate laser system all the components have to be adjusted to each other. In this part the main components of the lasers, that will be used on POLESat, will be discussed.

The resonator

The main component of a laser is the resonator or optical cavity. The optical cavity consists of at least two mirrors arranged in such a way that the light will bounce back

and forth with a standing wave. This means that alignment of the mirrors is crucial; the distance between the mirrors is dependent on the wavelength. On of the mirrors is partially transparent, this means that a small part, around 1%, of the light inside the cavity will propagate through the mirror. Practically most laser resonators consist of more than two mirrors. If an arrangement of several mirrors and lenses are used, this is called a folded cavity. Commonly, a pair of curved mirrors will create one or more confocal sections, while the rest of the cavity use plane mirrors and is quasi-collimated [38] (see figure 10.1). This will give better control over the divergence and the shape of the light beam inside the optical resonator.

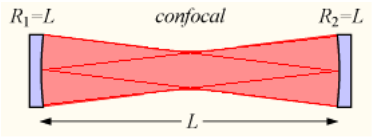

Figure 10.1: Confocal optical cavity.
In a confocal optical cavity the focal point of a mirror is at the center of the opposite mirror.

The gain medium

Inside the optical resonator is the gain medium. The gain medium is like the heart of the laser. The gain medium is the place where the actual amplification of the laser beam occurs.

Every gain medium consists of a material that can have an exited state, a quantum-mechanical energy level. After some time the atom or ion may decay into a lower state, this is called spontaneous emission. However it is also possible that the photon emission is stimulated by incoming photons with the right optical frequency [24]. In this case the emitted photon will have the same mode as the incoming photon; effectively amplifying the incoming radiation.

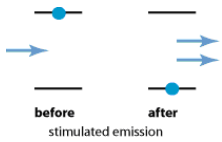

Figure 10.2: Stimulated emission.
An incoming photon stimulates an exited atom to undergo a transition from the excited to the ground state.

The pumping mechanism

Supplying energy to the gain medium is called pumping. Pumping is needed to bring the atoms or ions in the gain medium to an exited state. The goal is to achieve a population inversion in the gain medium and thus optical amplification via stimulated emission. Population inversion is a state in which the pumped energy is in equilibrium with the gain of the laser. Different kind of gain media require different types of pumping. Optical pumping is used to pump solid state lasers and some gas and liquid lasers. Optical pumping means to inject light in order to excite the medium to higher energy levels. Common optical pumping sources are flash lamps, laser diodes or other types of lasers; the last one is only used in very high power lasers. Flash lamps or laser diodes are commonly used to pump regular solid state lasers. Lamp-pumped lasers have a short lifetime and require regular maintenance, but are relatively cheap. Diode pumped lasers have a longer lifetime, because redundant laser diodes can be build in. Diode-pumped solid state lasers are the only lasers capable of producing the multibillion pulses needed on the POLESat mission

[65]. Another advantage of diode pumping is the relatively high efficiency of the diode lasers; this can result in a total efficiency of 4%-6% for a diode-pumped solid state laser configuration. Diode lasers are directly electrically pumped and therefore highly efficient; the only losses are due to imperfections in the crystalline structure of the semiconductor [56].

Pulse generation

For several purposes pulsed laser operation is needed instead of a continuous mode. A pulsed laser will have a highly increased emitted energy per pulse. Depending on the pulse duration, pulse energy and pulse repetition rate, different methods for pulse generation are used. The methods for pulse generation are gain-switching, mode-locking and Q-switching. Gain-switching is done by switching the pump source on and off. This is mostly applied in diode lasers. It will take some time before the stimulated emission starts, which will give the opportunity to excite the gain-medium. Gain-switching allows a highly controllable repetition rate. This is commonly used in telecom applications. Mode-locking works on the principle of creating a pulsed light already in the optical cavity (see figure 10.3).

The resonator of the laser contains an optical modulator which regulates the power transmission within the optical cavity. Mode-locking can be done both passively and actively. The repetition rate of a mode-locking pulsed system is fixed by the time to complete one round trip in the optical cavity. Mode-locking is capable of creating very short pulses in the order of picoseconds or even femtoseconds. The last method of creating a pulsed laser system is Q-switching. Q-switching works by modulating the intra-cavity losses, the Q-factor, of the resonator. Unlike mode-locking, there is a continuous standing wave inside the optical cavity. Like in mode-locking, Q-switching can be done both passively and actively.

Figure 10.3: Schematic setup of an actively mode-locked laser.

Active Q-switching uses an optical modulator to control the pulse build-up. The pulse energy depends on the energy stored in the gain medium and the repetition rate. Active Q-switching allows control over both the energy per pulse and the repetition rate. Passive Q-switching uses a saturable absorber to control a pulsing system (see figure 10.4). The pulse is formed as soon as the energy stored in the gain medium and the absorber has reached a high enough level. In the case of passive Q-switching the pulse energy and pulse duration are fixed. Varying the pump energy only influences the pulse repetition rate [56].

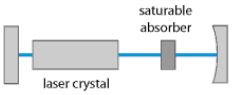

Figure 10.4: Schematic setup of a passively Q-switched laser.

The frequency doubler

To create light with a shorter wavelength a frequency doubler is used. A frequency doubler is a non-linear crystal material where an input wave generates another wave with twice the optical frequency. A small part, around 25%, of the energy of the infrared wave will be used to generate green laser light. The other 75% will pass through the crystal unchanged [31]. Several types of crystals can be used depending on the frequency of the laser. The crystal type most suitable for the POLESat laser is lithium niobate, $LiNbO_3$. This type

is capable of doubling the frequency of infrared light with a wavelength of 1064 nm. The conversion efficiency depends on the beam quality and the size of the $LiNbO_3$ crystal.

10.1.2 Requirements on the POLESat laser subsystem

Several requirements on the multiple laser subsystem arise from the base requirements. Some requirements are derived from limitations on other satellite subsystems. The requirements on the mission and the consequences on the lasers will be discussed in this paragraph.

Pulse repetition rate

The pulse repetition rate n_{rep} is mostly determined by the needed along-track resolution. The along-track resolution is the distance between two adjacent footprints along the ground track. The along-track resolution is a function of the velocity of the satellite and the pulse repetition rate of the laser;

$$d_{al} = V/n_{rep} \tag{10.1}$$

where d_{al} is the along-track distance between the footprints in [m], V is the velocity of the satellite in [m/s] and n_{rep} is the pulse repetition rate of the laser in Hz. In a circular orbit the altitude of the satellite determines its velocity [70]. To get a d_{al} of 100 m for altitudes of 450 km, 500 km and 550 km the n_{rep} are respectively 76.4 Hz, 76.1 Hz and 75.8 Hz. This means that a repetition rate of 75 Hz is sufficient to obtain enough measurements in the along-track direction. To increase the laser lifetime the repetition rate of 75 Hz should only be used over ice. On other terrain the repetition rate can be reduced to 40 Hz this will give an along-track resolution of 188 m -190 m. The repetition rate, along with the sampling rate and the range of interesting samples, determines the amount of data generated. This will influence the size of the data storage, data processing and telemetry subsystems (see appendix E).

Beam divergence

The divergence of the beam determines the size of the footprint. The total divergence consists of the beam divergence in the laser subsystem and the atmospheric divergence. The atmospheric divergence will give, in case of an ideal zero divergence beam, a footprint size varying from 20 m-60 m, in clear weather. For high water vapor contents this atmospheric divergence will even get larger. To create a useful footprint the divergence of the beam in the laser subsystem should be as small as possible. The footprint size due to the beam divergence of the laser needs to be smaller than 50 m to have useful measurements. The beam convergence needed can be calculated using

$$\tan\left(\mathrm{Div}\right) = R_{fp}/\left(H \cdot 1000\right) \tag{10.2}$$

where Div is the divergence of the laser beam after it leaves the laser, R_{fp} is the radius of the footprint size due to the beam divergence of the laser in [m] and H is the satellite's altitude in [km]. This requires that the beam divergence of the laser should be smaller than 50 µrad. All the optical components in the laser subsystem, like the gain medium, the amplifiers, the frequency doublers, the mirrors and the lenses, contribute to the divergence of the beam.

Beam angle and alignment

POLESat will have 5 lasers operating; this will result in 5 footprints for each pulse. One laser is pointing at nadir. The other lasers are slightly off nadir to create a swath. The angle between the beams is determined in such a way that at the polar regions an evenly spaced across-track resolution will be obtained. The across-track distance of the ground tracks is a function of the latitude, the altitude and the repeat cycle time. The repeat cycle is fixed at 91 days to be able to measure seasonal changes and still have a good coverage. In the worst case at 70° latitude, the across-track distance between two ground tracks, after a full 90 days repeat cycle, will be approximately 12 km. This results in an optimal across-track distance between the footprints of 2.5 km (see figure 10.9). This means that the optimal across-track resolution will be much worse than the along-track resolution. The angles needed for the five lasers to get the needed spacing are respectively −10 mrad, −5 mrad, 0 mrad, 5 mrad and 10 mrad. This is calculated using basic goniometric relations.

Pulse duration

The pulse duration is the length of the laser pulse expressed in [ns]. The shorter the pulse duration, the more accurate the measurements. The pulse duration for ICESat is 6 ns. The goal for the pulse duration on POLESat is set to 4 ns. It depends on the type of pulse generation what the minimum pulse duration can be. Pulses of 4 ns are still possible to produce with a Q-switched laser. Q-switching is preferable over mode-locking because of the higher energy per pulse that can be created.

Energy per pulse

The energy per emitted pulse is one of the main drivers of the accuracy that can be obtained. To increase the signal-to-noise ratio, the energy per pulse should be as high as possible. The signal-to noise-ratio is dependent on the energy per pulse, the effective detector area and the altitude. This design loop is iteratively done. For weight reasons the detector size is limited, to around 1.5 m. This will already result in a detector of approximately 500 kg (see section 10.2). The altitude selection is limited by the lifetime requirement. To keep the satellite in orbit for 10 years, the drag should be limited which requires a higher altitude. The altitude is a balance between the obtainable accuracy and the propulsion mass to counteract the drag (see appendix B). The power per pulse needed to obtain the 5 cm vertical accuracy for perfectly flat terrain is 175 mJ per pulse for the infrared laser.

The lasers are the main power users on the satellite and because they are not really energy efficient (4%) they are also the largest heat source. This means that the total laser power is limited by the heat generation and the solar panel area. The lasers will produce both, a laser beam at near-infrared (1064 nm) and green (542 nm) light. The total power of the lasers can be calculated as

$$P_{lasers} = n_{lasers} \cdot \eta_{laser} \cdot E_{pp} \tag{10.3}$$

where P_{lasers} is the total power of the lasers subsystem, n_{lasers} is the number of lasers (5 in this case), η_{laser} is the laser energy efficiency, n_{rep} is the pulse repetition rate and E_{pp} is the total power per pulse. After the laser, the beam will be split into a near-infrared (1064 nm) and a green (532 nm) laser beam. The infrared beam will be 75% of the emitted energy per pulse. This requires that the total emitted energy needs to be 235 mJ per pulse, resulting in a maximum total power requirement of the laser subsystem of 2.2 kW. From a thermal point of view the total power of the lasers is limited because 96% of the power will be transformed to heat.

Expected lifetime

To keep the satellite operating for the whole mission lifetime the laser should be capable of generating many pulses. The number of pulses can easily be calculated:

$$N_{pulses} = n_{rep} \cdot t_{life} \tag{10.4}$$

where N_{pulses} is the number of pulses during the lifetime, n_{rep} is the repetition rate and t_{life} is the expected lifetime. When the lasers operate at 75 Hz for 10 years it will require a lifetime of the lasers of $24 \cdot 10^9$ pulses. This is not feasible with lasers yet. The longest lifetime of a laser achieved so far (in a laboratory) is $7.2 \cdot 10^9$ pulses [65]. To reduce the pulses needed during the mission the laser will have a lower repetition rate 40 Hz over non-ice surfaces. This can easily be done by reducing the supplied power in case of a passive Q-switched system. This effectively means that the number of pulses needed can be reduced to $15 \cdot 10^9$ pulses. To reduce the number of pulses needed even further, the number of measuring campaigns can be reduced, e.g. two campaigns of 3 months a year. For redundancy two lasers will be used for every single footprint.

10.1.3 The POLESat laser

The laser needed for the POLESat mission will be a unique custom built laser. There are current off-the-shelf commercial lasers which have specs close to the repetition rate, energy per pulse, pulse duration and beam divergence parameters needed for the POLESat laser [54, 19, 43]. But especially the lifetime requirement will require thorough research on the POLESat laser design. In this section the layout of the laser will be described, which is, in theory, capable of meeting all the requirements. To create the POLESat laser, several stages are used to create the beam needed for the elevation measurements. The first stage is a single optical resonator where the pulsing laser beam is generated; this is like a small laser. The second stage is to amplify the beam and control its divergence quality. The next stage is the beamdoubler; here the green light is created. The last stage of the laser subsystem is a mirror on a piezo actuator to direct the light to the desired spot on Earth. This part is placed in front of the laser where the laser light can pass through the satellite bus to the Earth.

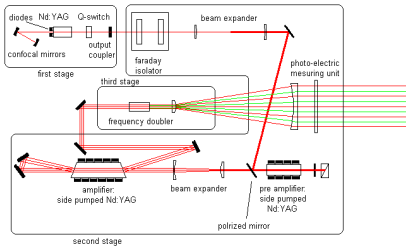

Figure 10.5: POLESat laser.

The type of laser

The number of laser types capable of meeting all the requirements is limited. A solid state laser is the only type of laser capable of generating the high power needed while still being mass efficient [54]. The lifetime requirements limit the pump source to diode pumped systems [54, 56]. For the crystal type there are numerous options [68]. A wavelength around 1000 nm is favorable for ice measurements. Neodymium is the mostly used dopant;

this will create light with a wavelength of 1064 nm. A Nd:YAG, neodymium doped yttrium aluminium garnet crystal is chosen, because this is the most common used and space proven solid state laser crystal. For the pulse generation Q-switching is preferable over mode-locking, because of the higher pulse power that is achievable and the higher reliability. Both passive and active Q-switching is possible. Passive Q-switching has the advantage that it is less prone to failure, and has a longer expected lifetime [54]. Passive Q-switching is only capable of adjusting the pulse repetition rate during operation, the energy per pulse of the system is fixed by the saturation level of the absorber. This has not a real disadvantages for the POLESat mission. A Cr^{4+} : YAG, Chromium doped yttrium lithium fluoride crystal is chosen as saturable absorber. This can absorb the 1064 nm light produced by the Nd:YAG crystal. A $LiNbO_3$ crystal will be used as frequency doubler. This will result in the passive Q-switched diode pumped solid state laser, which will be used on POLESat.

The first stage: the optical resonator

The optical resonator is like a small linear solid state laser. It consists of a end-pumped Nd:YAG crystal, which is pumped with 16 diode lasers. Two diodes are operating at the same time the remaining diodes are for redundancy. The average lifetime of a laser diode is approximately $10,000$ hours, depending on the power used. Behind the Nd:YAG crystal the saturable absorber, Cr^{4+} : YAG, is placed as a passive Q-switch. The size of the Cr^{4+} : YAG crystal determines the energy per pulse. These two crystals are placed inside an optical cavity. Behind the Q-switch is the output coupler, or partially reflective mirror. On the other side of the optical cavity is a confocal section to improve the beam divergence quality. The first stage will create a laser beam with the correct repetition rate and pulse duration, but with only 0.1% of the total needed power, 0.3 mJ. The cross-section of the beam will be around 0.5 mm [54, 56].

The second stage: the amplifier

Directly behind the first stage a Faraday isolator is placed. The Faraday isolator polarizes the beam and prevents deflecting light from the amplifier to damage the delicate first stage. After the beam emerges from the faraday isolator the beam will be expanded to 1 mm to allow faster amplification. Also the divergence is limited if the beam is larger. Then the beam will be directed to the pre-amplifier. This is also a diode pumped Nd:YAG crystal. This will be a side-pumped with 8 diode lasers. Eight times more diodes are placed for redundancy, coming to a total of 64 diodes. The beam will pass two times through this crystal for optimal amplification. The mirror behind the crystal will rotate the polarized signal 90° to allow further travel to the next amplifier. But first the beam will be expanded 3 mm diameter. The main amplifier will amplify the signal to the final 235 mJ per pulse. This is done by a diode side-pumped Nd:YAG crystal with a total of 128 powerful laser diodes. These diodes are places in arrays around the Nd:YAG crystal. 16 diodes need to pump at the same time to supply the crystal with enough power. The laser pulse will pass twice through this amplifier. Due to the polarization the light will be deflected after the second pass, to the next stage of the laser [3].

The third stage: the frequency doubler

After the laser beam has passed the amplifying stage, the frequency of a part of the light will be doubled to create green laser light. The crystal type most suitable as a frequency doubler for the POLESat laser is lithium niobate, $LiNbO_3$. After the frequency doubler the laser beam, with both green and infrared light, will be expanded further to a final 25 mm

diameter beam. This wide beam is favorable for the divergence properties of the beam. Especially the diffraction will be highly reduced with a wider beam. The beam divergence will have a much larger influence on the footprint size compared to the produced beam diameter. So a large beam diameter is favorable. The final beam, with 25 mm diameter, is measured with a photo-electric measuring unit. This is a dielectric lens which measures the amount of light that passes thought. This signal will be used to start the timer for the detector. The shape and energy of the pulse are also stored to be sent down, along with the detected return signal [3].

The final stage: the pointing mirror

The lasers are placed at the cold, dark side of the satellite and point towards the sun. With adjustable mirrors the beams will be pointed to the desired spot on the Earth's surface. This adjustment will be done with piezo actuators with mirrors attached to them. This gives control in the order of 5 μrad to the direction of the beam. These pointing mirrors are placed in such a way that the laser beams will be passing between the detector and the body mounted solar panel.

10.1.4 The challenges for further laser research

The laser needed on the POLESat mission is a custom laser. The lasers are one of the main components that determine the success of the mission. But they are also the most unreliable. This means that the lifetime requirement is difficult to obtain without redundancy. In theory it is feasible to build the POLESat laser, but further research need to verify and test the configuration before it is launched. To meet the requirements all components of the laser should be of the highest quality possible. Small defects can lead to catastrophic failure of a laser, because of the high power involved. To operate the delicate interior of the laser it should be protected as much as possible from space radiation. The main problem will arise from local heating of parts in the laser. The thermal conditions should be monitored very carefully. An emergency shutdown system should be coupled to the thermal measurements and the laser output to prevent a sudden death of the laser. Like in the GLAS laser a sealed atmospheric environment can be used to improve the control of the laser. The beam quality also highly depends on the impurities in the laser crystals, lenses and mirrors.

To verify all these parameters further research on the POLESat laser needs to be done. The design and full tests of the POLESat laser will take approximately 1.5 year [60]. This means that the launch in 2010 is unlikely. It is possible to have the satellite in orbit before the end of 2012.

10.2 Payload (detector)

The main objective of the detector is to convert the reflecting laser beams into digital signals. The detector consists of telescope with a size based on the amount of reflected light. The focal point of the detector is aimed at a plate where all dots are visible. The dots, which are the footprints on Earth, are transferred via glass fiber wires to the photon counter. The photon counter converts the signal in to a digital signal.

10.2.1 Telescope

The telescope is an essential part of the detector and is going to have a significant part in the total weight of the satellite. The lenses in the telescope will magnify the image which has been projected on the ground. The lens will need a certain diameter in order to catch enough photons in order for the detector to generate the required resolution. In order to estimate the size of the lens certain conditions are need. The worst possible albedo is taken that POLESat will encounter while measuring ice sheets. This will be 20% and is the albedo caused by the reflection of clear glacier ice (see [16]). Furthermore the atmosphere transmittance of 0.7 is taken into account and total optical efficiency is taken 0.4 [70]. The size of the lens is really a trade-off between the satellites orbit and the emitted laser power. Increasing the lens means less laser power or a higher altitude. appendix B lists all the calculations for the trade-off. Because POLESat has to achieve 5 cm vertical accuracy, the laser power is limited (see section 10.1) and the weight of the lens has to be kept as small as possible a diameter of the lens is chosen to be 1.5 m.

To reduce the length of the telescope one can make use of mirrors. By using two mirrors the length of the telescope can be reduced by a half (see picture 10.6). The light comes in via the telescope and is reflected via the first mirror and is magnified using the lens on the telescope. Because of defraction the light will converge and is being reflected by the second mirror. This finally sends the light to the plate which will guide it to the photon counter. This means that the lens has a hole in it and the effective area of the lens will be smaller. In order to keep the 5 cm vertical accuracy a lens with another diameter but with the same effective has to be calculated. For this we assume that the outer radius of the lens is 2 times the diameter for the hole (see picture 10.6). This gives a new diameter for the lens of 1.73 m.

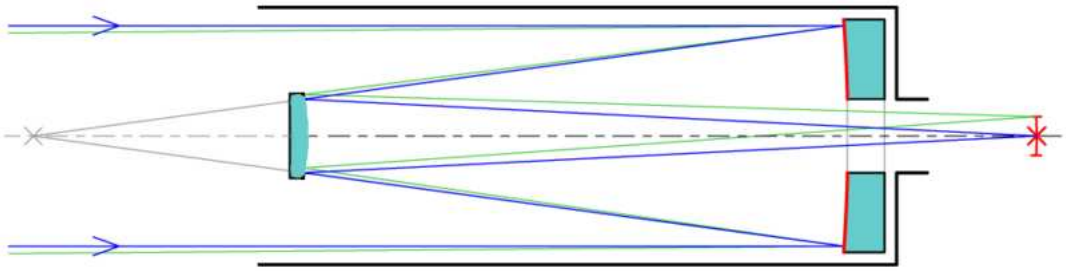

Figure 10.6: POLESat detector.

It's important to keep the focal length as small as possible as well, so the telescopes length will have an acceptable length. This can be done by increasing the curvature of the lens and therefore make it heavier. The equation used to estimate the curvature of the lens is called the lens maker equation and is given by:

$$\frac{1}{f} = (1-n)\left[\frac{1}{R_1} - \frac{1}{R_2}\right] \tag{10.5}$$

In this equation f is the focal length, n is the index of refraction, R_1 is the radius of one side of the lens and R_2 of the other. Because the other side of the used lens is flat because of the mirror the second term in the lens maker equation is zero. This is also a trade-off: the smaller the chosen curvature the smaller your telescope. However, this also means it becomes heavier. The density of the used optical glass is taken to be 3700 cm/m^3 and with

a index of refraction of 1.8 [63, p. 718]. The volume of the lens can be calculated using the fact that it is a sphere segment with a hole. The trade-off table for the lens lists all the curvatures with corresponding focal length and weights. Using the fact that the detector should have a weight around 450 kg a lens with curvature 2.5 is taken.

Curvature [m]	Focal length [m]	Weight [kg]
1.5	1.9	762
2.0	2.5	535
2.5	3.1	415
3.0	3.75	342
3.5	4.4	290

Table 10.1: Lens curvature versus weight.

10.2.2 Receiving the signal

A 5-optical-fiber array at the focal plane of the telescope each aligned to one of the five laser spots on the Earth's surface and delivers the signal to one of the five avalanche photodiodes (APDs).

The APD works using the principle in converting photons is electrons and comes in many forms. It works basically the same as solar cells. An avalanche photodiode is a semiconductor-based photo detector which is operated with a relatively high reverse voltage (typically tens or even hundreds of volts), sometimes just below breakdown. In this regime, carriers (electrons and holes) excited by absorbed photons are strongly accelerated in the strong internal electric field, so that they can generate secondary carriers, as it also occurs in photon multipliers. This gain usually has values between 30 or 100 times. The avalanche process effectively amplifies the photocurrent by a significant factor. In this way, avalanche photodiodes can be used for very sensitive detectors, which need less electronic signal amplification and are thus less sensitive to electronic noise ideal for the POLESat detector. However, the avalanche process itself is subject to quantum noise and amplification noise, which can offset the mentioned advantage. Tentatively, their noise performance is better compared with ordinary PIN photon diodes in the high-speed regime, but not for low detection bandwidths.

Silicon-based avalanche photodiodes are sensitive in the wavelength region from 450 nm to 1100 nm, at somewhat shorter wavelengths than for silicon PIN diodes. For longer wavelengths, APDs based on germanium or indium gallium arsenide (InGaAs) are used but these are used for telecommunications mostly. For this system we select a silicon base APD. When operated in the so-called Geiger mode with carefully designed electronics, avalanche photodiodes can be used even for photon counting. The Geiger mode means that the diode is operated slightly above the breakdown threshold voltage, where a single electron-hole pair can trigger a strong avalanche. In the case of such an event, the electronics reduce the voltage at the diode below the threshold voltage for a short time, so that it can recover. The largest manufacturer is Hamamatsu and the APDs are selected from this company with all the right sizes [34]. In total POLESat will need 5 of these detectors, able to detect wavelengths of 1064 nm and 532 nm.

Conversion from analog to digital signal

The analog signals coming from the APDs should be converted to raw digital data before they are processed into LIDAR. All current space based LIDAR missions (MOLA, ICESat, LOLA) use A/D convertors for quantization of the RAW APD data. In the POLESat mission a 16-bit A/D convertor is used. The down part of using an A/D convertor is the fact that saturation phenomena occur. A saturation phenomenon occurs when collecting and digitalizing raw data under such circumstances as signals with a larger dynamic range and inappropriate gain settings of the receiver. These signals exceeding the dynamic range of the selected A/D convertor should be truncated and digitized to be certain extrema. Another when the dynamic range of the AD convertor has been exceeded it needs to to desaturate. Especially using the green laser is important that the A/D convertor is desaturated before the next signal is received. Since POLESat is puling with 75 Hz the desaturation should be finished before $1/75 = 0.013$ s. Saturation caused the raw LIDAR data to degrade and therefore some more studying for correction methods is needed.

Researchers already have taken many approaches to minimize the data loss due to saturation. One method is to adjust gain for know across-track changes in signal strength. Another approach samples the incoming data and adjusts the gain during acquisition. The last method is currently used in the current space LIDAR missions.

10.2.3 Cost analysis

The telescope used with this detector is not off-the-shelf and therefore has to be devoped from scratch. The cost estimate is taken from a similar instrument namely the main optical instrument on board Hubble. Hubble carries a 2.4 m diameter telescope and the design cost in 1984 for this instrument where 69.4 million US dollars (source [47]). When this is corrected with the right inflation values this system becomes 123 million U.S. dollars. The telescope will be the main cost driver. The price of the S8890 si APD is around 6000 U.S. dollars (source [34]) and since 10 are needed the total price is 60.000 U.S. dollar, the same goes for the AD convertor. These values are small when compared with the telescope and can be neglected. The total cost for the detector will therefore be 123 million U.S. dollars.

10.2.4 Recommendations

The detector is the heaviest part of POLESat and this is mainly due to its telescope. The values which are used now are for very fine optical glass, but this could be different from other materials. Companies as Leica and Carl Zeiss use coatings on their lenses to increase the index of refraction and therefore increase the curvature of the lens. This means that a lower weight for the lens can be achieved. Also the material's density could be lower then the value which has been taken now. Lowering the weight of the lens will mean a significant change in the total weight of the satellite because of the snowball effect.

10.3 Orbit

The choice of orbit parameters like altitude, inclination, type of orbit etc, are of main importance since these influence almost every subsystem (power, thermal, propulsion, data handling). Change in orbit likely leads to a change in: sunlight and/or eclipse time, contact

time, coverage, power need, power for emitting signals, beam width of the lasers, propulsion need, data rate, dish size, detector size etc.

10.3.1 Orbit trade-off

The type of orbit (e.g. sun-synchronous, repeating, circular, etc.) already decreases a lot of orbit parameter possibilities. In this concept it is opted to use five single beam lasers all operating at the same time. The lasers use most of the power on-board of the satellite. To minimize the solar panel area together with the battery mass it was opted to fly in a sun-synchronous orbit. When using this type of orbit, the eclipse and sunlight time only depends on the orbital height. In this category there exist also a special orbit in which there is no eclipse, in other words the satellite is in the sunlight phase continuously. This type of orbit is called a dawn-dusk orbit which is a sun-synchronous orbit with a fixed value for the ascending node (the orbit insertion has to take place on a predefined time to be always in the sun). One of the advantages of the dawn-dusk orbit is that the solar panels can be put in a fixed position and still will be perpendicular to the solar radiation. In this way the panels are used in an optimal way, generating the maximum power. Also the sizing of the power subsystem is easier due to the fact of a constant sunlight time and no eclipse time. The disadvantage is mainly the solar pressure which is constantly working on the solar panel area. In this section different trade-off criteria are discussed. A final trade-off using all criteria is provided at the end of this section.

Power

The power needed to emit a signal depends on the required vertical accuracy and the altitude of the orbit. The objective is to reach an accuracy of 5 cm in the vertical direction over ice. This can be done by varying the diameter of the detector, the power of the laser per pulse and the orbital parameters. The detector diameter is limited by the launch envelope and was set to an effective diameter of 1.5 m (see section 10.2). The total laser power is sized in such a way that the 5 cm vertical accuracy over ice is met using 75% of the total power. The remaining 25% is used to achieve the highest possible accuracy over forest making use of green light (split laser principle as described in section 10.1. Ice has a higher reflectance than forest, the albedos are in the worst case 0.2 and 0.05 for respectively ice and forest [16]. Figure 10.7 (a) gives the power needed together with the obtained accuracy over ice and forest in function of the orbital height. Computations have been made using the equations provided in appendix B. From figure 10.7 (a) it follows that the accuracy over forest corresponding with the 25% available power is in the order of 9.3 cm. The total laser power is the sum of both the power for the laser over ice and over forest which ranges from 1.6 kW to 4 kW for an orbital height of 400 km to 650 km.

Atmospheric drag

When the satellite orbits the Earth, drag will be imposed on it. The magnitude of this drag depends on the orbit height, the frontal area of the satellite and the solar cycle of the sun. The solar cycle repeats itself every 11 years, from which the maximum emittance from the sun is known as the solar maximum and the opposite the solar minimum. During a solar maximum the atmosphere thickens due to heating of the Earth's gaseous envelope [57], causing an increased drag at higher altitudes. Orbit decay is a consequence of atmospheric drag which is much stronger for a solar maximum than for a solar minimum. The weighted average for a solar maximum and solar minimum equals respectively 80%

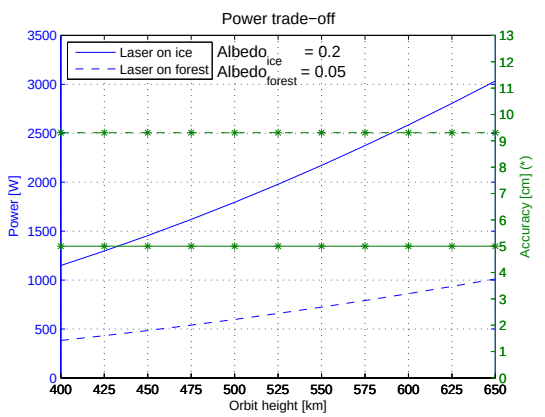

(a) Power need versus orbital heights

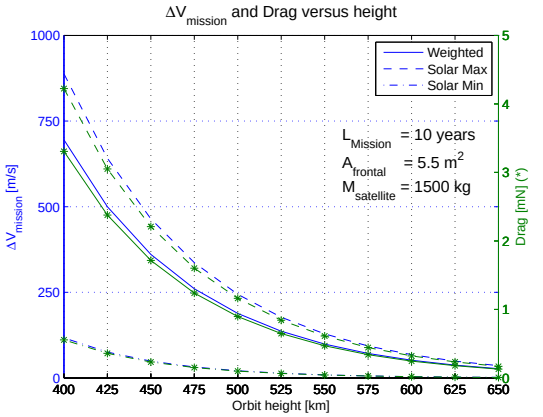

(b) ΔV and drag versus height as encountered during the mission lifetime

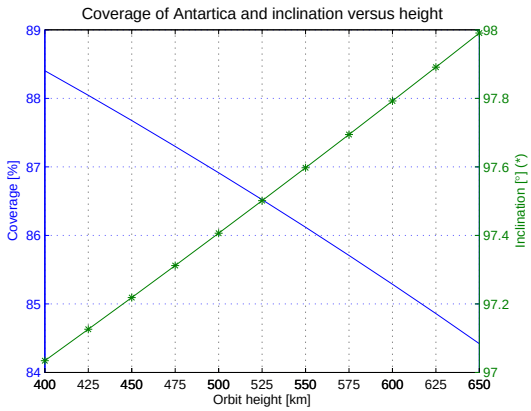

(c) Coverage of Antarctica and the inclination of the satellite versus height

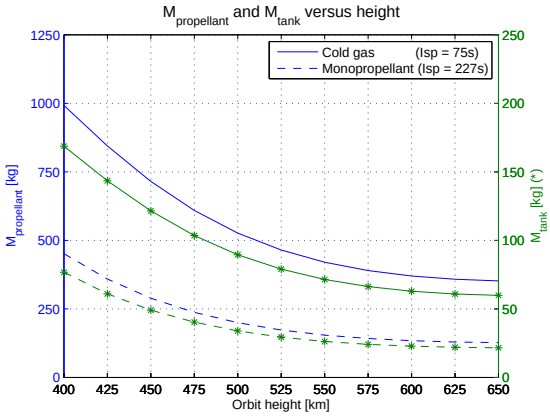

(d) Propellant trade-off versus height

Figure 10.7: Orbit calculations.

Interpretation of the figures: the legend describes the type of assumption. All starred lines correspond to the right axis, while the other ones correspond to the left axis.

and 20%. POLESat itself will encounter a solar maximum after the beginning and a solar minimum near the end of its lifetime, i.e. 2012 and 2018 respectively [51]. The engine should be able to overcome the drag force due to a solar maximum, namely to compensate for the worst case decay. The change in velocity needed to correct for the orbit decay is known as the ΔV budget for orbit keeping. This ΔV budget together with the drag encountered during the mission lifetime (10 years) for different heights are given in figure 10.7 (b). Figure 10.7 (b) includes also the three different cases, i.e. the solar minimum and maximum together with the weighted average of both solar maximum and minimum. All computations (equations are provided in appendix A.3 have been carried out with the assumption of a frontal area of 5.5 m^2 and a total satellite mass of around 1500 kg. From figure (b) follows that both the drag and the ΔV budget behave exponential, resulting in a higher propellant mass and engine thrust need (see figure (d)).

Coverage

The requirement was set to cover the whole of Greenland and at least 80% of the total area of Antarctica. The coverage itself is dependent on the inclination of the satellite (which is

fixed with height for sun-synchronous orbit) and the pointing angle of the lasers (section 10.1). The pointing angle of the lasers is changed in such a way that the ground tracks together with the footprints of the lasers cover the complete area of Greenland at the lowest latitude. This results in even more overlapping tracks near the poles. At the poles a gap will exist, where there is no coverage from the laser footprints and ground tracks. This gap is related to the inclination of the orbit. Figure 10.7 (c) gives the relation of the inclination and the coverage of Antarctica for different orbit heights. The closer the inclination to 90°, the smaller the polar gaps. From this figure it is clear that the 80% coverage is obtained within the complete range of heights as given in figure 10.7 (c). Computational equations are provided in appendix A.4.

Campaign time

The campaign time is the time needed for the satellite to collect all the measurements to complete one DEM. From a scientific point of view it would be interesting to observe even small variations in the mass balance. POLESats objective is to observe seasonal variations which can be achieved if the campaign time is no longer than three months. The best way to obtain fixed campaigns is to use repeating sun-synchronous orbits. This on the other hand restricts orbit heights but gives a fixed repetition of the ground tracks.

Trade-off

All paragraphs above are trade-off criteria. The weight of the campaign time will be the largest, since it is of main importance to observe the seasonal variations. Next, one should divide the loads in such a way that the power needed and drag (proportional to ΔV budget) are minimized, while the coverage is maximized. Orbits within the range of 475 km-500 km are the most attractive, since the solar panel area does not have to be larger than 12 m^2 (including 350 W estimated for the other payload equipment). The drag experienced within this range of heights differs by 0.3 mN and can be disregarded as trade off criteria for the orbit height. The coverage on the other hand can rise 0.5% when decreasing the orbit height. For the case of the campaign time the lowest orbit would be the one which is the most attractive, since this results in the highest coverage. The orbit height within the wanted range (475 km-500 km) corresponding to a repeating sun-synchronous equals 477.3 km (calculated using Satellite Tool Kit) .

10.3.2 POLESat orbit

POLESat will be flying in a sun-synchronous (almost) repeating orbit and more especially in a dusk-dawn orbit, leading to the fact that there is no eclipse. All corresponding orbital characteristics together with some important values are given in table 10.2. The

Altitude	477.3 km
Inclination	97.3°
Orbit time	94.2 minutes
Repeat time	91.3 days
Antarctica coverage	87.3%
Vertical accuracy ice	5 cm
Vertical accuracy forest	9.3 cm

Table 10.2: Overview of orbital characteristics.

track spacing will get denser towards the poles. The across track spacing is the distance

measured perpendicular between two neighbouring tracks. Figure 10.8 gives the across track spacing at different latitudes after 3 months of orbiting in case of POLESat. Figure 10.8 is constructed under the assumption that the tracks will be equally distributed after three months (equations are provided in appendix A.5). Since POLESat is in an almost repeating orbit, a real repetition will not occur resulting in an almost equally spaced track. The gap which is not covered on Antarctica contains also a part of water (coverage is

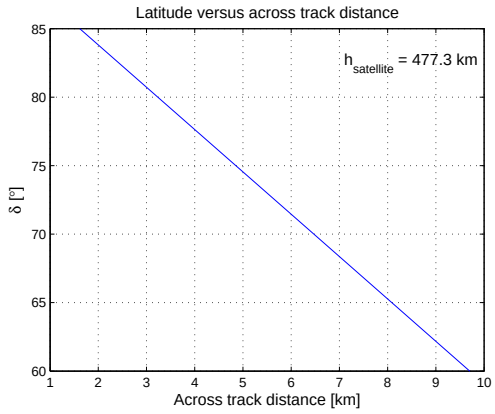

Figure 10.8: Latitude versus across-track resolution of POLESat.

limited by inclination). The tracks after two weeks of orbiting are provided in figure 10.10 (a). Remark that these are the ground tracks and not the footprints (to small compared to the covered area). When including the footprints of the laser the complete area will be covered excluding the gap. Also, Greenland is not completely covered when looking to the ground tracks as provided in figure 10.10 (b). These polar gaps can be partly made smaller by active pointing of the lasers/satellite in the neighborhood of the poles. On the other hand due to the dense track spacing POLESat will be able to take measurements of interesting areas like glaciers, transitions from water/ice and others. From scientific point of view is the Jacobshavn glacier one of the most researched areas of Greenland. This area covered by POLESat (1 campaign) and its predecessor ICESat after 91 days is provided in figure 10.9. ICESat uses a single-beam laser and covers only the area of the ground tracks, POLESat on the other hand uses multiple single-beam lasers pointed at different angles leading to a complete coverage of the Jacobshavn glacier (near the city of Llulissat).

10.4 Propulsion

The propulsion subsystem of the satellite is sized for keeping the satellite in its orbit together with the requirement of decommissioning it at the end of life. The propellant choice has consequences for the volume and mass needed for the propulsion subsystem. Besides choosing an appropriate propellant also a good corresponding engine should be identified which has to withstand the operational lifetime, required thrust but also the number of switch on/off cycles. Computations of the propellant mass are based on the ΔV budget and drag results as given in section 10.3.1 orbit trade-off and in appendix A.3.

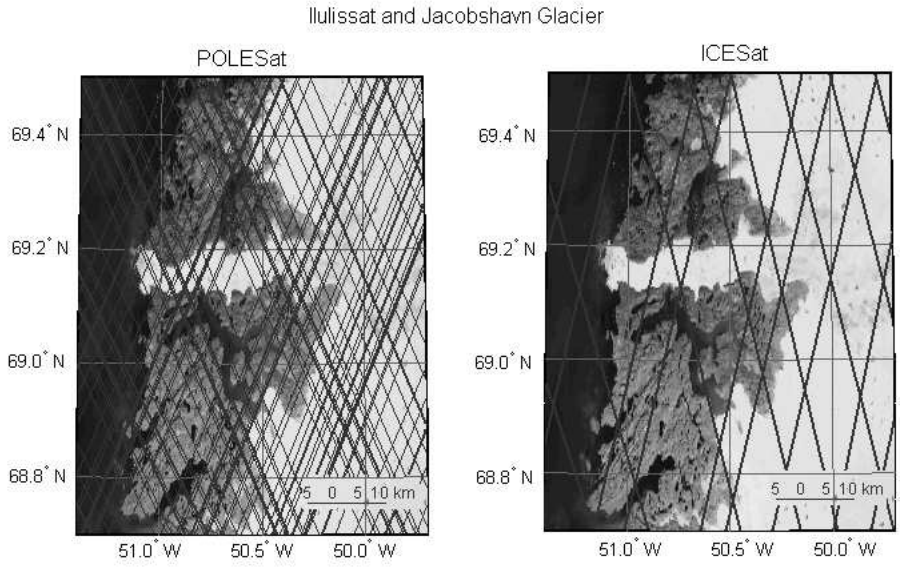

Figure 10.9: Ground tracks Jacobshavn glacier after 90 days.

Propellants

The main chemical rockets used are solid, liquid, hybrid and cold gas rocket engines. An overview of the different chemical propellant rockets is given in figure 10.11 [75]. When choosing an appropriate propellant one should consider the thrust range, the specific impulse (criterion for the exhaust velocity) and the average bulk density (the mass per volume). The chosen propellant has consequences for the type of engine and the tank size/mass, e.g. bipropellants have to be stored separately onboard of the satellite. The propulsion subsystem onboard POLESat needs to compensate for the atmospheric drag, which during the solar maximum (worst case drag) is in the order of 1.5 mN (see 10.3.1). Using this criterion already some propellant types can be eliminated:

Solid propellants burn from start until all propellant mass is depleted [70]. The thrust can be changed by varying the shape of the solid propellants. Solid motors cannot be switched on back again. Hybrid propellants provide thrust ranges [70, 46, 76] in the order of 150 N to 400 kN. The thrust range is too large and would over quantify the propulsion system. The same yields for bipropellants, were the thrust range is in the order of 5 N to 500 kN [70, 46, 76]. When using bipropellants, separated tanks would be needed causing more mass and an increased complexity of the structure.

The two remaining possibilities are liquid monopropellants and cold gas. Cold gas is a propellant stored at high pressure [74], which has as advantage that the gas can be compressed. The main disadvantage is the need for a special propellant tank that can resist the high pressure. Cold gas is often chosen for smaller spacecrafts since it can provide small thrusts in the order of 0.05 N to 200 N [70]. For monopropellants, the thrust range corresponds to 0.05 N to 5 N [70]. Monopropellants have a higher specific impulse compared to cold gas, respectively 227 s (hydrazine) versus 75 s [70], resulting in a lower propellant mass (principle of the Tsiolkovsky equation given in appendix A). Figure 10.7 (d) contains the comparison between cold gas and monopropellant. The computation of the propellant mass is based on the ΔV budget for orbit keeping (weighted) together with the change in velocity needed for decommissioning given in [70] for different orbital heights.

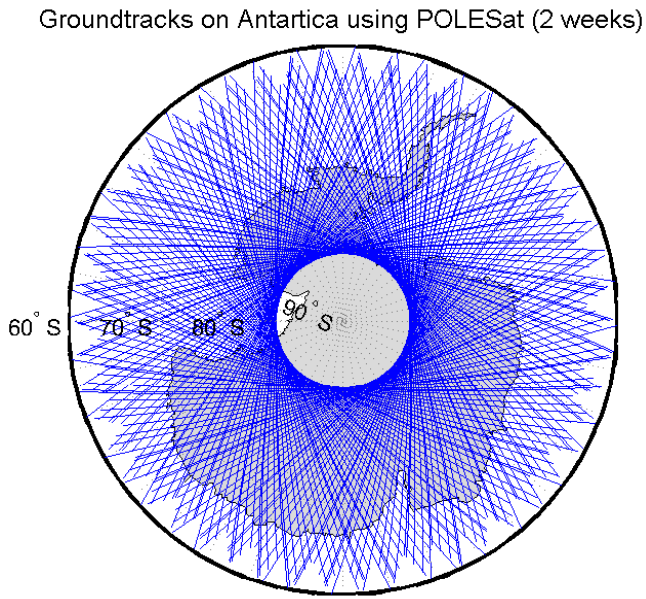

(a) Antarctica

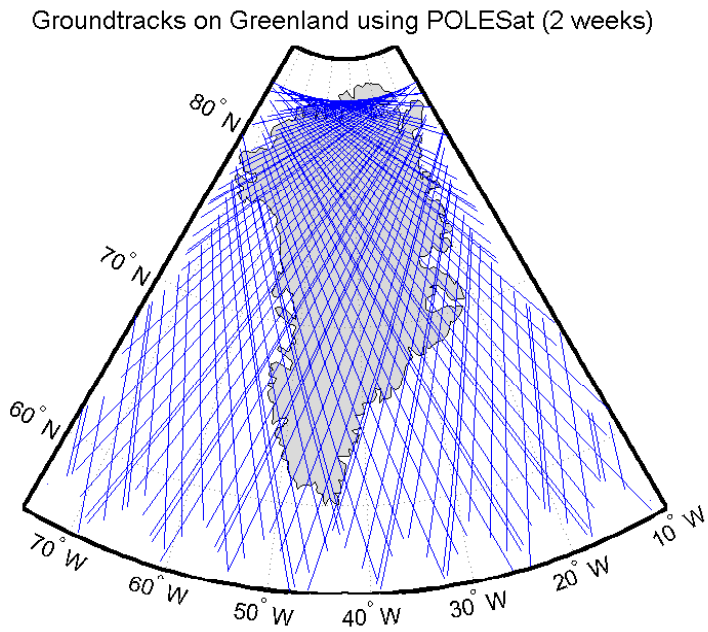

(b) Greenland

Figure 10.10: Ground tracks after two weeks.

The mass of the tanks is an estimated percentage (17% extrapolated from [22]) of the total propellant mass and will be further elaborated after choosing the propellant type. POLESat orbits the earth at a height of 477.3 km resulting in a ΔV for decommissioning of 123.5 m/s [70]. From figure 10.7 (d) follows that the mass when choosing monopropellant is in the order of 234 kg compared to 600 kg for cold gas. The volume corresponding to these masses can be calculated using the average bulk density given as 1.2 g/cm^3 and 0.6 g/cm^3 for respectively monopropellants and cold gas [70]. The choice in case of POLESat is to use monopropellant hydrazine, since this requires less propellant mass and volume compared to cold gas.

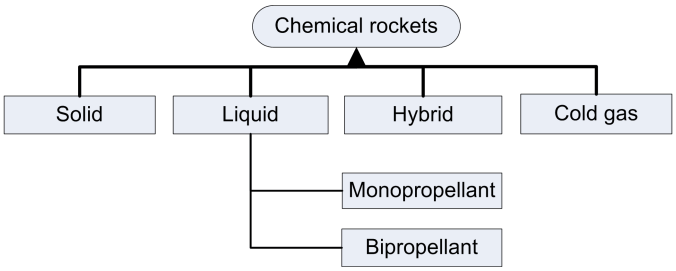

Figure 10.11: Overview of chemical rockets.

Tanks

Besides the propulsion subsystem also the AD&C subsystem (see section 10.5) needs propellants. Both subsystems use the same propellant, namely hydrazine. This makes it possible to store all the propellants in the same fuel tank. The AD&C subsystem requires 65 kg of hydrazine (elaborated in section 10.5), while the propulsion subsystem needs 234 kg. The chosen tank should be able to store a total of 299 kg hydrazine. To reduce costs and on the other hand to increase the reliability of the propulsion subsystem, off the shelf technology is used. The propellant tank chosen for POLESat is proven in flight and is produced by the aerospace company TRW [75]. The tank has the shape of a sphere with a diameter of 60 cm and is capable of storing 100 kg of hydrazine. The tank itself is constructed from titanium resulting in a structural tank mass of 14.3 kg per tank. For complete storage of the propellants at least 3 tanks are needed, resulting in a total tank mass of 343 kg including hydrazine. The propellant mass was calculated under the assumption of a total mass equal to 1500 kg. This results in an estimated dry mass of 1200 kg.

Engine

Some important parameters that should be taken into account when sizing the engine are the thrust in vacuum [N], the operational lifetime of the engine [s] and the number of switch on/off cycles. Besides this, often the total impulse [Ns] is given, this parameter corresponds to the thrust multiplied with the operational lifetime of the engine (eq. 10.6). The engine itself should be capable of correcting for the decay of the orbit during the satellites lifetime. The total impulse of the engine has to be larger then the total impulse resulting from the drag imposed on POLESat during the mission lifetime. The weighted drag (section 10.3.1) used for the calculation of the total impulse equals 1.2 mN resulting in a total impulse of 378.4 kNs.

$$I = F \cdot t \tag{10.6}$$

$$I_{mission} = 1.2 \cdot 10^{-3}\ \text{N} \cdot 10 \cdot 365 \cdot 24 \cdot 3600\ \text{s} = 378.4\ \text{kNs} \tag{10.7}$$

Corrections are not done continuously since these influences the laser measurements. Orbital corrections can be done when no important data is collected or when the lasers are switched off. The burning time of the engine depends on the thrust which it can provide together with the amount of correction it has to make. One can opt for a small thrust long burn or for a large thrust with a small burning time. The range of thrusts which are the best to correct for small drag forces are in the order of 0.5 N to 1 N. The CTH 0,5 engine chosen for POLESat is made by DASA [75, liquid rocket systems]. Characteristics of this engine are summarized in table 10.3.

Vacuum thrust [N]	Life span [s]	Cycle life [cycles]	Engine mass [kg]	Length [mm]
0.75	514800	> 55000	0.19	113

Table 10.3: CHT 0,5 hydrazine engine produced by DASA
Source: [75, liquid rocket systems].

To see if this engine satisfies the need to correct for the orbital decay some control calculations have to be made. The total impulse, I_{engine}, of the engine should be larger compared to total impulse due to drag.

$$I_{engine} = 0.75\ \text{N} \cdot 514800\ \text{s} = 386.1\ \text{kNs} \tag{10.8}$$

From this it is clear that the engine satisfies the demand of a larger total impulse. When assuming that the corrections are done once each week, this results in a total impulse of 725.8 Ns. The engine itself provides a thrust of 0.75 N resulting in a burning time of 16.5 min.

$$I_{week} = 1.2 \cdot 10^{-3}\ \text{N} \cdot 7 \cdot 24 \cdot 3600\ \text{s} = 725.8\ \text{Ns} \tag{10.9}$$

$$t_{burn} = \frac{725.8\ \text{Ns}}{0.75\ \text{N}} = 967.8\ \text{s}\,(= 16.5\ \text{minutes}) \tag{10.10}$$

$$n_{cycles} = \frac{10 \cdot 365}{7} = 522\,\text{cycles} \tag{10.11}$$

Correcting each 7 days results in 522 cycles which the engine can withstand (see table 10.3). During the mission it will not always be possible to make a correction, when delaying the corrections this will only result in a longer burning time of the engine. When correcting the decay after one complete campaign the burning time would be in the order of 3.5 hours.

10.5 Attitude determination & control

In this section, the attitude determination and control (AD&C) subsystem of POLESat is discussed. The attitude is the orientation of the satellite with respect to a fixed reference frame. This reference frame can be for instance the celestial reference frame. With this satellite attitude, also the pointing of the laser is determined and controlled since the laser has a fixed orientation with respect to the satellite.

In this section, first the attitude requirements are given and explained. Then the ways of determination are described, followed by the description of attitude control methods which are chosen for POLESat.

10.5.1 Attitude requirements

The use of a laser at about 500 km height requires accurate pointing of this laserbeam to make accurate measurements. Requirements on accuracy will therefore result in very high requirements on the accuracy of the AD&C system. The top level system requirements for POLESat originally include requirements on accuracy.

These requirements state that POLESat should be able to make measurements with a vertical accuracy of 5 cm and a horizontal accuracy of 5 m. When handling only a small slope, an error in the pointing can already evoke a large error in the vertical accuracy. For the horizontal or geolocation accuracy, 5 m is required.

The requirement for POLESat attitude determination is set at 1 arcsecond for roll and pitch. This requirement is taken over from the ICESat mission. This is a higher accuracy then eventually can be achieved for the pointing determination of the laser beam. This is mainly due to inaccuracies of the pointing with respect to the satellite. With post processing and measurements on the laser beam, this pointing can eventually be determined.

The yaw of POLESat needs to be determined with a smaller accuracy; the demand for yaw determination accuracy is 0.05 degree. This yaw determination requirement is relatively low, since it only affects the geolocation of the outer footprints of POLESat. The yaw will probably be determined far more accurate than this value. For this chapter, only the determination of the satellite will be discussed; post processing of the attitude determination will be discussed in section 10.7.

10.5.2 Determination

To determine the attitude of the satellite, several options are available. These include star sensors, a sun sensor, horizon sensors, inertial platforms such as gyroscopes and magnetometers. The design choices for POLESat will now be made clear. The main consideration for choosing a method for attitude determination for POLESat is the accuracy which needs to be obtained. This is a rather high required accuracy, due to the laser pointing errors described in the previous section

When observing the achievable accuracies ([70]) the choice for primary sensor can be made easily. The only sensor with an accuracy that meets the demands for POLESat is a star sensor. Since POLESat is a satellite with controlled attitude for all three axes, the appropriate star sensor is a star tracker.

Star tracker

A star sensor, as shown in figure 10.12 (a), consists of a small telescope which is oriented at the stars. It keeps track of several clear stars and constellations and with the on-board star catalog it can determine at which stars the sensor is pointing. Stars are projected through the telescope onto one or several charge coupling devices (CCD). For POLESat, a ready made star sensor is chosen. This is the ASTRO 15 produced by Jena-Optronik GmbH. This star sensor can determine the attitude around its roll axis with an accuracy of $10''$ and around its yaw and pitch axis with an accuracy of $1''$. It weighs 5.8 kg and uses 24 W of electrical power. It is 192 mm in diameter and 440 mm in length.

The database with stars which will be used by the star tracker is the Hipparcos star catalog. This is a catalog with contains data on roughly 118000 stars. The catalog has information

(a) Astro 15 star-tracker

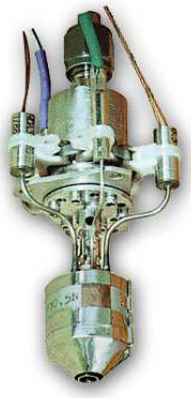

(b) EADS CHT 0.5 thruster

Figure 10.12: Star-tracker (a) and thruster (b).

on brightness and position about these stars. The position of the stars is accurate with an accuracy of 1-3 milliarcseconds. This catalog is roughly 800 Mb and can be stored on the solid state recorder on-board the satellite. More information on the Hipparcos star catalog can be found in [37] .

The attainable accuracy for the chosen star sensor is 1 arcsecond for the pitch and yaw of the star sensor and 10 arcseconds for the roll angle. These accuracies are with respect to the reference frame of the sensor. The sensor is attached in the satellite looking in zenith direction. This means that it is looking straight upwards. The roll angle for the sensor is therefore the yaw angle for the satellite. The other two satellite axes, roll and pitch, are therefore determinable with an accuracy of 1 arcsecond.

The star sensor also has some limitations. These limit the use of the star tracker and force the use of an extra sensor. The field-of-view (FOV) of the star sensor is 13.25°. Especially above the north pole, there is a chance of 2.1% that the star sensor will only see two or less stars [10]). Too few stars in the field of view can affect the accuracy in a negative way. Also, the field of view can be partially obscured by the moon. This will also decrease the reliability of the star sensor. The final limitation of the star sensor is the update-rate of the star sensor. This update rate is 4 Hz. The maximum pulse repetition rate of the laser will be 75 Hz. Because every pulse will need a corresponding determination of attitude, either a form of interpolation or alternative way of determining the attitude needs to be used.

Gyros

A gyroscope is an inertial sensor which measures the speed or angle of rotation. This is done from an initial reference. The absolute value for attitude cannot be determined with a gyroscope. Together with the fact that gyroscopes can have a higher output rate (up to hundreds of Hz), makes them ideal for the combination with the star sensor for POLESat. The attitude determination of the star sensor can be smoothed with the gyroscopes.

For POLESat, two gyroscopes are chosen. Both can determine attitude changes for two axes. This gives three axes determination and one redundant axis. The chosen gyroscopes

are the TARA I, produced by Kearfott, guidance and navigation corporation. These gyroscopes weigh 1.5 k each and both use 12.5 W electrical power (7.5 W operating and 5 W heating power). The lifetime of these gyroscopes is 10 years.

Operational details

Since these methods of attitude determination are now chosen, some extra remarks regarding their functioning can be made. The star sensor can determine the attitude of its own reference frame. This attitude will then be processed. To increase simplicity, the axes of the star tracker will be coinciding with the axes of the satellite. The roll axis of the star tracker will be the yaw axis of the satellite and the pitch and yaw for the star tracker will be the roll and pitch axes. (These two are interchangeable, since the star tracker can determine both of them with equally high accuracy). To decrease the chance in errors, the star tracker will be placed as close as possible to the optical instruments. Also the structure linking the tracker to these instruments will be as rigid as possible, so deformations in the structure will not cause errors in the measurements. The output of the star tracker is given in quaternions. Quaternions are an extension of complex numbers. They form a 4-dimensional space with one real axis and three imaginary axes. They can be used to describe the attitude for the satellite. The star tracker output is the attitude and the change of attitude. These are both described with a quaternion. Since the output rate of the star tracker is 4 Hz, 8 quaternions per second will have to be downlinked. These quaternions are 24 bits. The gyroscopes which are used to smooth the interpolation of the attitude between star tracker outputs, will also give four outputs per second. These will also be given in 24 bits. This means that the total date rate of the attitude determination will be $12 \times 24 = 288$ bits per second.

10.5.3 Control

The satellite also needs to be pointed correctly. This can be done with a lower accuracy than the determination of the attitude. If there is a misstake in pointing, it will be known due to the high accuracy determination and this can be taken into account. The sizing of the controlling actuators needs to be done A disturbing torque is often present on the satellite. This torque can consist of several components. This torque will disturb the attitude of the satellite.

Torque components

There are 5 types of disturbing torques acting on the satellite. These are affected by the orientation of the satellite and the design of the satellite. The types of torques are:

- Gravity gradient torques on the satellite,
- Solar pressure,
- Magnetic field torques,
- Aerodynamic drag torques,
- Internal disturbance torques.

The torques due to solar pressure and aerodynamic drag are caused by the offset from the center of gravity of the centers of solar pressure and aerodynamic pressure respectively. The gravity gradient torque is caused by the orientation and lay-out of the satellite and different gravitational forces. The magnetic field torques are created by the residual dipole created by electric circuits in the satellite acting on the earth magnetic field. Finally, the internal disturbances exist mainly due to internally moving parts and the inaccuracies of thrusters.

In appendix D are the calculations for all these components. When calculating these torques, they add up to approximately $4.6 \cdot 10^{-4}$ Nm. This torque is the combined torque over all axes. This is excluding the internal disturbance torques. These torques are considered negligible for the estimation of propellant mass, since they are small and will often counteract each other. Also no engines or moving parts are on board the satellite, apart from the AD&C components and the solar array at the start of the mission lifetime. Estimations are made using a contingency of 10%.

Momentum wheels

To counteract these torques, some actuators are needed. The first method chosen for POLESat is the use of momentum wheels. Momentum wheels are rotating disks. These disks often have a magnetic bearing to avoid friction. By spinning up or spinning down these disks, a reaction moment is applied on the satellite. This reaction moment can then be used to counteract the disturbing forces. Because the acceleration of the momentum wheels can be controlled precisely, counteracting moments can accurately be applied.

In POLESat, four momentum wheels will be used. One for each axis and one redundant wheel. This wheel will be placed with its axis oriented such that its vector is a combination of vectors of the axes of all the other momentum wheels. In this manner, when a random wheel fails, its function can be taken over by the redundant wheel. The largest momentum wheel of the Honeywell constellation series is the HR16. This momentum is suitable for POLESat. It can store up to 100 Nms. It weighs 12 kg and uses 22 W of electrical power. During spinning up it can use peak power of up to 195 W.

The momentum wheels on POLESat have a maximum rotating speed. For the momentum wheels chosen, this maximum speed leads to a maximum storage of momentum of 100 Nms. When the disturbing torques on the satellite have caused the moment wheels to spin at maximum speed, the momentum wheels need to be desaturated. This desaturation can be done using several actuators. The three options for this desaturation are: control moment gyros (CMGs), magnetic torquers and thrusters.

Dividing the capacity of the wheels by the torque components leads to a build-up time of 60 hours (see appendix D). Off course, this is calculated using the maximum torque. In reality, some torquecomponents will be cyclic, and some components can be manipulated to counteract other disturbance torques. The real maximum time between desaturating will therefore be higher.

Thrusters

The actuator type can now be chosen. CMGs are used to create high torques, are heavy and costly. CMGs will therefore not be used. Magnetic torquers are used to produce a very small counteracting torque. When desaturating the momentum wheels this will take

too much time. This time is not available, since desaturating needs to be done when not performing measurements. Therefore, for POLESat, thrusters are chosen to desaturate the momentum wheels. Thrusters are available in many types. For orbit maintenance, allready monopropellant hydrazine thrusters are chosen. These thrusters are available with thrusts down to 0.5 N.

To increase the simplicity of the design, hydrazine thrusters will also be used for the attitude control. The arm of the thrusters to the center of gravity is estimated to be 1 m for all axes. However for the long side of the satellite, this arm will be made larger. This increases contingency for the mass estimation of the fuel, especially since the largest contributor to the torques, solar pressure, works around the same axis due to the presence of the solar panels.

The chosen thrusters are produced by EADS Astrium, shown in 10.12 (b). They are CHT 0,5 thrusters, with 0.5 N thrust. They weigh 195 grams each and are 11.3 cm long. The thruster achieves a specific impulse of 227.3 s. The diameter is roughly 4 cm. 12 thrusters are needed, since there are three axes and for each axis, four thrusters are needed to create torques in both directions. A torque is created by two thrusters, and for both directions, this means four thrusters per axis.

With the arm of 1 m, a thruster-pair can create 1 Nm of torque. To desaturate a momentum wheel of 100 Nm, only 100 s are thus needed. The build-up time was estimated to be 60 hours. So, every 60 hours, 100 seconds of thruster firing is needed. The propellant mass needed for the entire lifetime is also calculated in appendix D. This is almost 65 kg. This propellant will be stored in the main fuel tanks together with the propellant for orbit maintenance.

In conlusion, the attitude determination consists of a star sensor. This star sensor determines the attitude of the satellite backed up by gyroscopes to smooth out the low refresh rate of the star tracker. The attitude control is performed with momentum wheels and thrusters to desaturate the wheels. The thrusters work on the same fuel as the main engine which is present to maintain the orbit.

10.6 Guidance & navigation

Navigation is defined in [70] as the determining of the satellite's position and velocity or determining its orbital elements as a function of time. Guidance on its turn is maintaining the desired position and controlling the orbit.

For POLESat an accuracy better than 5 cm for navigation is required. When a vertical accuracy of 5 cm is needed for measurements, the error margin for orbit-determination has to be substantially smaller, since the orbit determination error directly affects the measurement error.

GNSS

For navigation, several techniques are available. However, the only logical option to obtain a precision orbit determination (POD) is using a global navigation satellite system (GNSS). A GNSS is a constellation of satellites that send out timesignals. A receiving satellite can then determine its own position, using the signal from multiple satellites.

As of 2007, the only fully operational GNSS is the American Global Positioning System (GPS). The Russian Glonass is being restored and the European Galileo positioning system is still in development. It is planned to be operational by 2013.

GNSS antenna sizing The antennas used for POLESat to receive the GNSS signal are helical antenna's. These antenna's are approximately 20 cm diameter and 20 cm high. There will be two antennas on either side of the satellite. They are placed on two sides of the satellite in order to receive signals from enough GNSS satellites. Placing two antennas on either side is to increase redundancy of the measurements. This design can also be seen on GOCE, which is a mission that has a need for high accuracy to accurately map the Earth's gravitational field.

GNSS accuracy

The accuracy achievable today with GPS is in the order of 3 cm. This is enough for the requirements set for POLESat. It can be assumed that accuracies achieved with GPS will increase even more in the future. In section 10.7.4, an elaboration on POD via post-processing will follow.

ILRS (International laser ranging service)

To validate the reliability of the GPS orbit measurements, POLESat will be tracked by the International laser ranging service (ILRS). ILRS has a network of groundstations with laser rangers. ILRS already tracks several satellites and even the moon by pointing at a reflector placed on the lunar surface during one of the apollo missions. The reflector attached to exterior of the satellite is approximately 20 cm $\times$ 20 cm $\times$ 4 cm and weighs approximately 1.2 kg.

Laser ranging is currently the most accurate way to determine the geocentric position of a satellite. However this service is not present globally, because satellites cannot always be in the line of sight of laser rangers. The accuracy with which ILRS can determine the satellite position is in the order of millimeters. This measurement is used to calibrate the position of the satellite whenever it is in range of an ILRS groundstation. The data from this service is also used as an input for the post-processing of the precision orbit determination. Which is discussed in section 10.7.4.

Guidance

Guidance and orbit control can both be used to mean adjusting the orbit to meet the predefined conditions. Orbit control is described in section 10.3.1. The software and data handling needed for the guidance is not within the scope of this report. No further information is therefore needed on the guidance of POLESat.

In short, the navigation of POLESat is done with the help of the global positioning system. GPS nowadays can achieve accuracies around 3 cm and will probably become even more accurate. Additional, to increase reliability, ILRS is used to calibrate the orbit position and validate the post-processing. The ILRS can achieve accuracies in the order of millimeters.

10.7 Data processing & distribution

The data processing and distribution task is concerned with the entire data flow from sensor to data products delivered to customers. In this section most aspects of the data flow will be covered including the connections with the AD&C, G&N and TT&C subsystems.

10.7.1 Introduction

Based on previous missions the data flow can be roughly subdivided as shown in 10.13. The data obtained from the payload is much too large to store and telemeter to Earth (see section 10.2). Therefore a strategy is needed to reduce the dataset while keeping all relevant measurements. For POLESat this strategy is based on the one used by ICESat and is described in 10.7.3 [14].

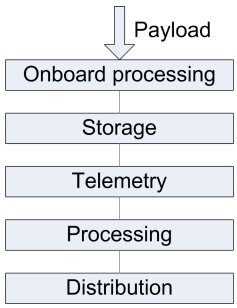

Figure 10.13: Data flow.

The reduced dataset then has to be telemetered to Earth during the contact time with a ground station, which is described in section 10.9. The ground station takes care of forwarding the dataset to mission control where it can be processed further. The products to be delivered are described in general in 10.7.5. The post-processing required for these products is described in more detail in 10.7.4.

The delivery of the data to end-users is given in 10.7.7.

10.7.2 Error budget

The ICESat the objective is to measure profiles of ice sheet surface elevation with sufficient accuracy, spatial density, and temporal coverage so that inter-annual and long-term elevation changes can be derived with an accuracy of < 1.5 cm/year for spatial averages of measurements over areas of 100 km $\times$ 100 km on the ice sheets [77]. For the chosen orbit and measuring parameters this resulted in a error budget for ICESat as shown in table 10.4 [10]. In [14] it is mentioned ICESat should be able to track surfaces up to 3°. For POLESat it is assumed the same terrain is of interest. However, as discussed in 3, POLESat should have a single shot error of no more than 5 cm and should enable the creation of a 100 m $\times$ 100 m Digital Elevation Model (DEM) of unspecified accuracy. What is feasible with our design in this respect will be discussed in section 10.7.6.

In [77, Fig. 6.2] it is shown the ICESat instrument, GLAS, stays within the set budget of 10 cm for both terrain and ice/snow for total slopes up to 5°. Using an implementation of formula C.1 (the pointing accuracy is not considered for this purpose), these figures can be reproduced. For the POLESat design as discussed in 10.1, 10.2 and appendix B this implementation gives the results shown in table 10.5 . It is obvious POLESat stays within the set boundaries, even with a relatively greater margin then ICESat stays within its boundaries.

Error	ICESat	P1	P2	POLESat
Single shot error	10	10	5	5
Radial orbit determination	5	5	5	3
Attitude determination	7.5	6.06	6.06	6.06
Troposheric delay	2	2	2	2
Atmospheric scattering	2	2	2	2
Other	1	1	1	1
RSS total error	13.8	13.07	9.78	8.93

Table 10.4: POLESat and ICESat single shot error budgets in cm for the 1064 nm laser [10]. Values are or a total slope of 1° [10]. P1 shows the effect of the lower orbit on the error budget with respect to ICESat (equal orbit and pointing accuracy). P2 show the effect of the improvement of the instrument over GLAS with respect to P1.

	Terrain				Ice/snow			
	Photons	Theoretical ranging error [m]			Photons	Theoretical ranging error [m]		
		0°	3°	5°		0°	3°	5°
ICESat	6963	0.0160850	0.032995	0.050711	19496	0.0098665	0.0207410	0.032015
POLESat	28553	0.0065746	0.012561	0.019039	79949	0.0052012	0.0088443	0.013025

Table 10.5: POLESat and ICESat single shot range error for different slopes (1064 nm laser). Terrain is assumed to have an albedo of 0.25, ice/snow of 0.7. Surface roughness is assumed to be 0, atmospheric transmission 50%.

10.7.3 On-board processing

The data received from the sensor is a continuous set covering both the transmitted and received pulse waveforms.

Since most of the data is useless except for determining noise, atmopsheric properties and background signal levels it can be processed and removed from the dataset. The range window is determined in two steps. First by looking up the expected terrain from an on-board DEM, and using it to reduce the dataset. Secondly, by using several filters, which are to be implemented in hardware, to determine the subset most likely to include the surface echo. This final subset will be stored together with the calculated noise levels and system parameters such as the APD gain and will be telemetered to Earth as described in section 10.9.

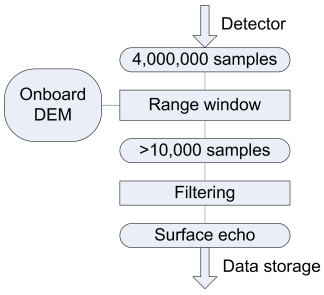

Figure 10.14: On-board processing flow.

10.7.4 Post-processing

Post-processing the onboard data is essential for keeping ranging errors for realistic terrain in the order of those mentioned in the error budget 10.4. Only the most important aspects of post-processing will be discussed here.

Full waveform analysis The analysis of the full waveform is explained in appendix C. From it, the uncorrected elevation, slope and roughness can be determined. There are several reasons why this is not always possible and/or useful.

Firstly, it is important to evaluate which measurements are to be disregarded for quality reasons. This is likely for measurements made in the presence of clouds. It might also occur that the onboard processing returned the wrong selection of data and no ground return signal can actually be found. Cloud returns are normally observed from measurements of the green laser, but in case of it's failure the near-infrared laser can be used to determince clouds, though with less accuracy. ased on the theory in [12] as applied in [36] the mean climatological probability of a nadir cloud free line of sight is roughly $0.5-0.6$ for Antarctica and $0.4 - 0.5$ for Greenland. Another reason for disregarding a meausurement is the saturation of the receiving system. For very variable terrain it is impossible to adapt the gain settings for the sensor between each measurement. Therefore some waveforms might be tainted by a saturated detector.

The precise implementation of the waveform profiling needs to be customized to POLESat. Both for the green and the near-infrared waveforms new predictions and fittings need to be evaluated for simulated data. One important reason for this is the fact that surface roughness is not random and its calculated value will have to be correlated with grounds surface measurements. Once the satellite is in flight the algorithms will have to be validated against known terrain. This procedure should benefit strongly from existing simulations and measurements from ICESat.

Precise attitude determination The attitude determination and control (AD&C) system as described in 10.5 delivers high quality data by itself, though it's real-time attitude knowledge is no better $20''$. The processing of this data will require knowledge of the systems thermal and optical behaviour as well as its exposure to stray light sources. This information will have to be obtained before hand by extensive testing. The data of the star-trackers and gyros will be combined, corrected for thermal optical and optical errors and possibly corrected for anomalous measurements. This is essential in obtaining the intended attitude determination for each laser pulse. It is expected the attitude determination should be at least equally accurate to that of ICESat and is therefore expected to be $1.5''$ or better. This results in a decrease in the contribution of the pointing error to the error budget as can be seen in table 10.4 due to POLESat's lower altitude compared with ICESat's orbit.

Precise orbit determination Determining an accurate ephemeris is done by estimating position and velocity from a series of observations. These observations are a function of the satellite's real position and velocity. Starting at a reference epoch the equations of motion are evaluated leading to predicted observations. These are then differenced from the real observations to produce observation residuals. The satellite state parameters at the reference epoch are then adjusted to minimize the observation residuals. Thus, it is required to know the equations of motion, the observation-state relationship and an estimation algorithm. The method chosen for POLESat is based on GPS observations:

GPS POD techniques A few different methods are available for post-processing the orbit data. The first is the geometric approach proposed in [73], which is based on phase the changes in the GPS carrier phase signals. The second is the kinematic approach in [17] using double- and triple-differenced GPS carrier phase measurements. A third option is

the dynamic approach described in [67] which requires precise models of all forces acting on the satellite. A combination of the last two is also possible as introduced in [72] and is known as the reduced-dynamic approach.

Analogous to ICESat the dynamic approach with gravtity tuning will be used for POLESat. This will allow leverage of existing knowledge and software development. This approach is expected to deliver increased accuracy compared to ICESat as the dynamic model parameters such as gravity fields have become more accurate. Validation of these results will be done using the reduced-dynamic approach, which should also benefit from the improved technology, specifically the advances in GPS measurements.

forces For the dynamical approach all forces on the satellite need to modeled as precisely as possible. The equations of motion of a near-Earth satellite can be described in an inertial reference frame as $\ddot{\bar{r}} = \bar{a_g} + \bar{a_{ng}} + \bar{a}_{emp}$ where r is the position vector of the center of mass of the satellite, $\bar{a}_g$ is the

$$\bar{a}_g = \bar{P}_{geo} + \bar{P}_{st} + \bar{P}_{ot} + \bar{P}_{rd} + \bar{P}_n + \bar{P}_{rel}$$

where P_{geo} = perturbations due to the geopotential of the Earth, P_{st} = perturbations due to the solid Earth tides, P_{ot}= perturbations due to the ocean tides, P_{rd} = perturbations due to the rotational deformation, P_n= perturbations due to the Sun, Moon and planets, and P_{rel} = perturbations due to the general relativity.

non-gravitational forces

$$\bar{a}_{ng} = \bar{P}_{solar} + \bar{P}_{earth} + \bar{P}_{thermal} + \bar{P}_{solar} + \bar{P}_{earth} + \bar{P}_{thermal}$$

where P_{drag} = perturbations due to the atmospheric drag, P_{solar} = perturbations due to the solar radiation pressure, P_{earth} = perturbations due to the Earth radiation pressure, $P_{thermal}$ = perturbations due to the thermal radiation,

empirical forces To adjust for unmodeled or incorrectly modeled forces, empirical parameters are added to the system. For satellites continuously tracked with high precision data the introduction of these parameters can significantly reduce orbit errors [62].

Processing The GPS range measurements need to be corrected for both propagation delay, relativistic effect, phase center offset and ground station related effects. The implementation of a precise orbit model will require a lot of work. The entire satellite has to be modeled and measured for the thermal model, the mass distribution model and the atmopsheric drag model. Many of the dynamic models are not constant and will require continuous optimization (e.g. the atmospheric drag is strongly influenced by the solar cycle). Once all these models are created they can be combined with the corrected GPS measurements and several of the parameters (especially the empirical ones) can be tuned to optimize the solution.

Performance In the case of ICESat this post-processing results in a 2-3 fold improvement of the orbit knowledge. For ICESat the design goals for orbit determination is < 5 cm RMS radial and < 20 cm RMS horizontal. Due to POLESat's lower orbit it is more sensitive to

atmospheric drag and variations in the Earth's gravity field. Compared with ICESat it is expected that use can be made of much improved gravity models and improved GPS sensors (see section 10.5). The validation by means of laser ranging and alternative processing of the GPS data should also benefit from increased accuracy that is will be available by 2012. It is therefore assumed a 3 cm radial error budget is feasible for POLESat.

Precise geolocation

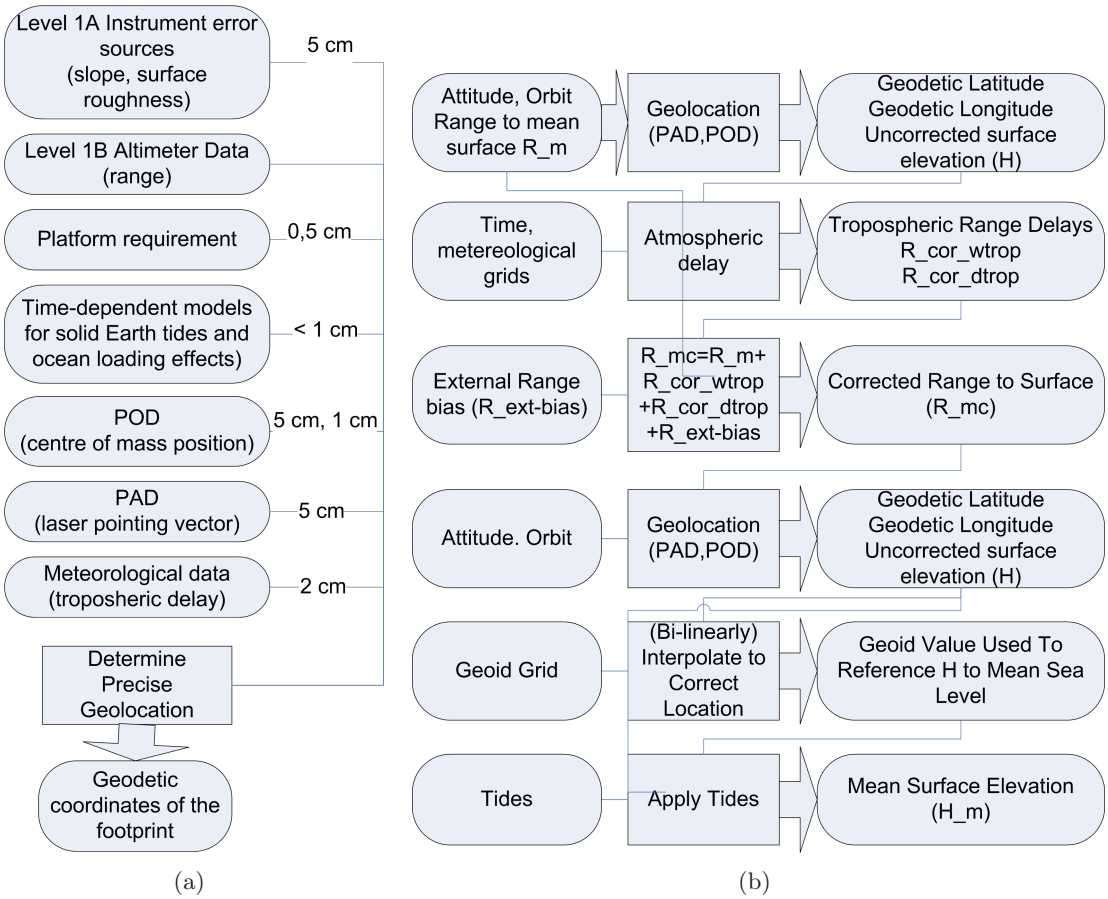

Figure 10.15: Precise geolocation with errors.

Once all the corrections have been calculated they can be used to determine the precise geolocation of the measured footprint. An overview of this process is shown in figure10.15 (a). The geolocation itself is shown in figure in 10.15 (b).

Error RMS [m]	ICESat	P1	POLESat
impulse	0.027104	0.0070658	0.0070658
roughness	0	0	0
curvature	4.6813E-05	1.1257e-05	1.1257e-05
angle slope	0.014857	0.0039298	0.0039298
Instrument error	0.030909	0.0080851	0.0080851
Pointing uncertainty	0.076172	0.060587	0.060587
Radial orbit	0.05	0.05	0.03
Tropospheric delay	0.02	0.02	0.02
Atmopsheric scattering	0.02	0.02	0.02
Other	0.01	0.01	0.01
Total	0.10078	0.084476	0.074405

Table 10.6: POLESat and ICESat errors.

Calculated using C.1: with, smooth terrain, 1° slope, albedo 0.2, pointing accuracy 1.5″ (1σ). P1 shows the effect of the improved instrument and equal pointing precision with respect to ICESat.

The end result for flat, though badly reflecting, terrain is shown in table 10.6. However, as can be seen from table 10.7 this is not a good approximation of reality.

Geomorphic features	Surface slope [°]		RMS Roughness	
	Σ50%	Σ90%	Σ50%	Σ90%
Glaciated continental shield	0.55	1.6	0, 5 m	0, 8 m
Shallowly Incised drainage	0.85	2.7	0, 9 m	1, 9 m
Ice cap	0.90	4.3	0, 3 m	1, 0 m
Moderately incised drainage	0.95	3.2	1, 4 m	3, 1 m

Table 10.7: Terrain characteristics for 50% and 90% occurence levels.

10.7.5 Data products

The main data products to be delivered by POLESat are shown in table 10.8. The raw telemetry (PS00) are only of interest to the mission engineering team. The most important level 1A products are: the almitery data PS01, containing the the transmitted and received waveforms, the atmospheric data PS02 containing normalized backscatter and low level instrument parameters, the engineering data containing the housekeeping data used in creation of PS01 and PS02, and the laser pointing data containing all spacecraft data required for calculating the precise laser pointing per pulse.

The main level 1B data products are: the waveform parametrization data, containing the results of the waveform characterization needed to calculate slope and roughness from the waveform, the elevation data PS06 containing the elevations and range corrections, and the backscatter data PS07 containing backscatter data from the lower atmosphere. Furthermore several data products will be created for other atmospheric data.

PS05 and PS06 data are used in conjunction to create level 2 data products of which the most important are P09 to P12 containing laser footprint geolocation and reflectance, and geodetic, instrument, and atmospheric corrections for range measurements.

PS00	Raw waveforms	0
PS01	Altimetry data	1A
PS02	Atmosphere data	1A
PS03	Engineering data	1A
PS04	Laser pointing data	1A
PS05	Waveform-based elevation corrections	1B
PS06	Elevation	1B
PS07	Backscatter	1B
PS08	Ice sheet products	2
PS09	Sea ice products	2
PS10	Land products	2
PS11	Ocean products	2

Table 10.8: POLESat data products.

10.7.6 Derived data products

One of the top level requirements for POLESat is to enable the creation of a digital elevation model (DEM) with a resolution of 1 km $\times$ 1 km. The coverage as described in section 10.3.2 can be combined with the expected weather (averaged over a ten year period for the summer [53]) to calculate the amount of useful measurements in one campaign. Using the POLESat error budget as in 10.4 in conjunction with the expected amount of measurements in a 1 km $\times$ 1 km area, an absolute minimal value for the DEM accuracy can be approximated using

$$E_{DEM} = \sqrt{\left(\frac{E_r}{\sqrt{N_{obs}}}\right)^2 + E_s^2} \tag{10.12}$$

where E_{DEM} is the root sum square total elevation error, E_r the random part of the root sum square error per measurement, N_{obs} the number of measurement within the area ,and E_s the systematic part of the root sum square error per measurement.

Assuming flat terrain and very low systematic errors due to long term effects and assuming all measurements are from different tracks (thus the orbit, attitude and atmospheric error are indepent, which does not hold for contiguous measurement from a single track) we thus obtain:

$$E_{DEM} = \frac{E_r}{\sqrt{N_{obs}}} \tag{10.13}$$

Now applying this to a grid of 1 km $\times$ 1 km areas on Greenland for which average values of the number of measurements have been made, figure 10.16 is obtained. It can be regarded as the best accuracy obtainable when the error equals the budgeted error of 8.93 cm.

10.7.7 Distribution

The most likely way of distributing all data products is via the internet via an organization like Earth Observing System Data and Information System [20] or the Earth Observation Principal Investigator Portal [58]. The distribution of the data is assumed to pose no challenge.

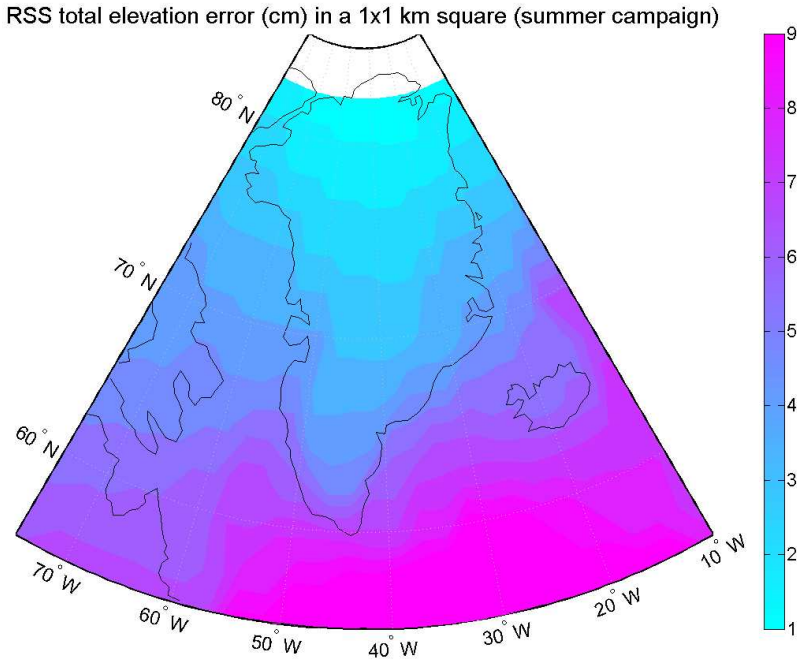

Figure 10.16: Maximal DEM accuracy on 1 km × 1 km areas on Greenland.

10.8 Thermal control

The thermal control subsystem regulates the temperature of the satellite components. The temperature control of the satellite is vital for the mission, as the lifetime of several important components will decrease rapidly if the temperature is not properly managed. The layout of the satellite and the components is described in section 10.12.

The configuration of the satellite has a number of important characteristics for the thermal control subsystem. First of all, the satellite has a dusk-dawn orbit, which means that the satellite has no eclipse periods. Secondly, due to the dusk-dawn orbit and the fact that the satellite by approximation doesn't spin, a fixed side of the satellite is always pointing to the sun. Additionally, the side of the satellite with the detector is always pointing to the Earth. Lastly, the time span of the operational status of the laser is in the order of months. As will be shown in a following section, the laser is the major contributor to the internal heat generation. The time span means that the satellite has plenty of time to reach an equilibrium temperature for each satellite component. An equilibrium temperature is reached for a component when the heat input equals the heat output of the component.

As a consequence of the aforementioned characteristics, the temperatures of the satellite components are always within a certain range of values. The lower bound for the temperature range is obtained when the least heat is generated within the satellite. In general, this occurs when the satellite is not taking measurements. The upper bound of the temperature range is reached when the satellite is generating the maximum amount of heat. In general, this is the case when the satellite is taking measurements.

For thermal control, heat pipes and louvers are used in addition to the commonly used other thermal control measures, such as applying white paint to the satellite surfaces.

Louvers, as shown in figure 10.17, are similar to blinds for windows to block incoming

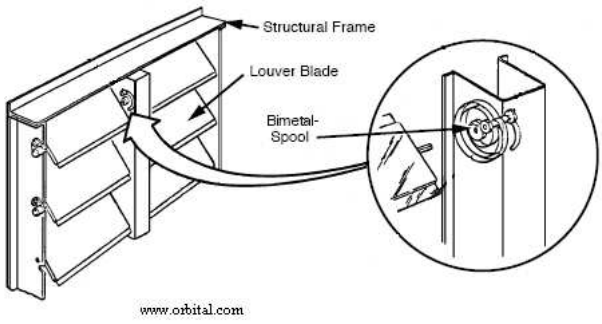

Figure 10.17: Layout of a louver.

sunlight, except that the louvers function to block radiation from leaving the satellite. Louvers react on the temperature of the satellite with strips of two materials with different thermal expansion coefficients, such that they deform with temperature change. The strips are positioned such that the louvers open when the satellites have a lower temperature and close when the satellite has a higher temperature. A drawback of louvers is that extensive exposure to sunlight may cause them to fail. This is not an issue however, since the louvers can be positioned on the side of the satellite directed away from the sun. An alternative to increase the temperature is using a heater. A combination of both will be used, this is both for redundancy reasons and because the temperature can be regulated better, as will be shown in the section about risk management for thermal control.

A heat pipe, as shown in figure 10.18, consists of a tube with high thermal conductivity.

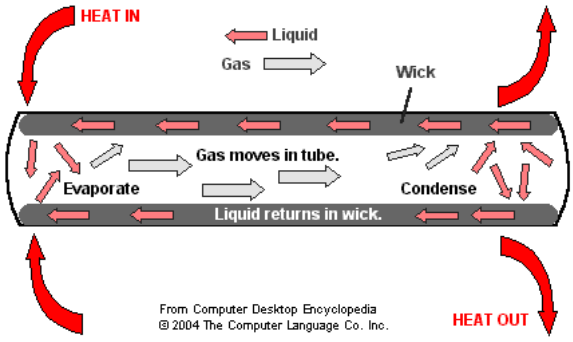

Figure 10.18: Layout of a heat pipe.

Inside is liquid and a material that soaks up liquid. When the temperature increases at a certain point in the tube, the liquid will evaporate. The gas will have an increased pressure and will move to a colder region where it condenses and is soaked up by the wicking material. This results in transport of the heat.

10.8.1 Requirements

The allowable temperature range for each component is listed in table 10.9. The listed temperatures are obtained from the specifications found in the sections for the verious

subsystems. The sensitive components are the electronic processing unit, detector housing and power control & distribution unit with a minimum temperature of −10 °C, in addition to the laser with an operational range between 10 °C and 35 °C. When the lasers are switched on, temperatures should be between 0 °C and 40 °C. This makes the laser system the most sensitive sytem.

Additionally, the avalanche photon detector and the antennas require a minimum temperature of −20 °C. The antennas are mounted on the body of the satellite and will therefore need extra attention.

Component	Minimum temperature [°C]	Maximum temperature [°C]
Lasers	0 (10)	35 (40)
Electronic processing unit	−10	50
Avalanche photon detector	−20	85
Housing	−10	55
Star sensor	−30	55
Gyros	−25	60
Momentum wheels	−30	70
S-band transceiver	−20	65
S-band antenna	−20	50
Mass memory unit	−40	80
Louvers	−85	120
Heater	−60	200
Battery	−55	85
Power control & distribution unit	−10	55

Table 10.9: Allowable temperature ranges.

10.8.2 Assumptions

Modeling the temperature of the satellite can become very complex. The more details available for the materials used and the lay-out of the satellite, the more accurate the model becomes. Adding more detials to the model can be very time consuming however. In addition, some information about factors that are important for thermal control may not be available accurately. For these reasons, some assumptions have been made to simplify the model.

- The detector is modeled to absorb 98% of the incoming radiation.
- The radiation emitted by the detector is negligible.
- Solar maximum conditions are considered for end of life, which is when the satellite wilil obtain its maximum temperature, even though solar minimum is expected.
- The satellite is modeled as a box of 3 m × 2 m × 2 m, with the square sides perpendicular to the velocity vector.
- It is assumed the side of the satellite with the main engine and the side with the solar array are covered for 95% with white paint. This is to account for non-uniformities.

Causes for non-uniformities include, but are not limited to the thrusters, the main engine, antennas, solar panel attachments plus deployment mechanisms. The fifth assumption also takes into account that the parts of the satellite that are not covered may absorb more radiation. It should be noted that the theoretical coverage is 87.5%. Any errors in the estimate can be calculated to only result in a negligible temperature change.

Errors introduced due to the second assumption can only lower the temperature. As will be shown later, the lowest expected temperature of POLESat is rather high. As a result, lowering the temperature slightly has no consequence for the satellite lifetime.

10.8.3 Energy balance

The temperature of the satellite is stable when the incoming energy and the outgoing energy are in balance. If this is not the case, the temperature will increase if the incoming energy is higher than the outgoing. The outgoing energy increases with increasing temperature, meaning that at some point a stable temperature is reached, where incoming and outgoing energy is in balance again.

The satellite has 5 sources affecting the temperature balance.

- Solar radiation Q_{in_solar} ,
- Earth reflected solar radiation, or albedo $Q_{in\_reflected}$,
- Earth infrared radiation Q_{in_IR},
- Internal heat generation Q_{in_heat},
- Heat dissipation by means of radiation $Q_{out\_radiation}$.

For an equilibrium temperature, the heat generation is equal to the heat dissipation:

$$Q_{in} = Q_{out} \tag{10.14}$$

where Q_{in} is the sum of the factors adding heat to the satellite:

$$Q_{in} = Q_{in\_solar} + Q_{in\_reflected} + Q_{in\_IR} + Q_{in\_heat} \tag{10.15}$$

and Q_{out} is the factor removing heat from the satellite;

$$Q_{out} = Q_{out\_radiation} \tag{10.16}$$

Absorbed solar radiation

The absorbed solar radiation is calculated with equation 10.17.

$$Q_{in\_solar} = G_s \cdot \Sigma \left(\alpha_i \cdot A_{sun\_i}\right) \cdot \cos\beta + G_s \cdot \Sigma \left(\alpha_i \cdot A_{side}\right) \cdot \sin|\beta| \tag{10.17}$$

where G_s is the solar constant, in W/m^2. Values vary from 1326 W/m^2 to 1418 W/m^2, depending on the solar activity. The mission lifetime of 10 years means that both the minimum and maximum value can be expected. A_{sun} is the area of the satellite illuminated

by the sun in m^2 and α is the absorption ratio of this area. The incidence angle β varies up to 23.5° in both directions. A_{side} is the area of either the side facing the flight direction, or the side facing away from flight direction, depending on whether the sun incidence angle is negative or positive. Taking either side for the equation will result in approximately the same values. The sum operator is present because the surfaces of the satellite can consist of different materials, each with individual absorption values.

Absorbed reflected solar radiation

The absorbed reflected solar radiation is found using equation 10.18.

$$Q_{in\_reflected} = G_s \cdot a \cdot \Sigma \left(\alpha_i \cdot A_{earth\_i}\right) \cdot \sin^2 \rho \tag{10.18}$$

Where a is the albedo of the earth, A_{earth_i} is the area of the satellite directed to the earth. As before a_i is the absorption ratio of this area. ρ is the angular radius of the earth, which is 1.1955 for an orbital altitude of 477 km [70]. The absorption value for part of the satellite surface covered by the detector has a value of approximately 0.98. As for the absorbed solar radiation, the sum operator is present because the surface of the satellite can consist of different materials, each with individual obsorption values.

Absorbed Earth infrared radiation

The absorbed Earth infrared radiation is obtained using equation 10.19.

$$Q_{in\_IR} = q_I \cdot \Sigma \left(\epsilon_i \cdot A_{earth}\right) \cdot \sin^2 \rho \tag{10.19}$$

Where q_I is the Earth's infrared radiation, values for q_I range from 216 W/m^2 to 258 W/m^2. ϵ_i is the emissivity ratio of the area A_{earth_i}. As a result of the first assumption, the emissivity of the detector is approximately 0.98 for the purpose of absorbing the infrared radiation. As for the absorbed solar radiation, the sum operator is present because the surface of the satellite can consist of different materials, each with individual obsorption values.

Heat generation

The internal heat generation Q_{in_heat} is derived from values for the power usage of various subsystems as found in table 10.10. The first column indicates the power consumption of the subsystems when the lasers are operating, the second column is for the case when the lasers are off. The main contributor is the laser, which uses 2.2 kW while it is operating. It is assumed that all electrical power by the subsystems is eventually converted into heat.

As comparison, ENVISAT has a power consumption of almost 5 kW, of which only a third, 1.7 kW, is used by the payload. For POLESat, 88% of the power consumption of 2.5 kW is used by the payload.

Heat dissipation

The only form of heat dissipation is radiation into space. The radiation can be calculated using equation 10.20.

$$Q_{out\_radiation} = \Sigma \left(A_{sat\_side} \cdot \epsilon\right) \cdot \sigma \cdot T^4 \tag{10.20}$$

Component	Power [W]	Power [W]
Lasers	2175	0
Star trackers	24	24
Gyros	25	25
Momentum wheels	88	88
S-band transceiver	36	0
X-band transmitter	30	0
Avionics unit	40	40
Mass memory unit	20	20
Processing unit	24	0
Thermal heater	0	2175
Total	2462	2372

Table 10.10: Power consumption of the various subsystems.

where A_{sat_side} is the surface area of a side of the satellite in m^2, σ is the Stefan-Boltzmann constant of $5.67051 \cdot 10^{-8}$ W/m^2/K^{-4} and T is the temperature of the satellite in K. Note that a satellite has multiple radiating sides that need to be considered, hence the sum operator.

Using equation 10.14, equation 10.20 can be rewritten to compute the temperature as a function of the other parameters:

$$T = \sqrt[4]{\frac{Q_{in}}{\Sigma \left(A_{sat\_side} \cdot \epsilon \right) \cdot \sigma}} \tag{10.21}$$

This concludes the required equations for the calculation of the average satellite temperature. Beside the average satellite temperature requirement, there is a requirement that no excessive heat concentrations should be present in sensitive components. Heat concentrations can only occur at places where heat is absorbed or generated. The batteries are not located in such places, but the lasers are, since they are a primary source of heat generation themselves.

10.8.4 Implementation

Since heating is easier to do than cooling, the thermal control configuration will first be constrained by the upper temperature limit. Keeping the laser within the operational temperature range is of primary concern. The generated heat should be transported to other parts of the satellite or it should be stored until the lasers are not operating. The latter is not considered an option, because the amount of heat and the amount of time the heat should be stored would require an excessively large and heavy heat storage device. Transporting the waste energy of the lasers to another part of the satellite is done using a heat pump, thermoelectric cooler or with transportation by means of conductance. The use of heat pumps will be avoided, as heat pumps have a relatively low reliability and lifetime due to the mechanical devices. Thermoelectric coolers do not have those problems, but their efficiency is relatively low [45]. Heat conductors, like heat pipes, do not use power and have high reliability [52]. Conductors can only transport heat to parts with a lower temperature. Lasers have a maximum operating temperature of 35 °C. Assuming that the colder regions have a maximum temperature of the average temperature of the satellite, the

average satellite temperature should be lower than 35 °C. Batteries have a lower maximum allowable temperature, but since they don't generate much heat themselves, it is easier to regulate their temperature. Taking into account the required temperature difference of 5 °C for the operation of the heat pipes [11] and a margin of 5 °C, the maximum allowable average temperature is 25 °C. The uncertainty margin is added because the lifetime of the laser can decrease very rapidly when subjected to an operating temperature of over 35 °C. The margin also ensures the proper heat transport of the heat pipes. Finally, the margin allows the louvers to react to temperature changes.

Maximum temperature

The maximum average temperature can be calculated using equation 10.21. The surface material types were iteratively selected until the temperature was just below the upper temperature bound. This approach resulted in aluminized Teflon for all surfaces except for the side facing the sun and the side facing away from the Earth. The side facing the sun is covered with solar cells. The side facing the Earth is covered with white paint. The aluminized Teflon is used because the maximum value for the absorption at end of life conditions is much lower than for white paint, resulting in a lower temperature, as the absorption is only affecting the absorbed solar radiation reflected by the earth. Additionally, the difference between beginning-of-life and end-of-life absorption values is much lower for aluminized Teflon, which means there is a decrease in the range of values for absorbed radiation, which in turn means that the satellite temperature has a smaller temperature range over the total lifetime.

Equation 10.17 has a maximum value for the absorbed solar radiation with values of 1418 W/m^2 for G_s, 0.52 and 6.0 m^2 for the maximum absorption ratio and area of the solar cells, respectively. The values for the aluminized Teflon present on either side are 0.316 and 3.8 m^2. The maximum absorbed radiation is obtained for a value of 22° for β. This results in a value of 4.7 kW.

Equation 10.18 has a maximum value for the absorbed earth- reflected solar radiation with values of 0.35 for the maximum albedo, 0.316 and 0.98 for the maximum absorption of aluminized Teflon and the detector, respectively, 1418 W/m^2 for G_s, 1.1955 for ρ and 4.23 m^2 for the area directed to the earth, minus the detector area. The detector area is 1.77 m^2. This results in a value of 1.0 kW.

The worst case hot value for the absorbed earth infrared radiation can be calculated with equation 10.19 with values of 258 W/m^2 for q_I, 0.7 and 0.98 for the emissivity of aluminized Teflon and the detector, respectively. Areas and the earth angular radius ρ are the same as for the calculations of the albedo. This results in a value for the maximum absorbed radiation of 1.1 kW. Note that this is not the maximum value of the absorbed radiation, as a minimum value for the emissivity is used. This is because for temperatures of above −15 °C, the emitted radiation increases more than the absorbed radiation with higher values for emissivity, causing a temperature drop.

The maximum internal heat generation is known to be 2.5 kW. This value is increased by 10% to account for variations in the power generation.

Adding the above values together results in a value of 9.8 kW for Q_{in}.

For equation 10.21, some additional parameters are required. The surface area of the satellite corresponding to a value of 0.825 for the emissivity is 6.0 m^2. Additionally, the top of the satellite has a surface area of 6 m^2 with an emissivity of 0.8. The sides also

have an affective area of 7.6 m^2 with an emissivity of 0.7. Finally, the side of the satellite directed away from the sun has an area of 6 m^2 covered with louvers. Note that this is in addition to the area directed to the earth mentioned for the calculation of the absorbed infrared radiation. For a temperature of 25 °C, the louvers will be partly closed with a value of 0.654 for the effective emissivity. A temperature rise in the satellite will cause the louvers to open up and decrease the temperature. The average satellite temperature is now calculated to be 25 °C with equation 10.21. Note that this value is obtained using an iterative approach, where values such as the emissivities and absorptions were optimized.

Minimum temperature

For the lower temperature bound, the same approach as for the maximum temperature can be used, but with different values. The values for the areas and ρ remain the same. G_s has a minimum value of 1326 W/m^2. The lowest absorption values for aluminized Teflon and white paint are 0.163 and 0.258, respectively. The highest emissivity for the same materials is 0.8 and 0.924. The albedo has a lower bound of 0.25 and the lowest value for the earth infrared emission is 216 W/m^2. The minimum heat generation equals 197 W. Inserting the known numbers results in a lowest average temperature of −16 °C. Since this value is lower than the allowable minimum, a heater and louvers will be used.

The heater will use the power that the lasers don't use when they are not operating. This means that the temperature is higher than the required minimum, but since roughly the same amount of power will be dissipated into heat as would be the case for operating lasers, the maximum temperature will never be higher than for the previously calculated maximum average temperature of 25 °C.

The heater will generate 2.2 kW heat. The higher power usage for the heater also means more area than required, this is to improve the reliability of the systems. For a power density of 3.9 W/cm^2 [1], this will require a heater area of about 0.056 m^2.

For the lowest temperature, the louvers will be nearly closed, changing the effective emissivity to 0.24. Recalculating the minimum temperature gives a value of 14 °C. The louvers are designed to be fully open at a temperature of 30 °C and to be fully closed at a temperature of 12 °C. Assuming a sinusoidal relation between the temperature and effective emissivity (with a maximum rate of change for fully open and a minimum for fully closed), the emissivity can be written as a function of current temperature as follows:

$$\epsilon_{eff} = \epsilon_{max} \cdot \sin\left(\frac{\pi}{2 \cdot (T_{max} - T_{min}) \cdot (T_{current} - T_{min})}\right) \tag{10.22}$$

where T_{max} is the fully open temperature (30 °C), T_{min} is the equivalent closing temperature for which ϵ_{eff} has a value of 0.115for the actual closing temperature, calculated to be 9.91 °C. $T_{current}$ is the current temperature and ϵ_{max} is the maximum effective emissivity (0.707).

Temperature range

The temperature of the satellite will range between 14 °C and 25 °C for nominal performance of the thermal control subsystem. This temperature range is very small when

compared to other satellites. This is the result of the more or less constant operating conditions due to the sun-synchronous orbit without eclipse. The satellite always has the same orientation and the internal heat generation is kept at a certain level.

Heat concentrations

If the temperature of the lasers would not be regulated, the temperature would rise to an unacceptable high level. To maintain the energy balance for an acceptable temperature, heat pipes are used to transport excessive heat to the colder parts of the satellite and parts that have tight lower temperature bounds. Each laser generates about 435 W, it is assumed that the heat pipes should have the capacity to at least transport this amount of energy. Four heat pipes transfer heat to the following locations:

- Detector housing at the side facing the sun,
- Detector housing at the side facing away from the sun,
- APD,
- Gyros.

These components have the highest minimum allowable temperature. With the extra heat transport, the minimum temperature of those components will certainly be above this lower limit. The last heat pipe will run along the inner side of the upper side of the satellite to improve the radiation of heat into space, as a higher temperature means more radiation. This amount of heat is transported for each pipe over a maximum distance of 1.75 m. The performance of heat pipes is measured in [Wm], which is the multiplication of the length of the pipe and the amount of heat transported. For 1.75 length and 435 W heat transport, a heat pipe with the performance of 760 Wm is required. The performance of heat pipes increases with the square of the increase in diameter. An 11 mm diameter heat pipe can transport 100 Wm. For 7.6 times as much heat transport, a heat pipe with $\sqrt{7.6} = 2.76$ times this diameter is needed This will require a pipe diameter of 30 mm.

The solar panel temperature can be calculated to have a maximum temperature of 25 °C in a similar way as for the rest of the satellite. The equations can be simplified to:

$$T_{soar\_panels} = \sqrt[4]{\frac{G_s \cdot \alpha}{(\epsilon_1 + \epsilon_2)} \cdot \sigma} \tag{10.23}$$

Where $\epsilon_1$and ϵ_2 are the emissivities of the front and the back of the solar panel. The back of the solar panel is covered with white paint with an end of life emissivity of 0.8. As mentioned earlier, the emissivity and absorption of solar cells is 0.825 and 0.52 respectively. This temperature is acceptable for solar panels and will therefore not need more temperature regulation.

In a similar way, an estimate can be made for the temperature of the sides of the satellite. This results in temperatures of 15 °C and 25 °C for the earth facing side and the sun facing side, respectively. The temperature of the earth facing side is calculated with the assumption that the interior face of this side is insulated for radiation. Without insulation, the temperature would be 31 °C. The temperature of the side of the satellite facing the sun

is not insulated, if it was, the temperature would increase to 80 °C, which is unacceptable. It should be noted that the antennas will be mounted on the side of the satellite facing the earth. As a result, the antennas will have a temperature above their allowable minimum.

Before the solar panels are deployed, the internal heat generation is zero. This results in a temporary minimum temperature of −8 °C. Since the batteries are located at the earth-facing side, the temperature will be higher than average and therefore within a suitable temperature range.

10.8.5 Risk factors

The reliability of the satellite components is often greatly affected by their operating temperature. If the thermal control system fails to provide a proper thermal environment, the satellite lifetime will decrease.

The following results were calculated using the equations 10.14 to 10.21. If the solar panels provide less power, or the heater has decreased performance, the satellite will have a lower temperature. The minimum temperature of the satellite with louvers closing normally is 3 °C. This is higher than the startup temperature for the lasers, so this is acceptable.

If the solar cells mounted on the body have degraded performance, the effective absorption will increase, causing a rise in temperature. As long as the degradation is lower than 37%, opening the louvers for an effective emissivity of 0.707 will cause the temperature to drop to 30 °C. It is very unlikely that the solar cells will degrade to this extend however, so this value is acceptable.

If the thermal subsystem is operating as expected, the louvers will never be entirely open, as the maximum obtained temperature of 25 °C is lower than the fully open temperature of 30 °C. If the louvers are stuck in the partly open position for regular operations, the temperature will drop, but as long as the heaters are operating at 32% of their initial capacity, the temperature will remain above 0 °C. This number will increase to 37% in case the louvers are completely open.

If the louvers are stuck in the closed position, the maximum temperature will increase to 43 °C. If this were to happen, a maximum of three lasers will have to be turned off, depending on the solar activity and the degradation of the satellite surface materials. It should be noted that louvers have an expected lifetime of 15 years and an expected minimum number of operation cycles of 30,000 and as such are not a high risk factor [55].

10.9 Telemetry, tracking & command

In this section, the telemetry, tracking & command (TT&C) or communications subsystem of POLESat will be discussed. The TT&C subsystem forms the interface between the satellite and the ground segment. In other words, it provides POLESat with a means to exchange information with the ground.

For a further discussion of this subsystem, it is first necessary to distinguish between two types of data: science data and housekeeping data.

The science data consists of all laser altimetry measurements, together with the information that is necessary for post processing these measurements, like data from POLESat's star tracker and GNSS receiver. Although the science data makes up the bulk of the data to

be exchanged with the ground segment, mission controllers cannot do without health and status information of the satellite. This information is contained in the housekeeping data.

Next to this, mission controllers need to be able to uplink commands to the satellite. This uplink includes the schedules for changing the pulse repetition rate of the lasers.

Now, the design considerations for the various data types will be discussed in detail.

10.9.1 Science data

Science data of Earth observation satellites like POLESat is generally downlinked in the so-called X-band (7145 MHz-8500 MHz), because it provides the highest possible data rates [28].

To downlink data in the X-band, a number of ground stations is available (see table 10.24). Because the orbit of POLESat is close to polar, it will pass more often over ground stations at higher latitudes. Since Kiruna, Sweden is the northernmost ground station available to both ESA and NASA, this ground station will be used to size the TT&C subsystem. In addition, it will be assumed that POLESat has to be at least 10° above the horizon to be able to communicate (according to [21] this is somewhat pessimistic).

(a) X-band transmitter XTRA-6

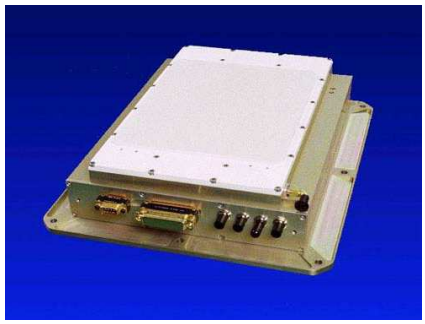

(b) X-band phased array antenna

Figure 10.19: X-band hardware.

With these assumptions, it is possible to calculate the minimum data rate required to downlink all science data to the ground. For this purpose, an orbit simulation program has been written, with which the minimum contact time can be calculated (see appendix A).

The simulation has shown that in the worst case, POLESat is only able to communicate for 3937 s during 15 orbital revolutions (= 84735 s). With an average storage rate of 3.7 Mbps (see appendix E), $3.7 \cdot 10^{-3} \cdot 84735 = 313.5$ Gb of laser altimetry data is generated during these 15 revolutions. All this data has to be downlinked in the 3937 s of contact time, thus requiring a minimum data rate of 79.6 Mbps.

It must be noted though that the 79.6 Mbps is no hard figure. It could be for example, that due to maintenance at the ground station, POLESat cannot communicate during one of its passes. Next to this, a different ground station or even multiple ground stations might be used to downlink the science data, therefore requiring a different minimum data rate.

In any case, the minimum data rate does not cause a problem for POLESat, since space-qualified X-band transmitters for high data rates up to 622 Mbps are readily available

[18, 40]. Of these X-band transmitters, the XTRA-6 from Tesat-Spacecom (see figure 10.19) was found to be most suitable for POLESat. This is because it combines a high data rate of 500 Mbps with a relatively low weight and low power requirement (1.1 kg and 30 W, respectively). Data encryption with this unit is possible as well (but optional), and it has built-in redundancy. Besides a transmitter, an antenna needs to be selected. One of the phased array antennas developed by Boeing Phantom Works seems to be a good choice for POLESat, as it is already proven in space to work with data rates of over 500 Mbps [49] (see figure 10.19).

10.9.2 Housekeeping data

Contrary to science data, housekeeping data of satellites is mainly downlinked in the so-called S-band (2025 MHz-2300 MHz) [28]. Although this band cannot support as high data rates as the X-band, many more ground stations are capable of receiving signals in the S-band. When something is wrong with the satellite, using the S-band for downlink allows fast access to the engineering parameters contained in the housekeeping data.

For an Earth observation satellite like POLESat, typically several hundred engineering parameters need to be monitored [30]. These are sampled at intervals somewhere between 30 seconds and 2 minutes. Suppose for POLESat it is necessary to sample 500 parameters with 8-bit values every 30 seconds. Then it follows from equation E.2 that in 84735 s (worst case scenario for the contact time), 11.3 Mb of housekeeping data is generated. To downlink this amount of data in 3937 s requires a minimum data rate of 2.87 kbps. This is far below current downlink capabilities in the S-band of several Mbps.

As far as the equipment is concerned, many manufacturers build S-band transmitters, like TRW Space & Electronics Group, L-3 Communications, WJ Communications, Tesat-Spacecom, General Dynamics and Surrey Satellite Technology (recently acquired by EADS Astrium). Several products from these manufacturers have been compared, and one that stands out is a multi-mode S-band transceiver, i.e. a combined transmitter and receiver, from General Dynamics [33](see figure 10.20). This unit can both be used for downlinking housekeeping data (6 Mbps) and for uplinking commands (512 kbps), which takes away the need to carry another communications unit for receiving data from the ground. In the end, this saves both space and power.

The S-band transceiver needs two antennas: one for uplink and one for downlink. An example of an antenna that can be used is the space-qualified S-band helix antenna of Surrey Satellite Technology (see figure 10.20), of which 8 have already flown in space [66].

10.9.3 Command uplink

Next to downlinking the science and housekeeping data, the satellite should also be able to receive commands from the ground. These commands include for example the schedules for changing the pulse repetition rate of the lasers and instructions to turn the main thruster on or off for orbit maintenance.

In general, the data rate needed for uplinking commands is very low, and it is expected that the data rate provided by the S-band transceiver discussed in the previous section (512 kbps) is more than enough for uplinking all commands.

(a) S-band transciever (b) S-band helix antenna

Figure 10.20: S-band hardware.

10.9.4 Overview

Now it's known what equipment will be used, an overview of the TT&C subsystem can be given, see table 10.11. Note that the table includes the parameters important for other parts of the satellite, like the power subsystem, thermal subsystem and structures & mechanisms.

	Quantity [–]	Mass [kg]	Max. power usage [W]	Size [mm^3]	Thermal operating range [°C]
S-band transceiver	1	2.2	36	203×160×86	−20 to +65
S-band antenna	2	0.5	–	100×100×500	−20 to +50
X-band transmitter	1	1.1	30	197×89×74	Unknown
X-band antenna	1	5.5	–	330×305×74	Unknown

Table 10.11: Overview of the TT&C equipment.

Although the thermal operating range for the X-band transmitter and antenna is unspecified, it makes common sense to assume it will be in the same range as the S-band equipment. Moreover, table 10.11 does not include weights for wiring/cabling and the supporting structure, as these will be specified in the structures & mechanisms part.

10.10 Command & data handling

In the previous section, the communications subsystem of POLESat was discussed. There, it was defined how POLESat exchanges data with ground stations on Earth. Yet, also inside the satellite a lot of data is exchanged between the various subsystems. The heart of this exchange is the command & data handling subsystem, which will be discussed now.

For a useful discussion, it is first necessary to know which data flows exist within POLESat. Therefore, a data flow diagram has been made, see figure 10.21. Note that this diagram

does not include the housekeeping data, which exists for every subsystem and will be dealt with later in this paragraph.

Now, let's look at the data flows from and to each subsystem in more detail.

10.10.1 Data flows

Payload

The payload, which was discussed in detail in sections 10.1 and 10.2, consists of five working lasers, five redundant lasers, a telescope and two photon counters. The working lasers have to be commanded in some way, to change their pulse repetition rate according to their operating schedule. Both the emitted pulse of the lasers and the corresponding reflection from Earth will be detected by the photon counters, which output an analog signal. This signal has to be sampled by an A/D converter, with a specific sample rate and quantization level.

As discussed in section 10.2, the required sample rate for the 1064 nm photon counter is 2 GHz with a quantization level of 16 bits. For the 532 nm photon detector, this is 500 MHz and 8 bits, respectively. After sampling, the now digital signal is sent to the processing unit, where the so-called waveform analysis is carried out. Appendix C describes this process in more detail.

Finally, the processed data from the photon counters is stored on board of the satellite, waiting to be transmitted to the ground segment.

Propulsion

Next to sending housekeeping data, the propulsion subsystem receives commands from the command & data handling subsystem. These commands are used to fire one or more thrusters for attitude control or orbit maintenance. For the latter purpose the main thruster will be used, which needs a command from the ground. The thrusters for attitude control will be commanded by the satellite itself, when it thinks an attitude correction is necessary. Of course override commands from the ground can also be used for making attitude corrections.

Attitude determination & control

The command & data handling subsystem receives input from the star tracker of the attitude determination & control subsystem. The signal from this star tracker is sampled at 4 Hz (as specified by the manufacturer), after which it is sent to the processing unit. The processing unit then computes the attitude of the satellite, by comparing the input from the star tracker with a stored database of stars. When an attitude correction is deemed necessary, an analog signal (i.e. a voltage) is sent to either the momentum wheels or thrusters, or both.

Guidance & navigation

POLESat receives its position and timing information from the GNSS receiver, which is part of the guidance & navigation subsystem. This data is used to synchronize the satellite's on-board clock, and to decide whether the pulse repetition rate of the lasers should be altered or not.

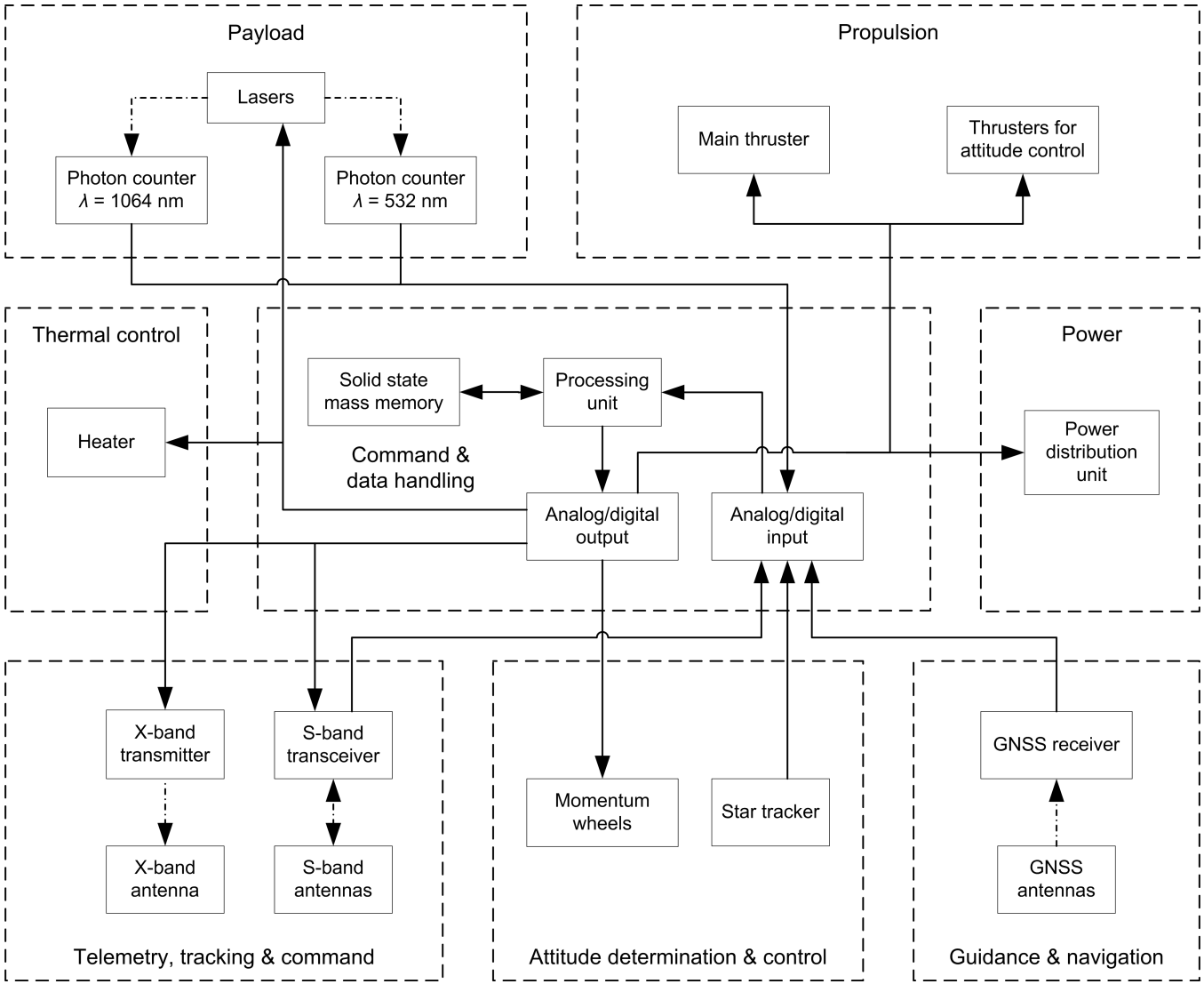

Figure 10.21: Data flows within POLESat (excluding housekeeping data).

Telemetry, tracking & command

The command & data handling subsystem has an important interface with the communications subsystem. One of its functions is for example to retrieve data from the storage system, encrypt it (when necessary), modulate it and send it as an analog signal to one of the transmitters. Next to this, the C&DH subsystem receives commands from the S-band transceiver, which have to be validated, decoded and distributed to the other subsystems.

Power

The power distribution unit of the power subsystem has an interface with the C&DH subsystem as well. As the name implies, this unit is used to monitor and distribute the power generated by the satellite over the various subsystems. It needs commands from command & data handling, for example to cut the power to one of instruments.

Thermal control

The only part of the thermal control subsystem that needs input from command & data handling is the heater. All other parts of thermal control work autonomously, but the heater has to be switched on and off, depending on the operating status of the lasers.

10.10.2 Housekeeping data

Next to the data flows discussed in the previous section, there is also a flow of housekeeping data in the satellite. This housekeeping data includes several parameters from the satellite's subsystems, like voltages, temperatures, pressures and status information. The command & data handling subsystem gathers, processes and formats this data, after which it is temporarily stored and eventually transmitted to the ground with the S-band transceiver.

Apart from being examined on the ground by mission controllers, the housekeeping data is used for various purposes in the satellite as well. For example, the voltage coming from the momentum wheels indicates their spinning rate, giving the processing unit the information needed to decide whether the momentum wheels need to be desaturated or not. Next to this, housekeeping data can also be used to generate commands when operations deviate from normal. Think for example about switching one of the lasers off for a while in case it becomes too hot.

10.10.3 Processing hardware

Up till now, only the functions of the C&DH subsystem have been discussed. In this subparagraph, the processing hardware itself will be looked at.

For the command & data handing subsystem, an integrated avionics unit manufactured by Broad Reach Engineering was selected [15], because it provides the most complete solution for our spacecraft. Basically, the unit consists of a box in which several modules or boards can be plugged (see figure 10.22).

In POLESat, the avionics unit will include a processor board, two digital & analog input/output boards and a data storage interface board. One of the input/output boards will be specifically used for the payload, because of the high sampling rates needed. It is likely this board needs to be custom built, but Broad Reach Engineering indicates they can do this.

Additionally, one of the boards needs a chip for timekeeping that is able to generate a timing signal in the order of picoseconds, allowing precision timing for the photon counters. Also a timer for the mission elapsed time has to be included, which is synchronized with time information from the GNSS receiver every 10 seconds or so.

The dimensions and maximum power consumption of the avionics unit (as specified by Broad Reach Engineering) are included in table 10.17.

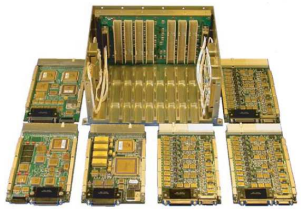

Figure 10.22: Avionics box with six boards.

10.10.4 Data storage

As discussed previously, the processing hardware includes an interface with the data storage system. The data storage of the satellite will be provided by so-called solid state mass memory, that will be mounted in a box similar to the avionics unit.

To size the data storage system, it is necessary to estimate the amount of data storage needed. When assuming only Kiruna, Sweden is used as a ground station, it can be calculated with the method described in appendix A, that the largest time without contact is 39793 seconds. In these 39793 seconds, 147 Gb of laser altimetry data is generated, assuming an average data rate of 3.7 Mbps (see appendix E).

Next to the laser altimetry data, also housekeeping telemetry and information from the star tracker and GNSS receiver needs to be stored. However, the corresponding data rates are very low (in the order of bits per second) compared with the laser altimetry data, which means they can be neglected from a data storage point of view.

Finally, a database with stars needs to be stored to be able to calculate the orientation of the satellite. The size of this database is 800 Mb, as described in section 10.5.

In total, a minimum data storage of about 148 Gb is needed. One of the companies that is able to provide this amount of data storage is EADS Astrium. A product suitable for POLESat is their "low cost smart mass memory" [8]. The problem with these memory blocks – and in general with solid state mass memory – is the reliability. For example, for a single memory block of 512 Mb, there is only 98% chance it still works after 5 years. Since failures of these memory blocks are unpredictable, the simple solution is to take more data storage than needed to make sure that even at the end of life enough data storage can be provided. Therefore, one box with 512 Gb (i.e. 1000 memory blocks) of data storage will be carried on POLESat.

10.10.5 Overview

Now the components of the C&DH subsystem have been sized, an overview of their most important parameters can be given, see table 10.12.

	Quantity [–]	Mass [kg]	Max. power usage]W]	Size [mm^3]	Thermal operating range [°C]
Avionics unit	1	5	40	$251 \times 118 \times 207$	Unknown
Mass memory unit	1	6	10	Unspecified	−40 to +80

Table 10.12: Overview of the CD&H equipment.

The exact size of a mass memory unit is not specified by EADS Astrium, but from pictures it is derived that one unit is about half the size of the avionics unit. On the other hand, the avionics unit does not have a thermal operating range specified. The avionics unit is not considered to be a critical part from the thermal control point of view though, in the sense that other components around it have more strict thermal requirements.

10.11 Power

The power subsystem is the most critical system on any spacecraft because nearly every other subsystem requires power. The electrical power system (EPS) provides, stores, distribute and controls the spacecraft electrical power. The average power needed at the end of life (EOL) determines the size of power subsystem.

There are four different sources for generating power in a spacecraft which can have advantage on other power sources depending on the mission. Photovoltaic solar cells convert solar energy into electric power. This is most common power source which is used in Earth orbiting spacecrafts. A Static power source uses nuclear reactor to generate power. Solar dynamic systems also use solar power but it use solar power to heat a working fluid to drive a heat engine which is used to generate electricity. Fuel cell power systems work similar to a conventional chemical battery, fuel cells convert the chemical energy of an oxidation reaction to electricity [70].

Most of the earth orbiting spacecrafts usually use solar cells as power source as it is the most reliable for such missions. Solar panel design depends on the required average power, operating temperature, radiation environment, mission life etc. this subsection is structured as follows first the solar panel selection is made, on the base of the chosen solar cells solar panel sizing is done. This will be followed by the batteries sizing and selection. After that the power distribution unit and the power control and regulation will be discussed.

10.11.1 Solar panels selection

There are many sorts of solar cells available which are space qualified. The highest theoretical efficiency of 42.5% has been achieved by University of Delaware [26] but yet they are not space qualified. BTJ Triple-Junction High Efficiency Solar cells are the most efficient space qualified solar cells [25] and are selected for the mission POLESat. Performances of many types of solar cells have been investigated, in the following table a comparison has made between three types of solar cells and the difference can be clearly seen between their performances.

Cell type	NeXt Triple Junction FaInP2/GaAs/Ge	Ultra Triple junction	BTJ Triple-Junction
Cell efficiency	27.0%	25.5%	28.5%
Mass [kg/m^2]	2.06	2.0	0.84

Table 10.13: Solar cells performance comparison [25, 64].

10.11.2 Solar panel sizing

Solar panel sizing depends on two factors which are the Mission life time and average power requirement during the mission. The solar panel area is sized according to the maximum power required at the end of life which results in over sizing of the power requirement at the beginning of life. This extra power is dissipated using shunt regulators as explained in section. To calculate the required solar-array area to run all the subsystems, first how much power, P_{sa}, the solar panels must generate, calculated according to following formula 10.24.

$$P_{sa} = \frac{\left(\frac{P_e T_e}{X_e} + \frac{P_d T_d}{X_d}\right)}{T_d} \tag{10.24}$$

Where P_e and P_d are the spacecraft power requirement during eclipse and daylight respectively. The terms T_e and T_d represent the length of eclipse and length of daylight per orbit respectively. The terms X_e and X_d are the efficiency of the paths from the solar arrays through the batteries to the individual loads and the path directly from the arrays to the load. From reference [70] the efficiencies are about $X_e = 0.65$ and $X_d = 0.85$ for direct energy transfer.

For POLESat orbit selection is such that it has no eclipse which will results in $P_e = 0$, $T_e = 0$ and equation 10.24 simplifies to:

$$P_{sa} = \frac{P_d}{X_d} \tag{10.25}$$

As the solar cell has been selected the power output per meter square, P_0, by the solar cells calculated according to following equation 10.24

$$P_0 = \eta \times G_s \tag{10.26}$$

G_s is the solar constant which has an average value of 1366 W/m^2 and η is the solar cell efficiency which is known for the selected solar cells. Now the next step is to calculate P_{BOL}, the power generated per square meter at the beginning of life

$$P_{BOL} = P_0 I_d \cos\theta \tag{10.27}$$

Where I_d is the inherent degradation which includes inefficiencies due to solar cells assembly, temperature variation etc. θ is the sun incidence angle between the normal to the surface of the array and the Sun line [70]. It means that if the sun's rays are perpendicular than the power generated will be maximum.

$$P_{EOL} = P_{BOL} L_d \tag{10.28}$$

P_{EOL}, power per meter square at the end of life and L_d life degradation factor which is different for different solar cells, the degradation for whole mission life can be calculated according to following equation from reference [70].

$$L_d = (1 - \text{dg/year})^{S_l} \tag{10.29}$$

where dg is the degradation per year and S_l is the satellite lifetime. The solar-array area A_{sa} required to generate the required power at EOL is computed using following equation

[70].

$$A_{sa} = \frac{P_{sa}}{P_{EOL}} \tag{10.30}$$

As the total area is known so it is also possible to calculate the total mass M of the solar cells.

$$M = A_{sa} \times \mu \tag{10.31}$$

μ is the mass of 1 m^2 solar cells and for selected solar cell it is known. All the known values are computed into equations 10.24-10.31 and their result can be found in table 10.14 .

Description and Parameters	Given values	Calculated values	Unit
Solar constant (worst case), G_s	1326		W/m^2
Solar cell efficiency, η	28.5		–
Solar cell mass, μ	0.84		kg/m^2
Satellite lifetime, S_l	10		years
Sun incidence angle (worst case), θ	23		degree
Inherent degradation, I_d	0.77		
Degradation per year, dg/year	0.005		
Required Power EOL, P_d	2500		Watts
Required solar panel area EOL		11.55	m^2
Total solar cell mass EOL		9.7	kg

Table 10.14: Solar power subsystem known and calculated values.

10.11.3 Batteries

Most of the spacecrafts which have a certain eclipse period requires batteries to store energy. POLESat orbits constellation is such that it has no eclipse period, which means power can be generated all the time by solar panels. Therefore no energy storage is needed. In the beginning phase of mission to deploy solar panels, start up computers, *G&N* subsytem etc., some power is required for a short period of time. Dischargeable batteries can be used to meet the required power need. Such battery cells convert chemical energy into electrical energy. There are many kind of such batteries but the most common space qualified batteries use silver zinc, lithium thionyl chloride, lithium sulfur dioxide, lithium monofolouride and thermal cells [70]. In table 10.15 the characteristic of some batteries are given which are suitable for our mission, the battery manufacturer can meet the power requirement within the specific ranges of specific energy density [70]. POLESat needs about 210 W in the beginning of the mission. For that purpose a Lithium Thionyle Choloride battery is chosen which weight about 1 kg, which can be used once and completely discharged. Lithium Thionyle Choloride battery which will be used in the POLESat will be manufactured by the EaglePicher Technologies, LLC USA which is one of the most reliable space qualified battery producer [23].

Primary battery	Specific energy density	Typical application
Lithium Thionyl Chloride	$175 - 440$	Medium rate, moderate life $<$ 4 hours
Lithium Sulfur Dioxide	$130 - 350$	Low rate, long life (days)
Lithium Monofluoride	$130 - 350$	Low rate, long life (days)

Table 10.15: Battery performance comparison [70].

Power control & distribution unit

The power distribution unit has to provide power and has to run the whole power system in the most efficient way. It consists of cabling, fault protection and switching gears to turn power on and off to the payloads. Power distribution is designed to meet the power requirements by the individual spacecraft loads. Different systems onboard require different (low to high) voltage of power converted from 28 Vdc power bus by the distribution unit [70].

Power distribution systems are centralized which means that the power is regulated to all spacecraft loads within the main bus. The power converters detach the noise from the load on the bus and they also prevent load failure damaging the power distribution unit. The Centralized system is the most simple one and has not to tailor-design the electrical power system (EPS) for different application [70]. Fault protection system within the EPS isolates a failed load which could cause the failure of spacecraft. Failed loads can cause a short circuit which can draw huge power and if this continues, the failed load may stress the cables and drain the energy sources. Using fuses these faults can be isolated from the EPS bus.

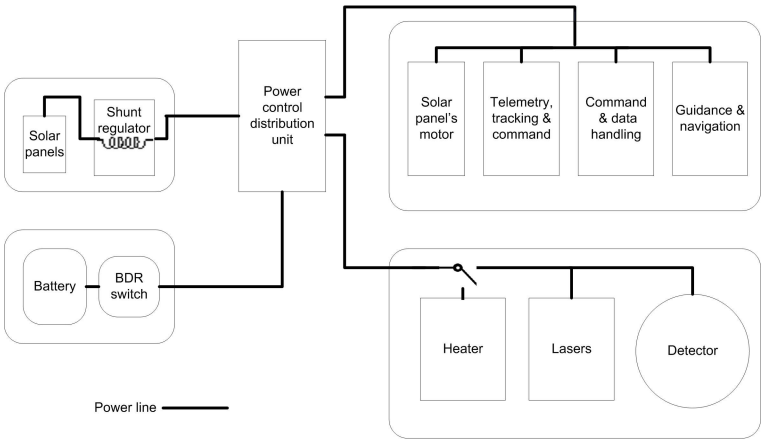

Figure 10.23: EPS block diagram.

There are two main power control techniques: the peak power technique (PPT) and direct energy transfer (DET). The DET is used for our mission; it dissipates the extra power not used by the system. The DET can dissipate extra power through external array of shunt resistor to prevent internal power dissipation. Shunt regulator unit operates in parallel to the solar array as can be seen in figure 10.23 and is designed to maintain the bus voltage to 28 V by dissipating the excess solar panels power in external resistive shunt. It is light weight, has fewer parts, and lower mass and has higher total efficiency at the end of life [70].

10.12 Structures & mechanisms

The functions of the structural subsystem are to enclose, protect and support the other spacecraft subsystems and to provide a mechanical interface with the launch vehicle. The enclose and protect functions are especially necessary during spacecraft assembly, handling and transportation from the manufacturing facility to the launch facility. Structural

members provide the mating and attachment points for subsystem components such as batteries, propellant tanks, electronics modules and so on. The structure must also sustain the stresses and loads experienced during environmental testing, launch and deployment of solar arrays and antennas. Spacecraft structures are mainly divided in two categories:

The primary structure or main structure, whose purpose is to transmit loads to the base of the satellite through specifically design components. This structure provides the attachment points for the payload and the associated equipments. Failure of the primary structure leads to a complete collapse of the satellite.

The secondary structures, such as detector support, thermal blanket support and solar panel must only support themselves and are attached to the primary structure which guarantees the overall structural integrity. A secondary structure failure is not a problem for the structural integrity, but it could have an important impacts on the mission.

For the design of the POLESat mission the determination of the spacecraft configuration and the initial design of the spacecraft structure is done by following the flow of elements in figure 10.24.

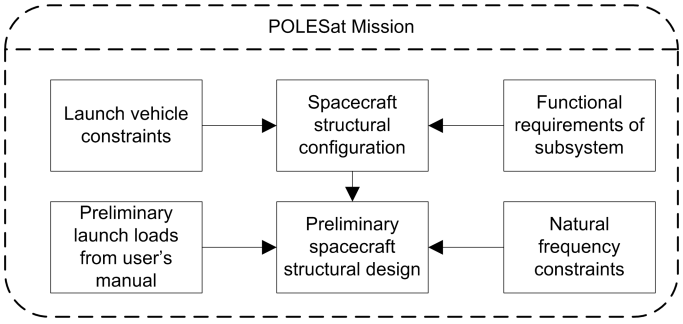

Figure 10.24: Design flow of spacecraft structure design (adopted from [4]).

10.12.1 Launch vehicle constraints

The satellite should fit in the flight envelope of the launcher, therefore it is important to consider the size of the flight envelope of the launcher. In table 10.23 the flight envelope for the suitable launchers are given. From this table the maximum size of the satellite can be derived as 2.5 m diameter and 3.7 m height. These launch vehicle constraints are considered during the structural design and choosing the layout

10.12.2 Functional requirements of subsystem

All the subsystems should be considered when designing the structure, because these subsystems determine the size of the structure and the layout of the satellite.

First of all, the engine should be placed at the back of the spacecraft bus structure on the center of gravity line. This will constrain the position of the detector, which is at the front of the satellite.

The lasers on-board should be directed downwards, but the laser bundle can be deflected by mirrors, so the position of the laser is not a constraint. An option is to place them above the detector in the external payload division. The solar panel is placed in front of

the spacecraft bus, which points in the flight direction of the satellite. This is because of the constant angle of the satellite with respect to the sun in a sun-synchronous orbit and because the engine is placed at the back of the spacecraft bus. This configuration leads to a smaller frontal area, which leads to a lower atmospheric drag. The fuel tanks should be placed near the engine; therefore the place of the fuel tank is important in the structure. During the mission the center of gravity shift should be minimized (changing inertia moments). To achieve this goal, the propellant tanks should also be placed in a symmetrical way such that the center of gravity stays more or less constant.

10.12.3 Spacecraft structural configuration

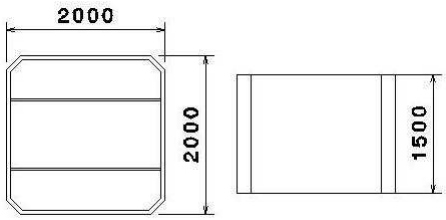

Figure 10.25: Schematic drawing of the spacecraft bus structure.

The square cross-section is chosen from experiences from other missions and it was the most suitable option for attaching the detector support on it. It is derived from the Ball aerospace BCP 2000 which is used for ICESat [2]. Some minor changes are made to fulfill our requirements. From the launch vehicle constraints and the functional requirements of subsystems the box dimensions are derived as 2 m $\times$ 2 m $\times$ 1.5 m, this is of course a first estimation.

The structure has three main sections. The middle one is for the fuel tanks and the other two are for the different subsystems in the satellite. The walls of the box are suitable for attaching different subsystems on it.

The schematic drawing of the space bus structure with respective dimensions is given in figure 10.25.

10.12.4 Preliminary launch loads and natural frequency constraints

The structure of the spacecraft should be designed to support the maximum quasi-static loads (QSL), including a factor of safety. The quasi-static loads are a combination of the steady-state static loads and the low frequency sinusoidal loads. Quasi-static loads can be used to dimension the spacecraft, provided the minimum frequency requirements with respect to mode shapes in the axial direction and the lateral direction are fulfilled.

The quasi-static loads of a Ariane IV launcher are given in table 10.16 to show the different forces which act on the satellite during its launch. These values are from the flight manual of the Ariane IV and are used as an example.

The natural frequencies of the spacecraft must be such that the fundamental natural (undamped) frequencies in all directions are larger than the first frequencies generated by the launch vehicle that excite the spacecraft, so dynamic decoupling is achieved.

Flight event	Axial axis	Lateral axis
Maximum dynamic pressure	$-3\,g$ (compression)	$\pm 1.5\,g$
Second engine cut off	$-7\,g$ (compression)	$\pm 1.0\,g$
Thrust lift off	$+2.5\,g$(tension)	$\pm 1.0\,g$

Table 10.16: Flight limit quasi-static loads (Ariane IV) at the payload center of gravity.

In table 10.17 the required lowest frequencies in the lateral and the axial direction are given for two different launch vehicles. In general, these frequencies are valid when the spacecraft is considered to be clamped at the interface between the spacecraft and the launch vehicle.

Axis	Launcher	Spacecraft	Internal equipment
Ariane IV			
Axial	> 31	$31 - 60$	< 80
Lateral	> 10	$10 - 40$	< 60
Delta			
Axial	> 35	$35 - 65$	< 80
Lateral	> 15	$15 - 45$	< 60

Table 10.17: Design-goal structural natural frequency bands [Hz] ([30]).

The launcher defines some important parameters which will be used for the actual sizing of the structure. These parameters are shown in table 10.18 and are estimated with use of table 10.32, table 10.16 and with experience with other launches. For safety higher values for load factor is taken.

Parameter	Symbol	Value
Axial load factor	n_{ax}	8
Lateral load factor	n_{lat}	3
First axial frequency	$f_{nat_{ax}}$	35 Hz
First lateral frequency	$f_{nat_{lat}}$	15 Hz

Table 10.18: Structural design parameters for the POLESat.

10.12.5 Preliminary spacecraft structural design

First a material selection is done and after that an initial sizing of the structure is done with some assumption using the initial sizing method from [70]. The secondary structures are discussed and an initial estimation of the mass is given.

Material Selection

The choice of materials on a mission can directly lead to its success or failure. If a material is chosen that cannot withstand the environment of space or forces experienced during launch and deployment, critical instruments and components could be damaged beyond repair. The material selected must meet standards of yield, ultimate and fatigue strength, specific stiffness, hardness and toughness, ductility, thermal expansion, creep resistance, melting point and also for ease of fabrication, versatility of attachment options and availability. Materials are classified into four groups: metals, polymers, composites and ceramics. Metals are very homogeneous and have constant properties throughout their

composition. Aluminium is the most commonly used metal for the spacecraft structure. It has good strength/weight capability, easy workability, moderate cost, high ductility and high corrosion resistance. In addition, it is non-magnetic and is available in numerous forms. The only disadvantages are the low yield strength at temperatures above 200 °C and the high coefficient of thermal expansion [9].

For the preliminary structural design of the POLESat use will be made of aluminium 7075. The most important properties concerning the elected material are presented in table 10.19 which is taken from [70].

Property	Symbol	Value
Density	ρ	$2.8 \cdot 10^3$ kg/m^3
Ultimate tensile strength	F_{t_u}	$524 \cdot 10^6$ N/m^2
Yield tensile strength	F_{t_y}	$448 \cdot 10^6$ N/m^2
Young's modulus	E	$71 \cdot 10^9$ N/m^2
Elongation	e	8%
Coefficient of thermal expansion	α	22.1

Table 10.19: Properties of Aluminium 7075.

F_{tu} is defined as the highest uni-axial tensile stress a material can sustain before rupturing. F_{ty} is defined as the compressive stress that causes a permanent deformation of $0,.2$ % of the specimen's length. e is defined as the percentage change in length caused by plastic deformation prior to rupture. α is defined as a measure of strain per degree temperature change.

Sizing of the primary structure

The primary structure carries the major loads for the spacecraft. The launch is the most obvious source of structural requirements; it dictates the spacecraft's weight, geometry, rigidity, and strength. Therefore the sizing of the primary structure will be based on the launch.

For the preliminary structural design, the structure bus will be assumed as a monocoque cylinder to make an initial sizing of the space bus structure. To make this assumption reasonable the cross-section area and the wall thickness of the space bus structure is taken equal to that of the monocoque cylinders. This method is often a good starting assumption for initial sizing. Monocoque structures are panels and shells without attached stiffening members.

The cross-sectional area of the box is estimated as $A \cdot b = 6 \cdot a \cdot t$ (with $a = 2.0$ m, the height of the box) which is equal to the cross-sectional area of the cylinder $A_c = 2 \cdot \pi \cdot R \cdot t$. When these cross-sectional areas and the wall thicknesses are equal to each others, then the radius of the cylinder becomes, $R = 3a/\pi = 3 \cdot 2.0/\pi = 1.9099$ m. The top-bottom length, L, of the box is off course equal to the length of the cylinder, $L = 1.5$ m.

Other important parameters are the estimated mass of the satellite, m_b, which is approximated at 2000 kg. The factors of safety are used to account for uncertainties that cannot be fully analysed. The qualification loads are often used as design loads, and subsequently the factors for yield strength and ultimate strength are applied. The ultimate factor of safety (U_{FS}) is equal to 1.25 and the yield factor of safety (Y_{fs}) is equal to 1.1.

Furthermore the following assumptions are made for the initial sizing [70].

- Mass equally distributed,

- Monocoque cylinder with the same cross-sectional area and wall thickness,
- Uniform thickness,
- No ring or longitudinal stiffeners.

The first step of the primary structure analysis is the determination of the minimum shell thickness capable to meet the natural frequency requirements. This procedure is also called sizing for rigidity. For the axial rigidity sizing process, it can be assumed that the primary structure is approximated by a uniform beam. The required cross-sectional area, A can be computed from equation 10.32

$$A = \frac{f_{nat_{axial}}^2 m_b L}{(0.250)^2 E} = \frac{35^2 \cdot 2000 \cdot 1.5}{0.250^2 \cdot 71 \cdot 10^9} = 8.2817 \cdot 10^{-4} \text{ m}^2 \tag{10.32}$$

The required thickness, t_{ax}, can then be computed from Equation 10.33.

$$\text{t}_{\text{ax}} = \frac{\text{A}}{2\pi\text{R}} = \frac{8.2817 \cdot 10^{-4}}{2 \cdot \pi \cdot 1.9099} = 6.9014 \cdot 10^{-5} \text{ m} \approx 0.0690 \text{ mm} \tag{10.33}$$

For the lateral rigidity sizing process, it can be also assumed that the primary structure is approximated by a uniform beam. The required area momentum of inertia of the beam's cross-section, I, can be computed from Equation 10.34.

$$I = \frac{f_{nat_{lat}}^2 m_b L^3}{(0.560)^2 E} = \frac{15^2 \cdot 2000 \cdot 1.5^3}{0.56 \cdot 71 \cdot 10^9} = 3.1167 \cdot 10^{-6} \text{ m}^4 \tag{10.34}$$

The required thickness, t_{lat}, can then be computed from Equation 10.35.

$$t_{lat} = \frac{I}{\pi \cdot R^3} = \frac{6.8211 \cdot 10^{-5}}{\pi \cdot 1.9099^3} = 3.1167 \cdot 10^{-6} \text{ m} \tag{10.35}$$

The limit or maximum expected loads can be derived by multiplying the spacecraft's weight by the load factors. The limit loads in axial direction, P_{axial}, lateral direction, $P_{lateral}$, and bending moment, M, are presented in table 10.20, in which a bending moment arm equal to 0.75 m has been used. This length is nothing else than half the size of the satellite bus.

Type of load	Weight [N]	Distance [m]	Load factor* [ ]	Limit load
Axial	19620		8	156960 [N]
Lateral	19620		3	58860 [N]
Bending moment	19620	0.75	3	44145 [N/m]

Table 10.20: Applied Loads.

* The load factors are taken from table 10.18 and for bending moment the load factor for lateral load factor is taken.

Using the computed limit loads presented in table 10.20, the equivalent axial load, P_{eq}, can be calculated from equation 10.36 and the ultimate axial load, $P_{eq_{ulitmate}}$, from equation 10.37.

$$P_{eq} = P_{axial} + \frac{2M}{R} = 156960 + \frac{2 \cdot 44145}{1.9099} = 2.0319 \cdot 10^5 \text{ N} \tag{10.36}$$

$$P_{eq_{ultimate}} = P_{eq} \cdot UFS = 2.0319 \cdot 10^5 \cdot 1.25 = 2.5399 \cdot 10^5 \text{ N} \tag{10.37}$$

The second step in the design is to size the primary structure for tensile strength. For this analysis use will be made of the ultimate load, $P_{eq_{ultimate}}$, and the material's allowable stress, F_{t_u}. Then, the required thickness, t_{t_u}, can be obtained by means of equation 10.38.

$$t_{t_u} = \frac{P_{eq_{ultimate}}}{F_{t_u} \cdot 2 \cdot \pi \cdot R} = \frac{2.5399 \cdot 10^5}{524 \cdot 10^6 \cdot 2 \cdot \pi \cdot 1.9099} = 4.0392 \cdot 10^5 \text{ m} \tag{10.38}$$

The sizing of the structure to meet the yield conditions obeys the same logics as the sizing for tensile strength. The only differences between both processes are: Firstly, in equation 10.37; the Yield Factor of Safety (Y_{fs}) should be used instead of the Ultimate Factor of Safety (U_{fs}) in order to compute the ultimate axial load. Secondly, in Equation 10.38; the allowable yield tensile stress, F_{t_y}, should be used instead of the material's allowable stress, F_{t_u}. The shell thickness, t_{t_y}, necessary to meet the yield conditions follows then from equation 10.38 after applying the changes explained above. The required thickness, t_{ty}, is equal to $4.1575 \cdot 10^{-5}$ m.

The third step in the structural design is to size the cylinder for stability, by using the largest thickness calculated in the previous calculations, namely the necessary thickness to meet axial rigidity conditions (0.0690 mm). The primary structure should withstand the ultimate axial load defined by equation 10.36. The reduction factor, γ, necessary for the calculation of the buckling stress, can be obtained from equation 10.40.

$$\phi = \frac{1}{16}\sqrt{\frac{R}{t}} = \frac{1}{16}\sqrt{\frac{1.9099}{6.9014 \cdot 10^5}} = 10.397 \tag{10.39}$$

$$\gamma = 1.0 - 0.901\,(1.0 - \exp(-\phi)) = 1.0 - 0.901\,(1.0 - \exp(-10.397)) = 9.9027 \cdot 10^{-2} \tag{10.40}$$

The buckling stress, σ_{cr}, corresponding to the primary structure can then be obtained from equation 10.41.

$$\sigma_{cr} = 0.6 \cdot \gamma \cdot E \cdot \frac{t}{R} = 0.6 \cdot 9.9027 \cdot 10^{-2} \cdot 71 \cdot 10^9 \cdot \frac{6.9014 \cdot 10^{-5}}{1.9099} = 1.5244 \cdot 10^5 \text{ N/m}^2 \tag{10.41}$$

The calculated buckling stress is not larger than the material's proportional limit. Consequently, it is not necessary to use additional methods for inelastic buckling. The corresponding critical buckling load, P_{cr}, can be obtained from equation 10.42; in which the cross-sectional area A is obtained by using the maximum thickness computed (0.0690 mm), $A = 2\pi \cdot R \cdot t = 1.9099 \cdot 6.9014 \cdot 10^{-5} = 8.21817 \cdot 10^{-4}$ m^2.

$$P_{cr} = A \cdot \sigma_{cr} = 8.2817 \cdot 10^{-4} \cdot 1.5244 \cdot 10^5 = 1.2625 \cdot 10^2 \text{ N} \tag{10.42}$$

From equation 10.42 follows that the structure used is not adequate for stability, because the applied ultimate load, $P_{eq_{ultimate}}$, is greater than the critical buckling load, P_{cr}. Structural integrity is often shown in terms of the Margin of Safety (MS), defined by Equation 10.43.

$$\text{MS } == \frac{P_{cr}}{P_{eq_{ulltimate}}} - 1.0 = \frac{1.2625 \cdot 10^2}{2.5399 \cdot 10^5} - 1.0 = -0.9995 \tag{10.43}$$

For stability conditions, the computed margin of safety should be equal or larger than zero. An increase of 1.957 mm in thickness should improve the stability characteristics of the primary structure. The first and final iteration is presented in table 10.21.

Iteration [ ]	Thickness [mm]	γ [ ]	σ_{cr} [N/m^2]	Area [cm^2]	P_{cr} [N]	MS
Initial	0.069	$9.9027 \cdot 10^{-2}$	$1.5244 \cdot 10^5$	8.282	$1.2625 \cdot 10^2$	-0.99935
First	2.026	0.2312	$1.0450 \cdot 10^7$	243.1	$2.5405 \cdot 10^5$	0.0003

Table 10.21: Initial and first estimation of the primary structure.

The new Margin of Safety is equal to zero, and therefore the primary structure satisfies the stability requirement. To obtain stability, a plate or shell thickness, t, equal to 2.026 mm has been used. This thickness will be used for the computation of the total mass of the primary structure as defined by Equation 10.44.

$$m = \rho \cdot 2 \cdot \pi \cdot R \cdot t \cdot L = 2.8 \cdot 10^3 \cdot \pi \cdot 1.9099 \cdot 2.0260 \cdot 10^{-3} 1.5 = 102.1 \text{ kg} \tag{10.44}$$

The mass, m, of the primary structure is then computed to be approximately equal to 102.1 kg. Any fasteners, attachments and access doors would increase this mass somewhat, making allowances for material lost in drilled holes and cut outs.

10.12.6 Secondary structures

Solar array deployment mechanism

Power generation is another important part of a spacecrafts design. Power is generated by the solar arrays that collect solar rays and convert them into energy. Solar arrays have a large area in order to produce the amount of power required by the system. A part of the arrays are directly attached to the spacecraft and other part is stored as a series of folded panels hinged together. The majority of the mechanisms that attach and release the solar arrays have been designed for rapid, reliable, one-time deployment of the folded panels. The body mounted solar panels are attached using a support structure. The mass of the solar array deployment mechanism is estimated as 10 kg and the total mass of the solar panel structure including both deployable and body mounted solar panels is estimated as 25 kg.

Detector support mechanism

The detector is attached to the primary structure with use of support mechanisms. The detector is located in front of the spacecraft bus. The detector support mass is estimated

as 20% of the detector mass, which is 86 kg [70]. This mass is included in the total mass of the detector which is given in 10.2.

Other support

Other support structures are estimated as 26.9 kg, which includes the attachments of the detector and the solar panels on the primary structure, but also al the mechanisms such as support structures for other subsystems, like the supporting for the fuel tanks, momentum wheels, antennas. All of these subsystems should be mounted in the primary structures and therefore other support structures have to be considered.

10.12.7 Total Mass calculation

The total mass of the structures and mechanisms subsystem can be found by summing up the primary and the secondary structures. These masses are given in table 10.22.

Primary structure	102.1 kg
Secondary structure	
Solar panel deployment	10 kg
Solar panel structure	25 kg
Detector support	86 kg
Other support	26.9 kg
Total structure mass	250 kg

Table 10.22: Masses of the structure and mechanisms subsystem.

10.12.8 Layout

All the components are set into a preliminary layout of POLESat. The 3D perspective pictures of the POLESat are given in figure 10.26 to create a visualization of the POLESat. Also the 2D drawing is given in figure 10.27 which gives a schematic overview of POLESat with the respective dimensions.

10.13 Launch segment

At this stage of the design, all constraints are known, like spacecraft dry mass, dimension, mission orbit, mission lifetime, therefore launch-system configurations can be designed. To deliver the spacecraft to its final orbit. The launch system is selected in the conceptual stage to minimize the program risk, at this stage the negotiation can be made with contractor for the launch system to decrease costs and schedule downstream [70].

Launch vehicle selection depends on at least four criteria: the launch vehicle performance capability, vehicle availability, compatibility and costs. Vehicle performance means whether the selected vehicle is capable to bring the satellite to the desired orbit. Launch vehicle availability consideration is whether the preferred launch system will be available on the required launch date, it also includes the availability of launch site as well as the use of any unique facilities for the group processing. For example, on the requested launch date, the

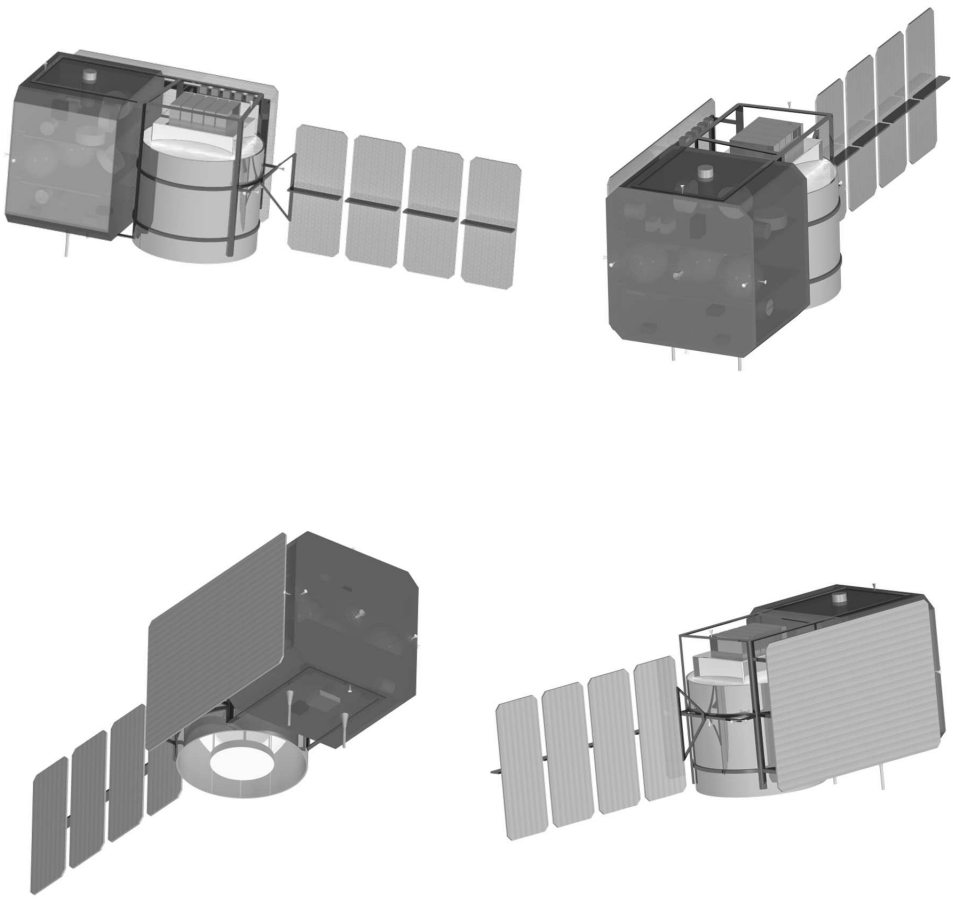

Figure 10.26: 3D dimensional perspective view of the POLESat.

launch pad may be available but the activities nearby the launch site may keep us from launching for safety reasons. Thus all such factors such as ground-support equipments and network for tracking and communications have to be examined for launch vehicle availability [70]. For many spacecraft contractors cost is one of the most important factors to choose the launch vehicle. To reduce the cost it is also possible to share the launch vehicle with other satellite companies. For that purpose such launcher are selected which are capable of transporting bigger masses into a sun-synchronous orbit and share the fairing space inside of the launch vehicles.

To keep the mission price competitive the tradeoffs have been made between selection criteria such as vehicle performance capability, vehicle availability, compatibility and cost of many launcher systems. For the POLESat mission the Dnepr rocket is selected to inject the spacecraft into its final orbit.

The Dnepr rocket is a converted ICBM designed by the Yuzhnoe Design Bureau in Dnipropetrovsk, Ukraine [50]. It has a high reliability of 97% and is very cost effective compared to many other launchers. In table 10.23 some performance criteria of launchers which are possible suitable for our mission are given. It is launched from the Baikonur site which is managed by the Russian Federal Space Agency; this site is suitable for high inclination orbit injection. This launcher will be available until 2020, as it is converted from an ICBM, it posts no problem regarding availability in the required year of launch which is 2010.

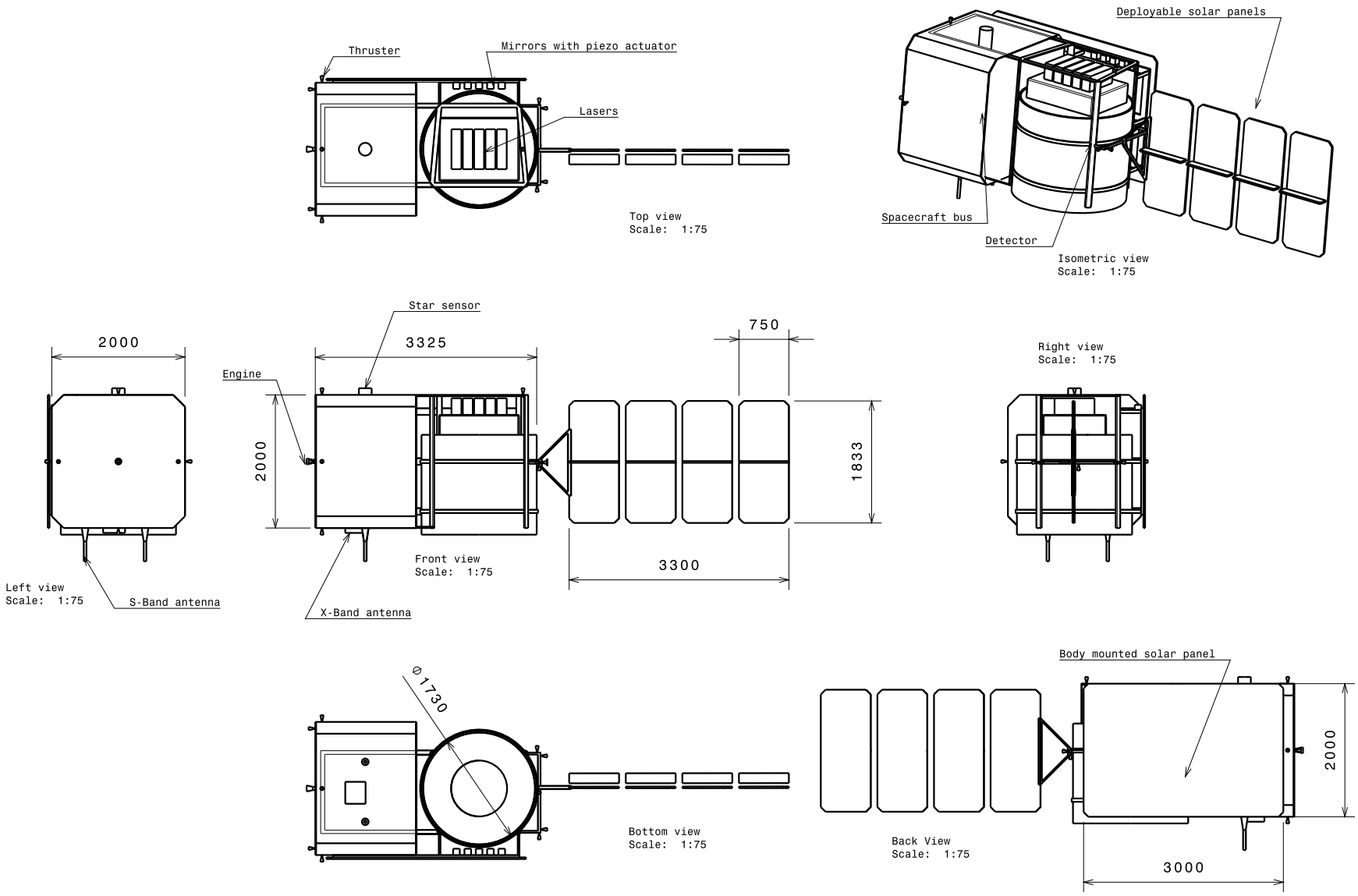

Figure 10.27: 2D Layout.

Launcher	Payload capacity to LEO [kg]	Envelope size Diameter [m]	Height [m]	Succes rate [%]	Cost per launch [USD 1,000,000]
Delta II	2700 – 6100	2.44	3.5	98.5	36
Soyuz	7000	3.7	7.7	97.7	32 – 50
Dniepr Rocket	4500	2.7	4	90	10 – 13
Cosmos	1500	2.44	2.7	97.4	10 – 12
Polar Satellite Launch Vehicle	3200	3.2	7	84.5	30

Table 10.23: Launcher data.

10.14 Ground segment

In this paragraph, the ground segment of the POLESat mission will be discussed. The ground segment is the part of the mission that supports POLESat from the ground and distributes data to all users.

More specific, the functions of the ground segment are (derived from [30]):

- Tracking the satellite,
- Acquiring and recording data from the satellite,
- Commanding the satellite,
- Pre-processing satellite data,
- Distributing data to mission control and processing centers.

The latter two of these functions is discussed in section 10.7, which is about data processing & distribution.

Tracking the satellite is the first function listed for the ground segment. This function comprises the ability to determine the orbit of the satellite; not for navigation purposes, but to verify the measurements of the on-board GNSS receiver, which remains the primary source of orbit information.

Determining the orbit of a satellite at a ground station can be done in various ways, for example by pointing a directional antenna at the satellite and registering the azimuth & elevation angles or by doing laser ranging. The latter is considered to be the most accurate method (with errors in the same order as the GNSS receiver), and will therefore be used for POLESat.

The second function listed at the beginning of this section is acquiring and recording data from the satellite. As discussed in section 10.9, the satellite downlinks data in the X-band and has a two-way communications system for the S-band. From a cost point of view, it is undesirable to set up a whole new ground segment for POLESat, which means an existing ground segment has to be used. This in turn means, that the ability to downlink data in the X-band will be the most restricting requirement, as there are far more S-band ground stations available.

To downlink data in the X-band, three existing ground networks can be used: ESTRACK, NASA's ground network and KSAT. ESTRACK is the ground tracking network of the

European Space Agency, with X-band ground stations in Kiruna, Kourou and Perth [27] [27]. NASA has only one ground station capable of receiving X-band signals in Poker Flat, Alaska. When this ground station does not suffice, NASA either cooperates with ESA at Kiruna or contracts satellite tracking out to the third network [5]: KSAT. KSAT is the network of a commercial company called Kongsberg Satellite Services, which has ground stations in Tromsø, Grimstad and Svalbard in Norway, and a ground station facility called TrollSat in Antarctica [39].

An overview of the available X-band ground stations, sorted by latitude, is given in table 10.24. Each of these ground stations is also capable of receiving and transmitting data in the S-band, and capable of doing laser ranging.

Ground station	Operator	Latitude	Longitude
Svalbard, Norway	KSAT	N78°14′	E15°24′
Tromsø, Norway	KSAT	N69°40′	E18°56′
Kiruna, Sweden	ESA/NASA	N67°51′	E20°58′
Poker Flat, Alaska, USA	NASA	N75°06′	W147°30′
Grimstad, Norway	KSAT	N58°21′	E8°36′
Kourou, French Guyana	ESA	N5°15′	W52°48′
Perth, Australia	ESA	S31°48′	E115°53′
Troll, Antarctica	KSAT	S72°01′	E2°31′

Table 10.24: X-band ground stations.

Because the orbit of POLESat is close to polar, the satellite will be visible more frequent from ground stations at higher latitudes. Suppose ESA or NASA does not want to outsource communications to a commercial company, then this makes Kiruna in Sweden the most obvious choice. This ground station is therefore used to size the communications subsystem of the satellite (see also paragraph 10.9).

When a KSAT ground station at a higher latitude than Kiruna is used, lower data rates are required for communications. However, it was already discussed in section 10.17 that the data rate is not a restricting requirement, so from this point of view it has no obvious advantage to choose a different ground station.

Another alternative for the ground segment is to use multiple ground stations. This makes the operations & logistics of the mission more complicated though, so if one ground station is sufficient, it is advised that only this ground station is used for normal mission operations. In case something is wrong with the satellite and status information of a command uplink over the S-band is directly necessary, the use of another ground station is still an option of course.

11 Interface charts

An N^2 or interface chart is a block diagram showing relations between various functions. The interface chart for POLESat is shown in figure 11.1. The data flow is what POLESat is all about; the measurement data should in some way reach the users.

In the interface chart, two related functional groups are visible. These functional groups correspond to the satellite (top-left) and the ground segment (lower-right). They are connected with the critical functions of the C&DH and TT&C subsystems, and the ground station. The C&DH forms a direct control loop with all the other functions on board of the satellite, except for the detector. From the C&DH there is a simple flow down to the primary users. During this process, the science data of POLESat will be refined from raw science data to level-2 data.

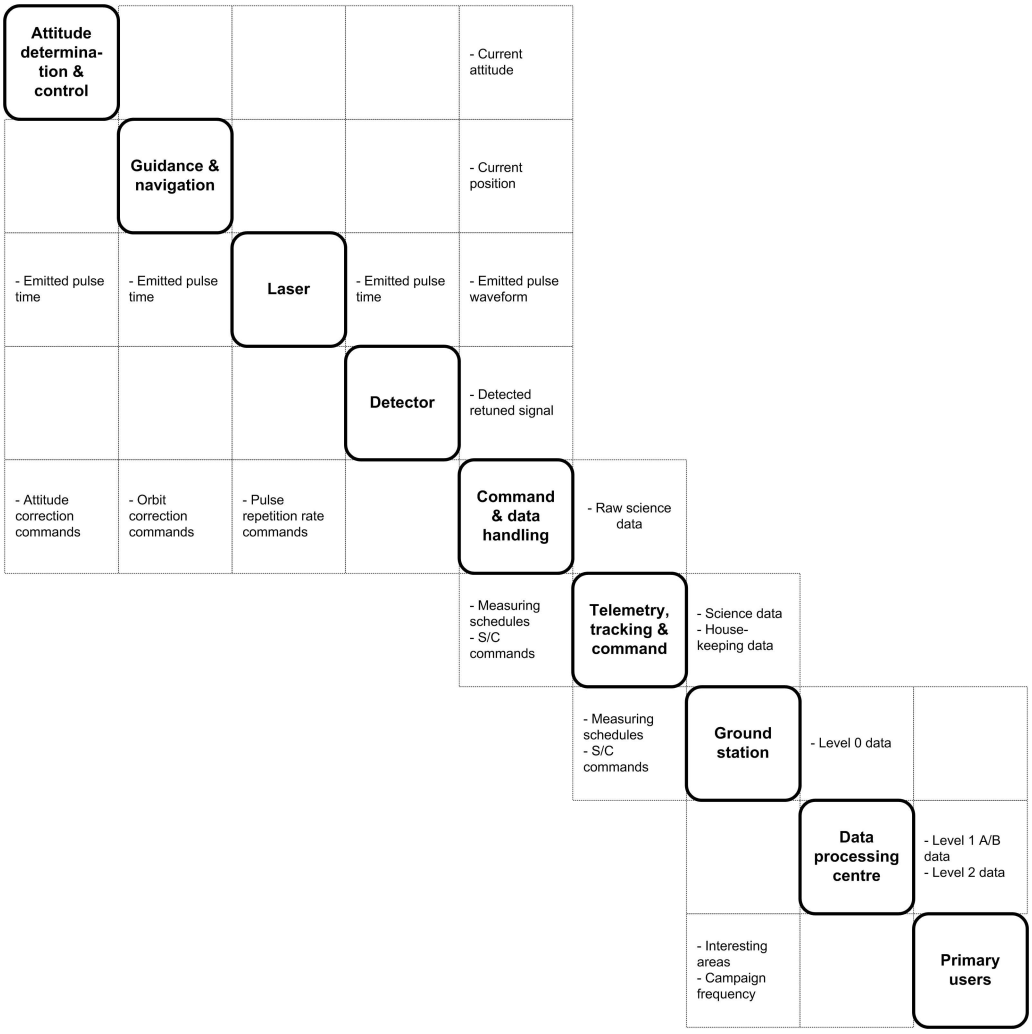

Figure 11.1: Interface chart

12 Operations & logistics concept

To reduce both cost and risk of the POLESat mission, it is necessary to think about the operations and logistics concept at the current stage of the design process. Hence, a general operations and logistics concept description will be given in this chapter. This concept will be worked out further during a later stage of the project.

It is clear the satellite has to take laser altimetry measurements over the Earth's poles. When not considering other applications of laser altimetry, it is preferred that the lasers are only turned on over the poles to lengthen their life time. There are two ways of achieving this. The first is to send a command from the ground every time the laser has to be turned on or off. Although this can be done automatically, the satellite always has to be in view of a ground station when nearing the polar ice sheets. Since this is hardly feasible, a second option is to let the satellite work autonomously by uploading a schedule containing the times for switching the lasers on and off. This will be done by Mission Operations Control (MOC) when necessary.

Next to this, MOC is responsible for uplinking commands to the satellite (e.g. for attitude control) and analyzing the housekeeping data of the satellite. The housekeeping data will be downlinked from the satellite to one or more ground stations and sent to MOC, together with the raw science data. The raw science data will be processed by a processing center, which will also generate a DEM. This DEM is then finally distributed to scientists either by DVD or secure connection over the Internet.

To perform all operations & logistics tasks, 24/7 staffing is definitely not necessary. Although it is difficult to know in advance how much personnel will be needed exactly, the equivalent of two full-time-employment seems enough at this point.

13 Cost analysis

To be able to compete with other feasible earth observation missions, POLESat should be competitively priced. Therefore, this was also one of the requirements set for the design of POLESat. This means that for POLESat, the costs should be analyzed. This is done in this chapter. To have a clearer overview of the total costs of the POLESat design, first a cost breakdown structure is given. After this, the costs for POLESat are estimated.

13.1 Cost breakdown

The cost breakdown structure (figure 13.1) gives an overview of the cost elements for the life cycle phases of POLESat. These phases are the research, development, test and evaluation (RDT&E) phase, the production phase and the operational phase. The RDT&E phase gives an overview of non-recurring costs, while the production phase indicates the recurring costs. These costs are only recurring by definition however, as it is likely that only one operational POLESat unit will be produced. The final phase includes the costs to keep the satellite and supporting systems operational.

The RDT&E phase is further subdivided into the categories research & development, testing, test equipment developed, program management and systems engineering. The production phase is divided into the categories manufacturing and logistics. Finally, the operational phase is divided into operations, maintenance and system- & equipment modification.

13.2 Cost estimate

The cost of the satellite mission is an important factor that may be decisive for whether the design will be used or rejected. The estimated cost for various factors of POLESat can be found in table 13.1 and 13.2. The total cost is eastimated at $1,077$ million U.S. dollars (in 2012) or €697 million (see table 13.3). The main cost driver is the design and development of the payload, which consists of both the laser system and the detector. In addition to the payload, other cost drivers are the spacecraft bus, program level and integration, assembly & test. The cost drivers will be explained below.

Most of the values for the cost were found using the cost estimation method as described in [70]. The payload is a special case however and is estimated separately, the details of which can be found in sections 10.1 and 10.2 for the lasers and detector, respectively.

The entries that can be found in tables 13.1 are divided into two categories. The first category is the cost estimate for research, development, testing and evaluation (RDT&E). The second is the cost for producing the first unit, indicated as theoretical first unit (TFU). The costs for RDT&E are generally the non-recurring costs and TFU includes the recurring costs of the design and production of the satellite. Finally, the remaining cost factors are grouped into several smaller categories.

For the first and second category, a number of cost drivers are defined. The first category (RDT&E) includes the highest values for the cost. Per subsystem, the second category (TFU) is usually between 10% and 40% of the first category. The payload includes the detector and the laser subsystems and communication subsystems. The spacecraft bus is the part of the spacecraft that does not include the payload. The primary cost driver is the mass of the bus [70]. Structures & mechanisms includes the spacecraft components that carry and protect the satellite during launch and deployment. Like the spacecraft bus, the structure has as primary cost driver the weight of the system. Thermal control indicates the devices and materials that are used for regulating the temperature of the satellite. The thermal subsystem cost can vary depending on the type of thermal control used for the satellite: passive thermal control generally costs less than active. For POLESat, mostly passive systems are used. The electrical power subsystem includes everything necessary for the proper power distribution over the various subsystems. The components used are commonly used in other spacecraft and have no special attributes that require large modifications. TT&C/C&DH combines the costs of the telemetry, tracking & command and the command & data handling subsystems. Along with thermal control, this subsystem has the lowest cost of the listed subsystems. The cost of the AD&C subsystem increases with attitude precision. The attitude determination for POLESat should be known quite precise.

Integration, assembly and test (IA&T) costs involve the labor and material costs for integrating the satellite subsystems into a complete satellite. This part also includes costs involved with testing the spacecraft, design & scheduling analysis required for subsystem integration, systems test & evaluation and test data analysis. IA&T is one of the major cost drivers.

The program level is comprised of the costs that accompany the system engineering and project management activities. This part of the cost can also be described as everything that is not an activity involving hard- or software. Program level is one of the main cost drivers, because the activities often require a lot of time.

Ground support equipment includes all facilities, tools and equipment needed for the development, assembly and tests of the satellite.

Finally, launch and operations support are the costs involved with the activities for the launch of the satellite.

The remaining categories are the costs for the launch vehicle, ground segment and software. The launcher is about 50% of the cost for these remaining categories.

The costs listed in tables 13.1 and 13.2 are in American dollars for the year 2000. An inflation factor is introduced to convert the costs to the year the money is spent. The total costs are shown in table 13.3, both including and excluding inflation corrections. The value of the inflation factor over the period 2000 to 2012 is 1.279.

Space segment cost [Y2000 million US dollars]		
Component	Cost (RDT&E)	Cost (TFU)
Payload	256	5
Spacecraft bus	128	55
Structures & mechanisms	13	3
Thermal control	5	1
Power subsystem	21	4
TT&C / C&DH	3	2
AD&C	17	7
Integration, assembly & test	97	13
Program level	110	26
Ground support equipment	40	N/A
Launch support	N/A	6
Total	691	123

Table 13.1: Cost components for RDT&E and TFU.

Other costs [Y2000 million US dollar]	
Software	
Flight software	0.9
Ground segment & operations	
Ground software	2.2
Facilities	0.4
Equipment	1.8
Logistics	0.3
Systems level	
Management	0.4
Systems engineering	0.7
Product assurance	0.3
Integration & test	0.5
Operations & support	
Maintenance	4.4
Contractor labor	3.2
Launch vehicle cost	
Launcher	12.7
Total	27.8

Table 13.2: Cost components for the remaining categories.

Total costs [Y2012 million US dollars]	
Total cost excluding inflation ($):	841.8
Total cost excluding inflation (€):	545.0
Total cost including inflation ($):	1076.7
Total cost including inflation (€):	697.0

Table 13.3: Total costs (inflation factor 1.279).

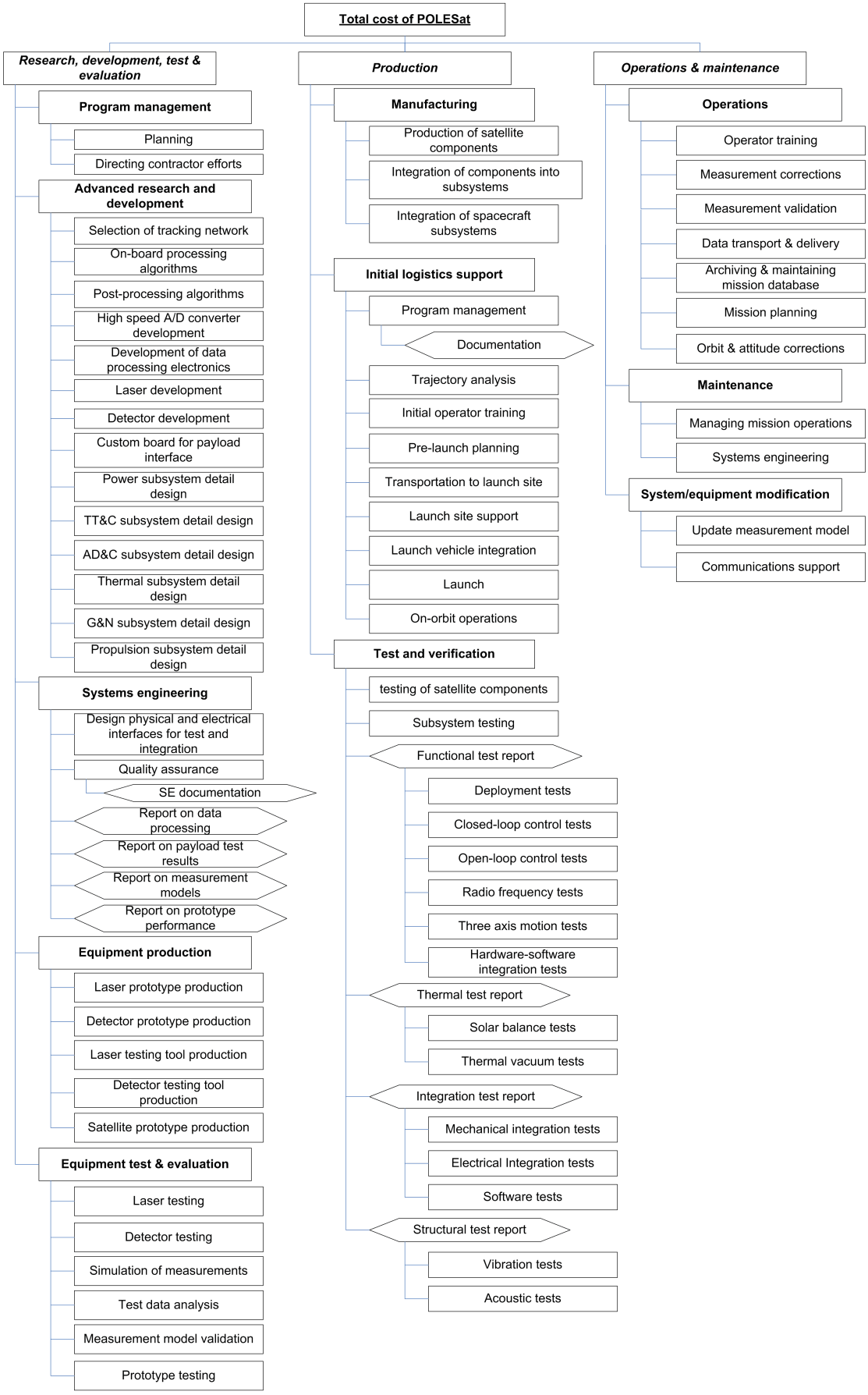

Figure 13.1: Cost breakdown structure.

14 Requirements compliance

With the final design of POLESat known, it is now possible to make an overview of the requirements and review whether POLESat can meet them. To do this, a compliance matrix (table 14.1) is made to sum up the top level requirements which were given in the project guide.

Requirement	Compliance
Minimal lifetime 5 years, expected lifetime 10 years.	v
Mission start in 2010	–
Full waveform, multi-beam laser altimeter	v
The obtained elevation data should enable the construction of a 100m resolution Digital Elevation Model covering:	
the whole of Greenland	–
at least 80 % of Antarctica.	v
Vertical precision under clear sky and over flat terrain: 5 cm; Horizontal precision: 5 m.	v
The sustainability of the mission objective should be reflected in the design.	v
The mission should be able to face competition with a number of highly attractive alternative Earth observation missions. In able to besuccessful, a competitive price is required.	v

Table 14.1: Compliance matrix.

Operational lifetime POLESat is built to last 10 years. Parts of POLESat have been selected with lifetimes of 10 years and preferably more. Systems with uncertain lifetimes have been made redundant by adding more parallel systems. Overall the requirement is met by POLESat.

Preferable mission start The mission start of POLESat in 2010 can not be achieved. Too much testing, building and development time is still needed on subsystems and the payload in particular to be able to launch in 2010. The estimated launch time 2012.

Main payload The main payload consists of a multibeam laser altimeter which stores the full received waveform.

Spatial resolution With the obtained data it is possible to construct a DEM of over 80% of Antarctica. So this part of the requirement is met. However, in the north of Greenland is a small strip of land, which is not covered by POLESat. This strip is relatively small and fortunately not in the most interesting parts of Greenland.

Accuracy The horizontal accuracy stays within 5 m depending on atmospheric conditions. For a clear sky and low humidity, the vertical accuracy stays within 5 cm.

Sustainability Sustainability is a driving factor for the DSE group and will be the main point of consideration for future POLESat teams

Costs The costs for POLESat are estimated at $1,000$ million U.S. dollar. This is comparable to the price of ICESat, while POLESat has largely improved capabilities. It therefore is competitive.

15 Further planning to launch

In this chapter all phases after the basic design concept will be briefly discussed. For simplicity, the next stages of the mission after basic design are divided into three phases. The first phase will be the research, development, test and evaluation phase, which will be followed by the production phase and finally the operational phase.

Research, development, test and evaluation phase

After the initial concept design, the broad definition of the mission is clear. The next step will be to start with Research, development, test and evaluation phase This phase will start with the research on the payload. As for this mission a new laser, as well new Detector technology, will be used. This will require an extensive amount of research on the mentioned components. The research and development of the payload will be followed by production of the prototype laser, detector and their testing tools. Payload is the subsystem with the highest impact on the spacecraft design. Parameters such as size, weight and power influence various characteristics of the spacecraft. All the subsystems are designed according to the payload requirement. Most of the subsystems and their components are already space qualified and in operation in various missions and therefore do not require a lot of additional research. A spacecraft prototype is produced after the detail design of all the subsystems and the testing of the payload.

Production phase

This phase will start with the production of spacecraft components and will last until the in-orbit operations are completed. The components are designed and produced by different companies; these components are integrated into different subsystems. Subsequently, each subsystem has to go through space qualification test. Finally, the payload and all the subsystems are assembled together to get an end product in the form of the spacecraft. The spacecraft also has to go through tests such as vibration test, acoustic test and thermal vacuum test. A component must be able to withstand the vibrations caused by the launch vehicle engine rumble. For the vibration test of a component, an electromechanical shaker perturbs the base of the component at a specified level of acceleration. Components can experience shocks from explosive release devices such as aerodynamic fairing separation mechanisms or spacecraft separation bolts. For this test, the electromechanical shaker produces a shock pulse instead. The thermal vacuum test is performed in a vacuum chamber. The walls of the vacuum chamber have a thermal shroud for cooling or heating. Selecting the launch vehicle, selecting the launch date, initial training of operator personnel, transporting the spacecraft to the launch site, launch site activities, launch and in-orbit operation are also part of the production phase. Launch site activities include installing and validating the test equipment, testing the performance of the spacecraft, installing the propulsion, loading the propellant, integrating the spacecraft into the launch vehicle, and monitoring.

Operational phase

The operational phase is the final phase of the mission, it consist of the activities performed by the operational teams during the flight phase of the mission, together with the operations training activities they perform pre-launch. Some activities which are performed by the team during the flight phase of the mission are mission control, establishing communication links and managing data flow, determining where the spacecraft is and planning maneuvers, managing the spacecraft bus, as well as the payload, data processing and managing all the data generated by the mission etc.

An overview of the entire process is shown in figures 15.1, 15.2 and 15.3.

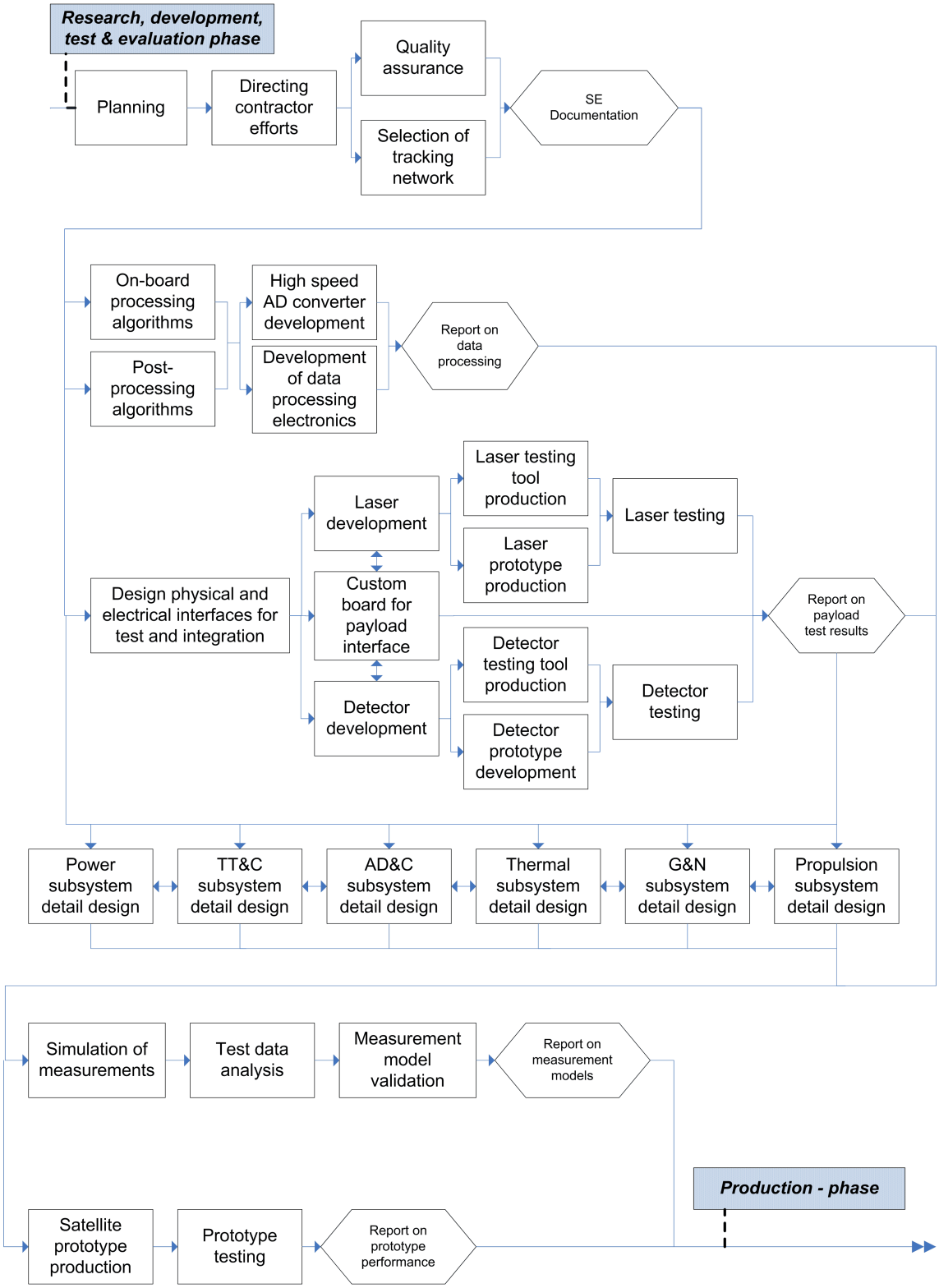

Figure 15.1: Work flow diagram (part 1).

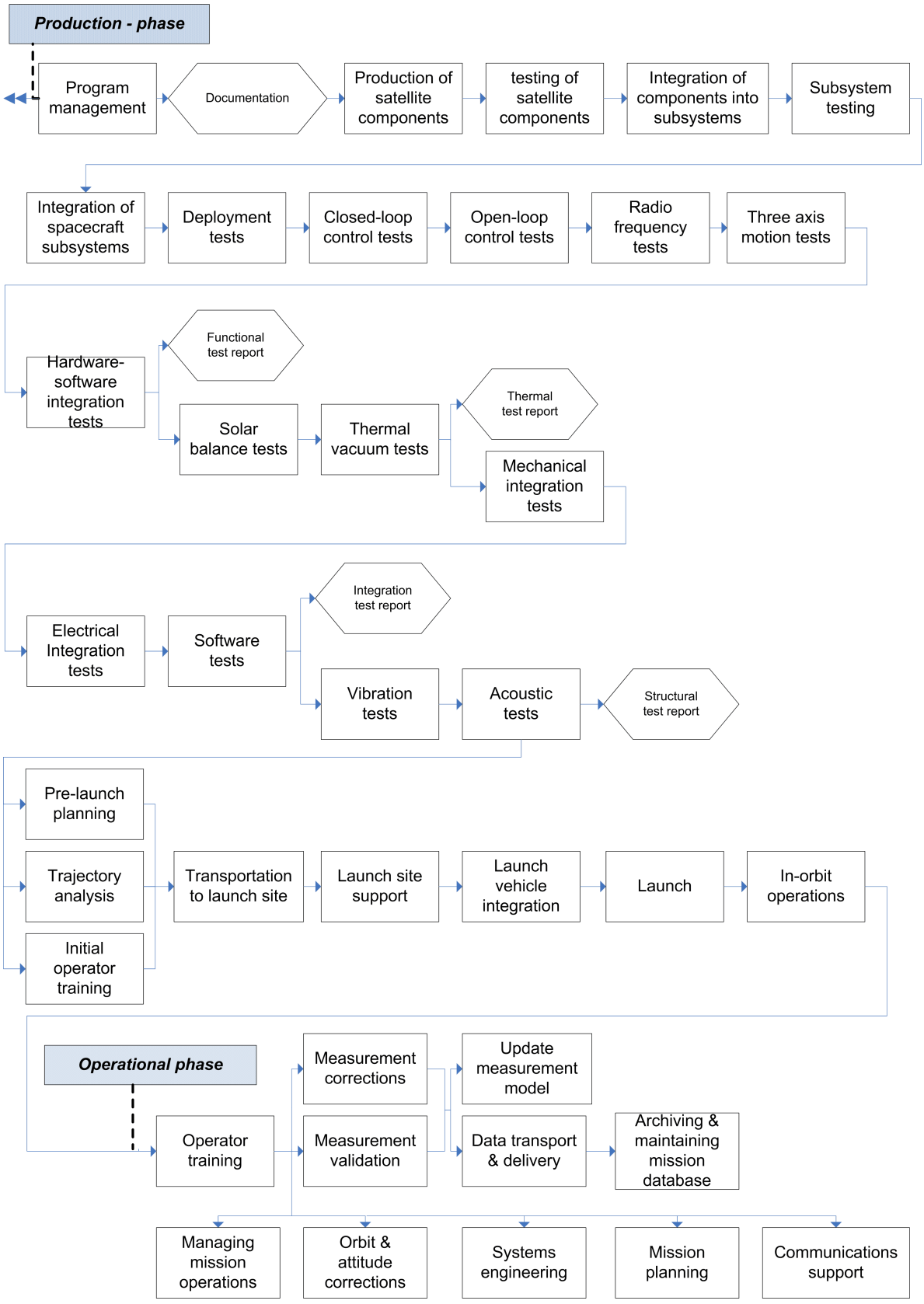

Figure 15.2: Work flow diagram (part 2).

ID	Task Name	Duration
1	**POLESat mission**	**1115 days**
2	**Research, development, test & evaluation p**	**635 days**
3	Project planning	0.25 mons
4	Directing contractor efforts	0.5 mons
5	Quality assurance	0.25 mons
6	Selection of tracking network	0.5 mons
7	SE documentation	0.25 mons
8	Power subsystem detail design	6 mons
9	TT&C subsystem detail design	6 mons
10	AD&C subsystem detail design	6 mons
11	Thermal subsystem detail design	6 mons
12	G&N subsystem detail design	6 mons
13	Propulsion subsystem detail design	6 mons
14	On-board processing algorithms	3 mons
15	Post processing algorithms	3 mons
16	High-speed A/D converter	2 mons
17	Development of data processing electronic	2 mons
18	Report on data processing	0.25 mons
19	Design physical and electrical interfaces fo	1 mon
20	Custom board for payload interface	1 mon
21	Detector development	5 mons
22	Detector prototype development	2 mons
23	Detector testing tool production	2 mons
24	Detector testing	3 mons
25	Laser development	9 mons
26	Laser prototype production	2 mons
27	Laser testing tool production	2 mons
28	Laser testing	6 mons
29	Report on payload testing	0.25 mons
30	Simulation of measurements	1 mon
31	Test data analysis	1 mon
32	Measurement model validation	1 mon
33	Report on measurement models	0.25 mons
34	Satellite prototype production	6 mons
35	Prototype testing	4 mons
36	Report on prototype performance	0.25 mons
37	**Production phase**	**480 days**
38	Program management	0.25 mons
39	Documentation	0.25 mons
40	Production of satellite components	6 mons
41	testing of satellite components	1.5 mons
42	Integration of components into subsystems	1 mon
43	Subsystem testing	2 mons
44	Integration of spacecraft subsystems	1 mon
45	Deployment tests	0.5 mons
46	Closed-loop control tests	1 mon
47	Open-loop control tests	1 mon
48	Radio frequency tests	0.5 mons
49	Three axis motion tests	0.5 mons
50	Hardware-software integration tests	1 mon
51	Functional test report	0.5 mons
52	Solar balance tests	1 mon
53	Thermal vacuum tests	1 mon
54	Thermal test report	0.5 mons
55	Mechanical integration tests	0.5 mons
56	Electrical Integration tests	1 mon
57	Software tests	1 mon
58	Integration test report	0.5 mons
59	Vibration tests	0.5 mons
60	Acoustic tests	0.5 mons
61	Structural test report	0.5 mons
62	Pre-launch planning	0.25 mons
63	Trajectory analysis	0.5 mons
64	Initial operator training	1.5 mons
65	Transportation to launch site	0.25 mons
66	Launch site support	1 mon
67	Launch vehicle integration	0.25 mons
68	Launch	0.25 mons
69	In-orbit operations	0.25 mons

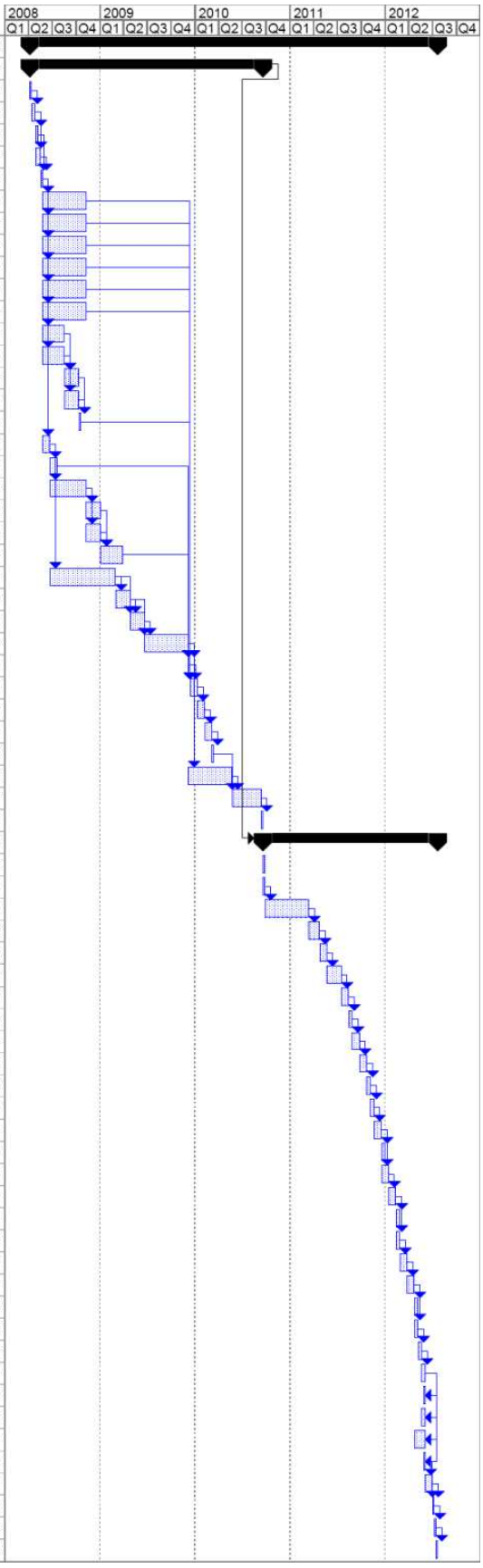

Figure 15.3: Gannt chart.

16 Conclusions and recommendations

In this report, the design of POLESat, the Pole Oriented Laser Elevations Satellite, has been discussed. POLESat will be the follow-up mission of ICESat. Its main goal is therefore to take elevation measurements over Greenland and Antarctica, from which the mass balance of the polar ice sheets can be derived.

The final design of POLESat is comprised of a satellite with five operating lasers, which will take full waveform measurements at infrared (1064 nm) and green (532 nm) wavelengths. This is to improve the accuracy of measurements taken by ICESat.

Some top-level requirements have been mentioned that POLESat should be able to fulfill. These are:

- Measurements taken by POLESat should allow the construction of a DEM of Greenland and at least 80% of Antarctica.
- The minimum lifetime must be 5 years, with an expected lifetime of 10 years.
- The mission should start in 2010.
- The single measurement accuracy in clear sky and over flat terrain has to be 5 cm vertical and 5 m horizontal.

The final design discussed in the report is able to fulfill all these requirements, except for the mission start in 2010. A mission start in 2012 is more likely, because extensive testing of the laser system is recommended before it's flown in space. Next to this, it is advised tests are done on the custom electronics and the detector.

In the end, the estimated price for the POLESat mission was found to be around 1,000 million U.S. dollars (€700 million). This is only slightly more expensive than ICESat, which costs 900 million U.S. dollars.

It is concluded the estimated costs, in combination with the improvement in coverage and accuracy, make POLESat a suitable option as follow-up mission for the ICESat.

A Orbit calculations

In this appendix, various calculations will be shown that have to do with POLESat's orbit and are used in the design process. In paragraph A.1, computations will be given to calculate the position of POLESat at an arbitrary time. The time that the satellite is visible from a ground station is discussed in A.2, followed by computations that have to do with atmospheric drag in A.3. Finally, the coverage of POLESat and the across-track distance will be looked at in paragraphs A.4 and A.5, respectively.

A.1 Satellite position

In order to be able to show the ground tracks of POLESat or to calculate its contact time with a ground station, it is necessary to know where the satellite will be at a specific time instance. In this paragraph, it will be explained how the position of POLESat or any other satellite can be predicted, knowing its initial position. All equations in this paragraph are taken from [70, 6].

The position of a satellite is generally given in so-called classical or Keplerian orbital elements, see figure A.1. These elements are:

- Semi-major axis a [m], which is the largest radius of the orbital ellipse.
- Eccentricity e [–], which defines the shape of the orbital ellipse.
- Inclination i [°], which defines the angular distance of the orbital plane from the Earth's equatorial plane.
- Right ascension of ascending node Ω [°], which is the point where the satellite passes through the equatorial plane moving from south to north.
- Argument of perigee ω [°], which is the angle from the ascending node to the eccentricity vector.
- True anomaly ν [°], which is the angle in the orbital plane between the eccentricity vector and the satellite.

The values of all these elements at an arbitrary time $t = 0$ have to be known, in order to make a prediction of the satellite's position at a different time t.

First of all, the initial mean anomaly M_0 has to be calculated, which is the angle the satellite would have traveled if its orbit was circular and its velocity constant. For a circular orbit (i.e. $e = 0$), the initial mean anomaly equals the initial true anomaly ν_0. For an elliptical orbit, it has to be calculated using the following two equations:

$$E_0 = \cos^{-1}\left(\frac{e + \cos\nu_0}{1 + e \cdot \cos\nu_0}\right) \tag{A.1}$$

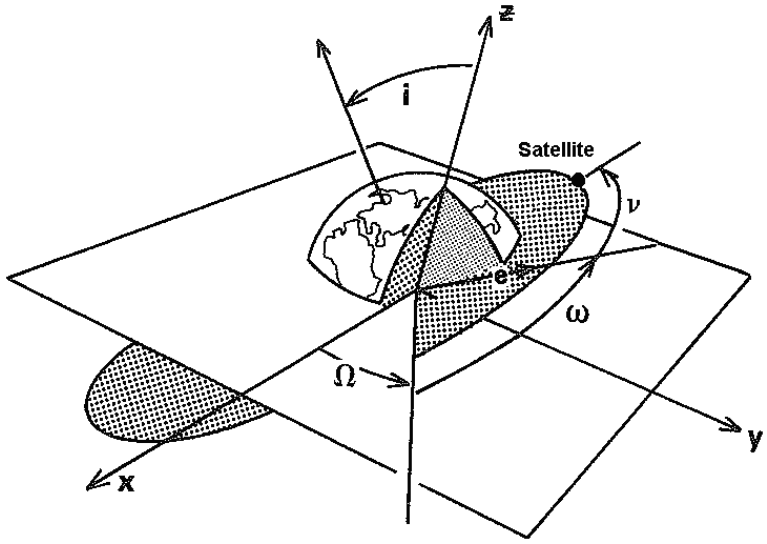

Figure A.1: Definition of classical orbital elements (adopted from [70]).

$$M_0 = E_0 - e \cdot \sin E_0 \tag{A.2}$$

At an arbitrary time t, the mean anomaly is shifted and given by

$$M = M_0 + n \cdot t \tag{A.3}$$

where n is the average angular velocity of the satellite, computed by

$$n = \sqrt{\frac{\mu}{a^3}} \tag{A.4}$$

where, μ is the universal gravitational constant times the Earth's mass ($\approx 3.986 \cdot 10^{14}$ $\mathrm{m}^3/\mathrm{s}^2$).

Next, a new value for the eccentric anomaly (the angle the satellite would have traveled if its orbit was circular) can be computed, using

$$E = M + e \cdot \sin E \tag{A.5}$$

When the eccentricity of the orbit is zero, the eccentric anomaly equals the mean anomaly. However, when $e \neq 0$, equation A.5 cannot be solved explicitly. In this case, it is possible to take E_0 as first approximation to E and find an iterative solution working down to the precision level of the numerical solver (e.g. a calculator or pc). Alternatively, a Taylor expansion can be used.

After this, a new value for the true anomaly can be calculated with the following expression:

$$\nu = \cos^{-1}\left(\frac{\cos E - e}{1 - e \cdot \cos E}\right) \tag{A.6}$$

Now, the position of the satellite is basically known, but not yet in an Earth fixed reference frame. For this, the rotation of the Earth during the time interval considered has to be taken into account as well. Since the Earth rotates once in 23h 56m (or 86164 s), the

change in the right ascension of ascending node will be (t in seconds)

$$\Delta\Omega_E = -\frac{2\pi \cdot t}{86164} \tag{A.7}$$

At this point, it is important to note that the predictions made here are not exact, because of unknown perturbations of the satellite orbit. The largest perturbation, the so-called J_2 factor ($1.0826267 \cdot 10^{-3}$, from [51]), is caused by the flattening of the Earth. This causes a drift of both the right ascension of the ascending node and the argument of perigee, given by (t again in seconds):

$$\Delta\Omega_{J_2} = -2.39629 \cdot 10^9 \cdot a^{-\frac{7}{2}} \cdot \cos i \cdot \left(1 - e^2\right)^{-2} \cdot t \tag{A.8}$$

$$\Delta\omega = 1.19815 \cdot 10^9 \cdot a^{-\frac{7}{2}} \cdot \left(4 - 5 \cdot \sin^2 i\right) \cdot \left(1 - e^2\right)^{-2} \cdot t \tag{A.9}$$

The resulting right ascension of ascending node, after taking Earth's rotation and J_2 into account, will be

$$\Omega = \Omega_0 + \Delta\Omega_E + \Delta\Omega_{J_2} \tag{A.10}$$

The corresponding argument of perigee is

$$\omega = \omega_0 + \Delta\omega \tag{A.11}$$

Knowing these quantities, the satellite's position with respect to the centre of the Earth (in Cartesian coordinates) can be computed:

$$x = r \cdot \left(\cos\Omega \cdot \cos\left(\nu + \omega\right) - \sin\Omega \cdot \sin\left(\nu + \omega\right) \cdot \cos i\right) \tag{A.12}$$

$$y = r \cdot \left(\sin\Omega \cdot \cos\left(\nu + \omega\right) + \cos\Omega \cdot \sin\left(\nu + \omega\right) \cdot \cos i\right) \tag{A.13}$$

$$z = r \cdot \sin\left(\nu + \omega\right) \cdot \sin i \tag{A.14}$$

where r is the distance from the centre of the Earth to the satellite, given by

$$r = \frac{a \cdot \left(1 - e^2\right)}{1 + e \cdot \cos\nu} \tag{A.15}$$

Example

The equations listed above can be used to simulate POLESat's orbit during one day. For this purpose it is assumed that the orbit of POLESat is perfectly circular, i.e. that $e = 0$. Using the known orbit parameters $a = 6855.4$ km and $i = 97.3°$, and taking any value for the remaining orbital elements, results in the tracks shown in figure A.2.

A.2 Ground station access time

In the previous paragraph, it was discussed how the position of a satellite can be calculated. An example illustrated the use of this position for plotting the satellite's ground tracks. Another application of the previous section is computing the contact time between the satellite and a ground station, the so-called ground station access time. This is a geometric problem, as is shown in figure A.3.

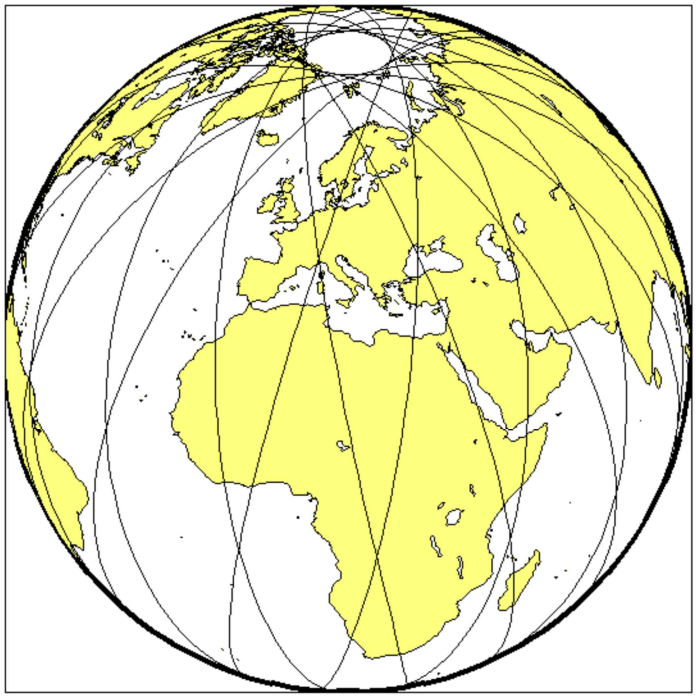

Figure A.2: POLESat's orbit during one day.

In this case, the goal is to calculate the elevation angle ϵ. If $\epsilon > 0$, the satellite is above the horizon at the ground station, which means contact with the satellite is theoretically possible. Due to horizon obstructions, the minimum elevation angle for which contact with the satellite is possible is usually larger, like 5 or 10 degrees.

As can be seen in figure A.3, ϵ is given by

$$\epsilon = 90 - \eta - \lambda \tag{A.16}$$

which means η and λ have to be calculated first. To do so, it is necessary to know the distance r_r between the satellite and the ground station. This value can be computed using

$$r_r = \sqrt{x_r^2 + y_r^2 + z_r^2} \tag{A.17}$$

where x_r, y_r and z_r are the relative Cartesian coordinates between the satellite and the ground station.

Next, the true outer horizon angle ρ as seen from the satellite can be calculated:

$$\rho = \sin^{-1}\left(\frac{r_e}{r}\right) \tag{A.18}$$

where r is the distance from the satellite to the Earth's centre. Now, the latitude δ_s and longitude λ_s of the sub-satellite point can be calculated, using the following two equations:

$$\delta_s = \tan^{-1}\left(\frac{z}{\sqrt{x^2 + y^2}}\right) \tag{A.19}$$

$$\lambda_s = \tan^{-1}\left(\frac{x}{y}\right) \ (-180° < \lambda_s \leq 180°) \tag{A.20}$$

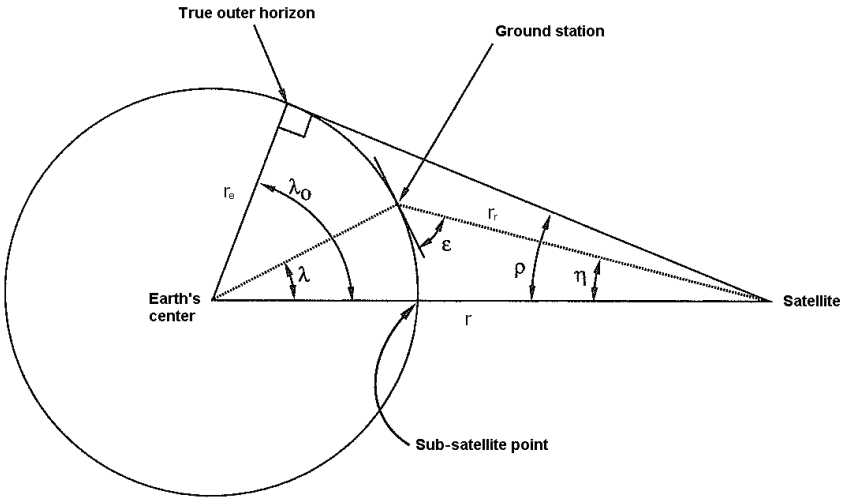

Figure A.3: Geometry of ground station access problem (adopted from [70]).

Knowing the location of the sub-satellite point allows to calculate the Earth's centre angle λ, given by

$$\lambda = \cos^{-1}\left(\sin\delta_s \cdot \sin\delta_t + \cos\delta_s \cdot \cos\delta_t \cdot \cos|\lambda_s - \lambda_t|\right) \tag{A.21}$$

where δ_t and λ_t are the latitude and longitude of the ground station, respectively.

Finally, the angle η can be calculated using

$$\eta = \tan^{-1}\left(\frac{\sin\rho \cdot \sin\lambda}{1 - \sin\rho \cdot \cos\lambda}\right) \tag{A.22}$$

after which ϵ is known, according to equation A.16.

Two examples

With the equations just discussed, it is possible to extend the simulation of the previous paragraph with a computation of the angle ϵ. When ϵ is larger than the minimum required elevation angle, let's say 10°, it can be assessed whether a satellite is visible from a specific location on Earth or not. This can be used for example, to show all POLESat tracks that are visible from Delft within a month, providing the satellite is more than 10° over the horizon. See figure A.4. Note that in the figure also the 10° elevation mask and the true horizon (i.e. $\epsilon = 0$) are shown.

Another example includes the calculation of the longest time between two passes over a ground station. In the worst case scenario, POLESat is just not visible over the westerly horizon of a ground station. For the ground station in Kiruna, Sweden, figure A.5 shows three complete revolutions of the satellite for this scenario, assuming an elevation mask of 10°.

As can be seen in the figure, POLESat starts over the equator near Africa and moves northbound, passing just outside the view of Kiruna. The ground track then moves westward because of the rotation of the Earth, which causes the satellite to be not visible from the ground station for more than 11 hours.

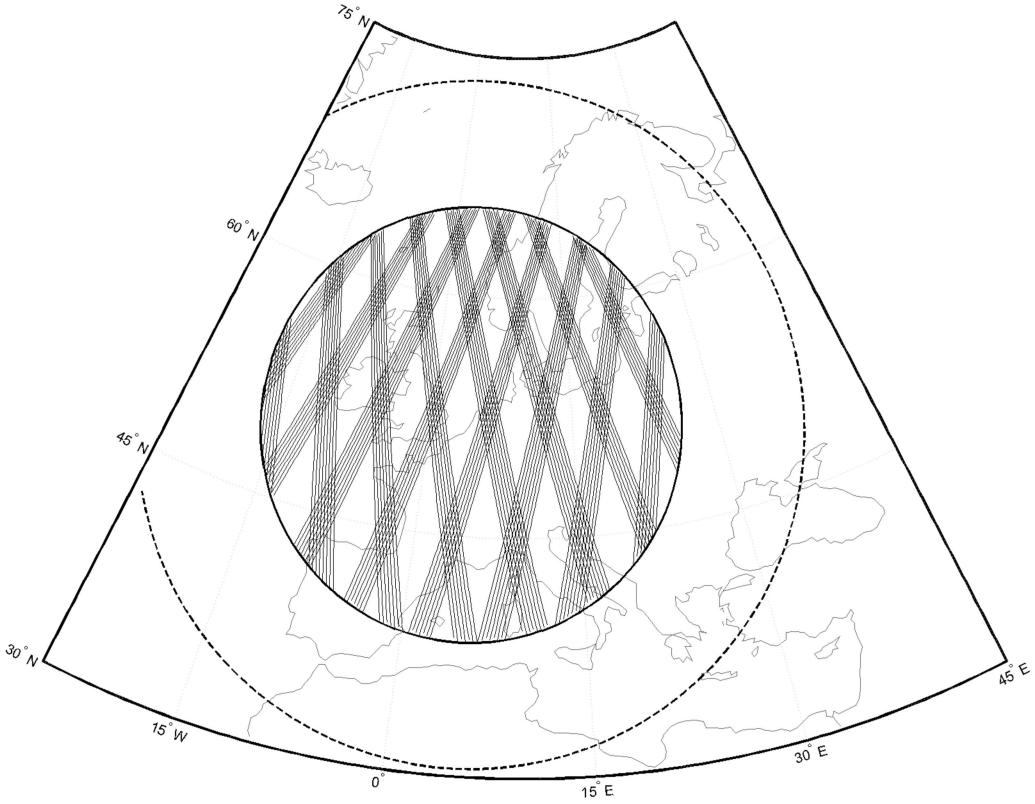

Figure A.4: One month of POLESat tracks visible from Delft.

A.3 Atmospheric drag

Orbital mechanics can be used for various types of aspects. This can be sizing of the different subsystems but also for making estimations or calculations of important mission parameters. Orbit parameters like height, inclination, eccentricity (circle is assumed) have its influence on eclipse time and/or sunlight time, drag, lifetime, ΔV budget, etc. The equations from [51] used to calculate these variables are given below. All the equations given assume a circular orbit, i.e. $e = 0$.

The orbit time t_{orbit} in seconds follows from the height h [m] given by [6]:

$$t_{orbit} = 2\pi\sqrt{\frac{(r_e + h)^3}{\mu}} \tag{A.23}$$

The eclipse time $t_{eclipse}$ and sunlight time t_{sun} (both in seconds) can be calculated from the orbit altitude h in mand the equatorial radius r_e (6378136 m) using trigonometric relations presented in figure A.6

$$t_{eclipse} = \frac{t_{orbit}}{\frac{360}{2 \cdot \lambda}} \tag{A.24}$$

$$\lambda = \arctan\left(\frac{r_e}{r_e + h}\right) \tag{A.25}$$

$$t_{sun} = t_{orbit} - t_{eclipse} \tag{A.26}$$

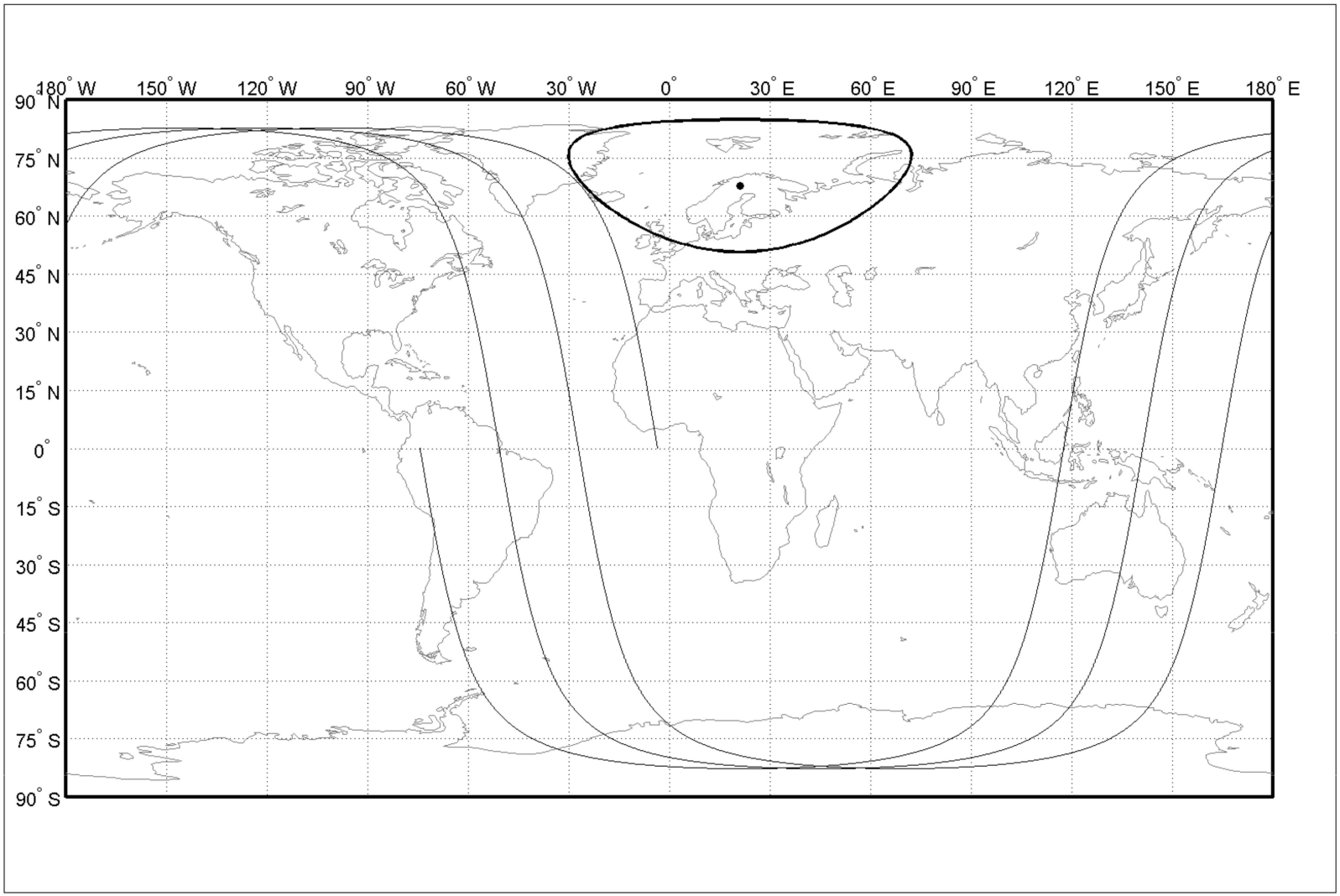

Figure A.5: A worst case scenario for the contact time.

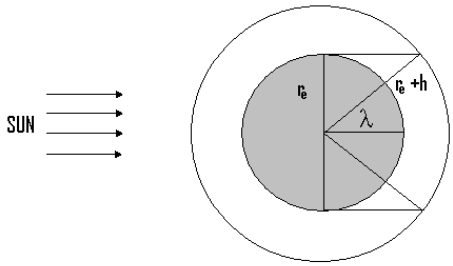

Figure A.6: Eclipse time.

The estimated value for the eclipse time is a raw approximation due to assumption of spherical Earth. Software tools like Satellite Tool Kit (STK) give a better estimate since all factors are taken into account (like flattening). A dusk-dawn orbit is a sun-synchronous orbit in which the satellite is inserted at a fixed time. When using a dusk-dawn orbit there will only be sunlight time.

Decay due to atmospheric drag

The influence of decay due to atmospheric drag depends not only on the orbit altitude, but also the solar radiation pressure (solar minimum or maximum). Values for the density ρ versus height are provided in [51, table 4-1], together with values for the scale height H. Atmospheric drag has its influence on the semi-major axis of the orbit, the drag acting on the satellite and also the lifetime of the satellite. The drag D [N] experienced by a satellite can be computed using the following relation [51]:

$$D_{satellite} = -\frac{1}{2} \cdot \rho \cdot V_{sat}^2 \cdot S_{frontal} \cdot C_D \tag{A.27}$$

Both the drag coefficient C_D and the frontal area [m^2] of the satellite can be estimated using already existing mission data. The drag coefficient is often in the order of 2.2 [70, table 8-3]. The speed of the satellite V_{sat} [m/s] can be calculated by using:

$$V_{sat} = \frac{2\pi \left(r_e + h\right)}{t_{orbit}} \tag{A.28}$$

The decrease in semi-major axis Δa [m] due to atmospheric drag after one orbital revolution is given by:

$$\Delta a_{2\pi} = -2\pi \cdot \frac{C_D \cdot S_{frontal}}{m_{satellite}} \cdot \left(r_e + h\right)^2 \cdot \rho \tag{A.29}$$

The satellites lifetime L expressed in years, is the life time of the satellite in case nothing is done to compensate for the height losses. The lifetime is the ratio of the density scale height H and the decrease in semi-major axis, both expressed in meters.

$$L = -\frac{H}{\Delta a_{2\pi}} \tag{A.30}$$

Orbit keeping ΔV budget

ΔV is a change in velocity given in m/s. The ΔV budget for orbit keeping equals the change in velocity needed to compensate for the atmposheric drag and other non-periodic perturbations. An estimate of this budget per orbital revolution is given below (eq. A.31). Using the orbit time, it is possible to determine the number of orbital revolutions per year, from which the ΔV budget for that year can be computed.

$$\Delta V_{rev} = \pi \cdot \frac{C_D \cdot S_{frontal}}{m_{satellite}} \cdot \rho \cdot \sqrt{(r_e + h) \cdot \mu} \tag{A.31}$$

Propellants mass and volume

Once the ΔV budget is known, it is possible to size the propellant mass $m_{propellant}$ using Tsiolkovsky's equation:

$$\Delta V = I_{sp} \cdot g_0 \cdot \ln\left(\frac{m_{dry} + m_{propellant}}{m_{dry}}\right) \tag{A.32}$$

The dry mass m_{dry} represents the total mass of the satellite excluding the propellant mass (all masses expressed in [kg]). Each propellant type has it's own specific impulse I_{sp} [s], which is a measure of the exhaust velocity of the burned propellant.

A.4 Coverage

When a satellite is flying in a polar orbit (i.e. $i = 90°$) no gap will exist near the poles. Often this is not the case, and a gap will exist leading to non-covered areas (two gaps, one at each pole). This paragraph deals with the equations needed to estimate the gap area, assuming a perfect sphere. A graphical representation of POLESat's orbit is given in figure A.7. The gap existing at the poles increases when the inclination i of the orbit deviates more from 90°.

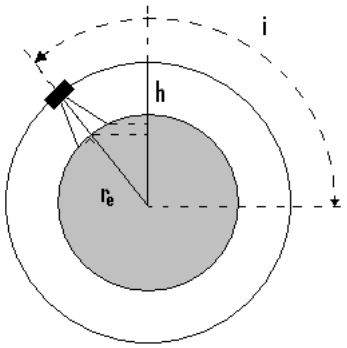

Figure A.7: Satellite representation of coverage.

When considering POLESat, laser beams are not only pointing at nadir (straight down to the Earth's surface) but some also have a small angle deflection, causing an offset between

the different laser footprints. As represented in figure A.8, x equals the distance between the footprint located at the outside and the center footprint. The location of the outer footprint results in a decreasing polar gap, compared to the case of only the center footprint. To make the estimate more precise it is important to take this offset x into account.

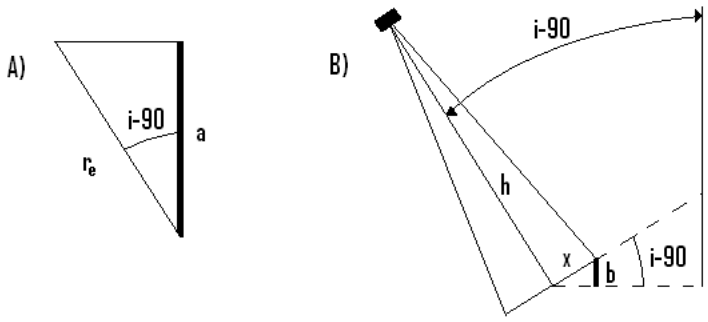

Figure A.8: Geometric relations (coverage).

Using goniometric relations, it is possible to calculate the distance a and b, as given in figure A.8 from the inclination i in [°], the distance x in [km] and the equatorial radius r_e (6378.136 km).

$$a = r_e \cdot \cos\left(i - 90^\circ\right) \tag{A.33}$$

$$b = x \cdot \sin\left(i - 90^\circ\right) \tag{A.34}$$

The gap at the poles corresponds to a small circle. Using the height h_{cap} in km, it is possible to compute the corresponding cap area S_{cap} expressed in km^2 using the equation as given in [69].

$$S_{cap} = \pi \left(r_{cap}^2 + h_{cap}^2\right) \tag{A.35}$$

$$h_{cap} = r_e - (a + b) \tag{A.36}$$

r_{cap} is defined as in figure A.9 and relates the distance a and b by

$$\frac{r_e}{r_e} = \frac{r_e - (a + b)}{r_{cap}} \tag{A.37}$$

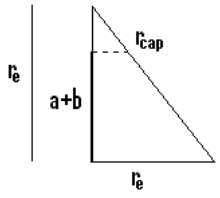

Figure A.9: Radius of a spherical cap.

A.5 Across-track distance

The distance between ground tracks gets smaller towards the poles, leading to the fact that for each different latitude δ there is a different value for the across track distance $D_{across\,track}$ (measured perpendicular to the ground track). This paragraph deals with the formulas needed to estimate the across track distance for different latitudes, assuming that the ground tracks are equally spaced.

When one wants to compute the across track distance between neighboring ground tracks after a time t, the following steps have to be carried out. First one needs to determine the number of revolutions n_{rev} after a time t using the orbit time t_{orbit}, both expressed in seconds.

$$n_{rev} = \frac{t}{t_{orbit}} \tag{A.38}$$

The orbit time can be calculated using equation A.23. From the number of revolutions it is possible to compute the distance between neighboring tracks at the equator expressed in km using the assumption of equally spaced (equatorial radius r_e expressed in [km]).

$$D_{across\,track\,eq} = \frac{2 \cdot \pi \cdot r_e}{n_{rev}} \tag{A.39}$$

Once the spacing at the equator is known, one can estimate the spacing between neighboring ground tracks at other latitudes δ. The relations between the latitude and the across track spacing is given in figure A.10.

$$\frac{90^\circ}{D_{across\,track\,eq}} = \frac{90^\circ - \delta}{D_{across\,track}} \tag{A.40}$$

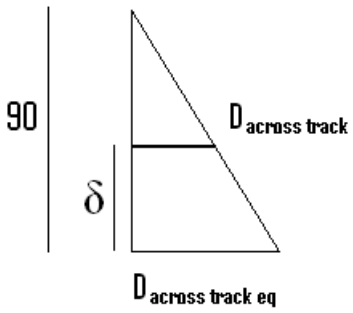

Figure A.10: Across track distance goniometric.

B Required laser power

To calculate the required laser power E_0, the following equation[29] is used:

$$E_0 = \frac{16ER^2}{\alpha D^2 \eta \tau} \tag{B.1}$$

where R is the orbit altitude, α the albedo of the Earth's surface, D the effective lens diameter of the detector, η the efficiency of the optical system and τ the atmospheric transmittance.

In equation B.1, the only unknown variable is the required energy at the detector E. In reference [29], E is given by

$$E = \frac{S^2 hc}{\lambda} \tag{B.2}$$

where S is the signal-to-noise ratio at the detector, h is Planck's constant ($h \approx 6.626 \cdot 10^{-34}$ $\mathrm{m^2 kg/s}$), c is the speed of light ($c \approx 2.998 \cdot 10^8 \mathrm{m/s}$) and λ is the wavelength of the laser.

S can be calculated using the following equation (also taken from [29]):

$$\epsilon = \frac{c}{2}\sqrt{\frac{T}{BS}} \tag{B.3}$$

where T is the laser pulse duration, B the detector bandwidth and ϵ the measurement error in slant direction.

For POLESat, the goal is to achieve a slant range accuracy of 5 cm. With the known laser pulse duration of 4 ns and detector bandwidth of 200 MHz, it is possible to compute the required signal-to-noise ratio at the detector. For the infrared laser ($\lambda = 1064$ nm), the corresponding energy at the detector can then be calculated with equation B.2.

When looking at ice sheets, the lowest albedo expected is 0.2 for glacier ice [16]. Moreover, the optical system efficiency is estimated to be 40%, which is in line with the performance of ICESat [77], and empirical measurements show the average atmospheric transmittance is about 0.7 for a wavelength of 1064 nm [42].

Knowing these values makes it possible to visualize the relation between the laser power, orbit altitude and detector size, according to equation B.1. See figure B.1.

From this figure, it can be derived that for an altitude of 477.3 km and a detector with an effective lens diameter of 1.5 m, the laser power per pulse should be 173 mJ to achieve 5 cm slant range accuracy.

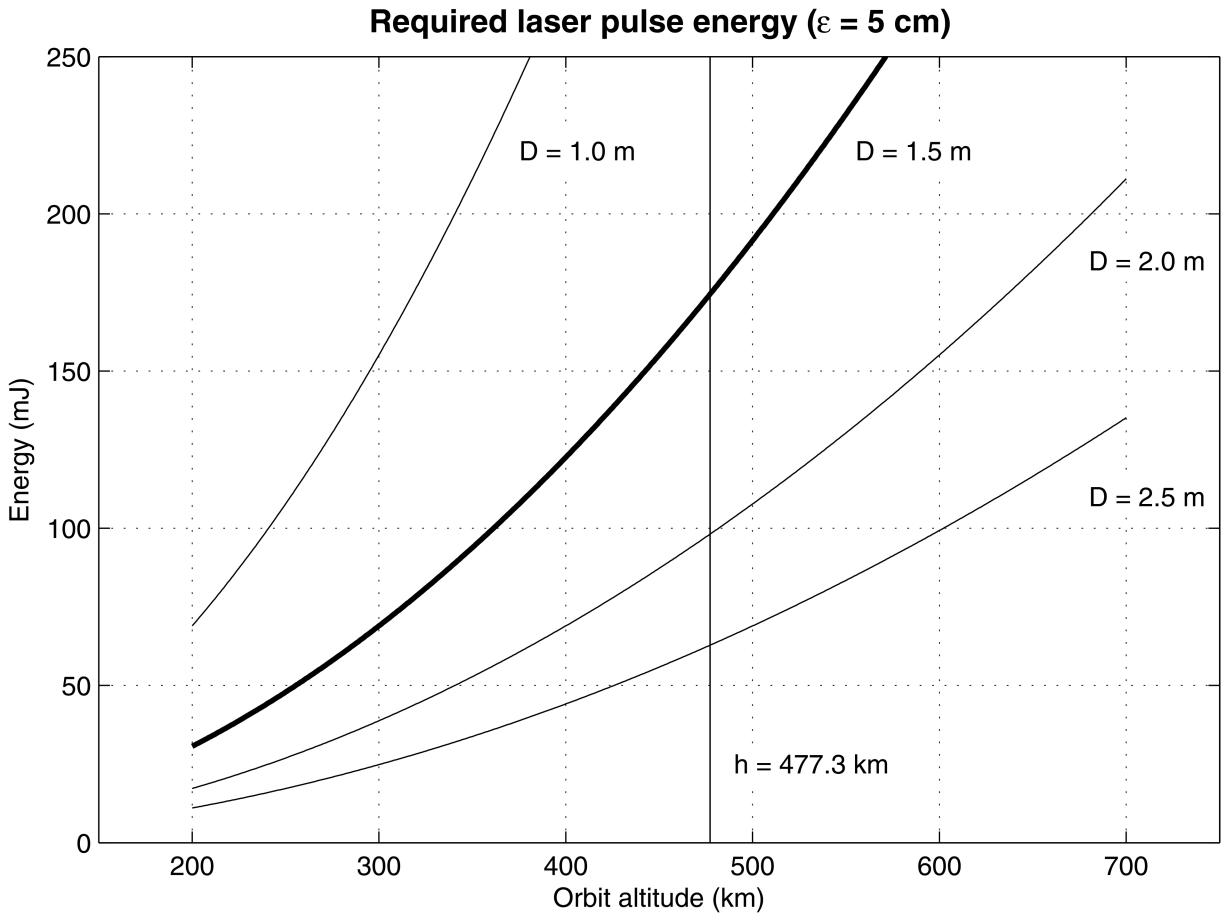

Figure B.1: Required laser pulse energy.

C Full-waveform analysis

Full-waveform analysis is done to distill as much useful data as possible from laser altimetry measurements. It allows for estimations of terrain surface characteristics such as roughness and reflectivity and therefore calculating corrections to the height estimation. Full-waveform analysis is discussed in detail in [32], [36] and [14], and is shortly summarized here.

Figure C.1 shows a schematic overview of laser ranging on sloping terrain. Errors associated with a single shot in this situation are given in [36] as in formula C.1 $N_S = \left(\frac{E_t \eta}{h\nu}\right)\left(\frac{A_r}{Z^2}\right)\tau_{sys}\tau_{atm}^2\left(\frac{r_{sur}}{\Omega_{sur}}\right)$ and $N_B = \left(\frac{E_s \eta}{h\nu}\right) B_0 A_r \tau_{sys}\left(\frac{A_{sp}}{Z^2}\right)\left(\frac{r_{sur}}{\Omega_{sur}}\right) T_p$. The terms used are listed in table C.1.

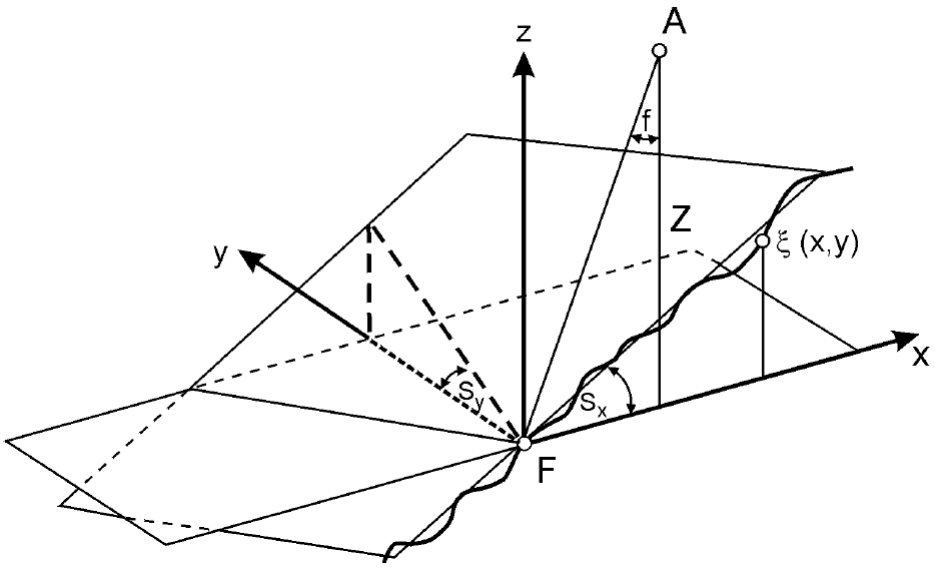

Figure C.1: Generalized geometry of the terrain (taken from [14]).

$$
\begin{aligned}
\mathrm{var}(T) = & \\
& \underbrace{\mathrm{var}\frac{T_0}{N_S} + (FN_B + N_D)T^3 \cdot (N_S^2 12\Delta t) + \frac{\Delta t^2}{12}}_{\text{impulse response}} \\
& + \underbrace{(\frac{F}{N_S} + \frac{1}{K_S})\frac{4\mathrm{var}(\Delta R)\cos^2(Sx)}{c^2\cos^2(\phi + Sx)}}_{\text{surface roughness}} \\
& + \underbrace{(\frac{F}{N_S} + \frac{1}{2K_S})\frac{4Z^2\tan^2 D}{c^2\cos^2\phi}}_{\text{beam curvature}} \\
& + \underbrace{(\frac{F}{N_S} + \frac{1}{2K_S})\frac{4Z^2\tan^2 D}{c^2\cos^2\phi} \cdot \left[\tan^2(\phi + Sx) + \frac{\tan^2(Sy)\cos^2(Sx)}{\cos^2(\phi + Sx)}\right]}_{\text{nadir angle and slope}} \\
& + \underbrace{\frac{4Z^2(1+\tan^2 D)^2}{c^2\cos^2\phi}\left[\tan^2(\phi + Sx)\mathrm{var}(\Delta\phi x) + \frac{\tan^2(Sy)\cos^2(Sx)\cos^2\phi}{\cos^2(\phi + Sx)}\mathrm{var}(\Delta\phi y)\right]}_{\text{pointing uncertainty}} \qquad \text{(C.1)}
\end{aligned}
$$

Definition of terms	
T_S	Pulse waveform centroid time.
$\mathrm{var}(T_0)$	Variance of transmitter laser pulsewidth.
ϕ	Laser pointing angle off nadir.
$\Delta\phi x$	Laser pointing angle uncertainty along track
$\Delta\phi y$	Laser pointing angle uncertainty across track.
var (ΔR)	Variance of surface roughness.
S_x	Surface slope along track.
S_y	Surface slope across track.
Z	Range to the surface.
c	Speed of light.
D	Laser beam divergence angle.
N_S	Mean signal photoelectrons.
N_B	Mean solar background photoelectrons.
N_D	Mean detector dark counts.
F	Avalanche photodiode excess noise factor.
Δt	Time-interval-unit resolution.
T	Detector integration time.
A_R	Receiver area.
λ	Laser wavelength
K_S	Speckle signal-to-noise ratio $= \pi AR[2\frac{\tan D}{\lambda})]^2$

Table C.1: Definition of terms for the single short error budget.

Waveform characterization

As described in [14] the waveform is characterized as shown in figure C.2. The waveform is analyzed by the fitting of one or more Gaussians and trying to determine the origins of the pulse spreading in terms of the factors of equation C.1. The effect of the surface on the return pulse is illustrated in figure C.3. No unique solutions exists for determining

the slope and roughness from the fitted waveform. Extensive simulation, testing and validation are required to achieve maximal accuracy with this technique, particulary for land measurements.

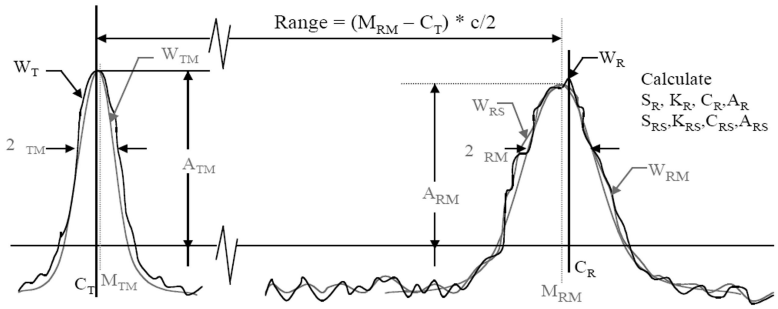

A	Max Amplitude	$()_T$	Transmitted pulse
W	Waveform	$()_{TM}$	Model of Transmitted pulse
M	Gaussian Mean	$()_R$	Return pulse
	Gaussian 1/e halfwidth	$()_{RM}$	Model of Return Pulse
C	Centroid (abscissa value)	$()_{RS}$	Smoothed Return Pulse
S	Skewness		
K	Kurtosis		

Figure C.2: Waveform characterization (taken from [14]).

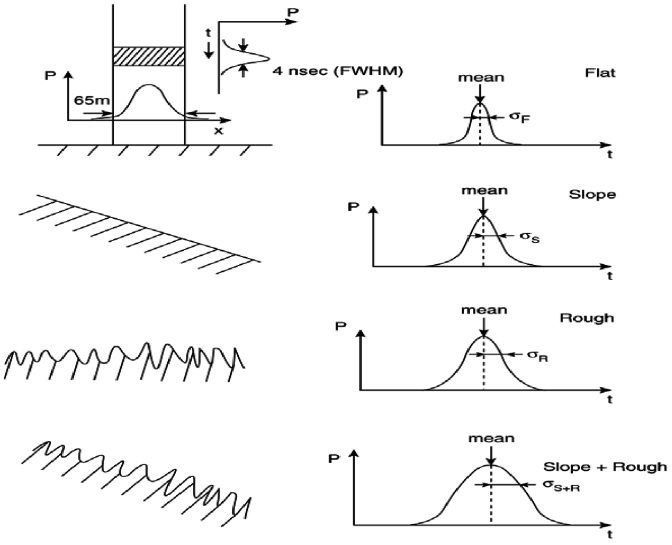

Figure C.3: Characteristics of returned laser pulse as a function of surface type (from [14]).

D Disturbing torques

On a satellite orbiting the earth, four typical torques are present. These are:

- Gravity gradient torques on the satellite,
- Solar pressure,
- Magnetic field torques,
- Aerodynamic drag torques.

Gravity gradient

The gravity gradient can be calculated with:

$$T_G = \frac{3\mu}{2 \cdot R^3} \cdot |I_z - I_y| \cdot \sin(2\theta) \tag{D.1}$$

In this, μ is the Earth's gravity constant ($3.986 \cdot 10^{14}$ m^3/s^2). Because the satellite is looking at nadir, $\theta = 0$. This is the maximum deviation of the z-axis from the local vertical. R is the orbit radius, which is the Earth radius plus the orbit altitude. Finally, I_z and I_y are two moments of inertia in kg/m^2.

Solar pressure

The radiation from the sun exerts a small force on the satellite. An offset of the center of solar pressure from the center of gravity will create a torque. This torque is calculated by:

$$T_{SP} = F \cdot (C_{sp} - C_g) \tag{D.2}$$

Here, C_{sp} and C_g are the centers of solar pressure and gravity respectively. F is the force exerted on the satellite, given by:

$$F = \frac{F_s}{c} \cdot A_s \cdot (1 + q) \cos i \tag{D.3}$$

F_s is the solar constant, which is 1367 W/m^2 at 1 astronomical unit from the sun. c is the speed of light in [m/s]. A_s is the surface area of the satellite facing the sun and i is the incidence angle of the solar rays on the satellite surface. Finally, q is the reflectance factor of the satellite surface material.

Magnetic field gradient

The magnetic field of the Earth will try to align the satellite to its own coordination. This results in a torque on the satellite:

$$T_G = \frac{2 \cdot D \cdot M}{R^3} \tag{D.4}$$

In this equation, D is the residual dipole of the satellite, expressed in $A \cdot m^2$ and M is the Earth's magnetic moment, which is $7.96 \cdot 10^{15}$ T/m^3. R is just like in previous equations the orbit radius.

Aerodynamic drag

The last contribution to the torques is the aerodynamic drag. This torque can be written as:

$$T_A = \frac{1}{2} \cdot \rho \cdot C_D \cdot A \cdot V^2 \cdot l \tag{D.5}$$

This is the basic aerodynamic drag function multiplied by the arm of the aerodynamic force. For calculating the drag, ρ is the density, A is the frontal area, aerodynamic drag is the speed, C_D is the drag coefficient and l the arm of the aerodnamic force.

Desaturation

To estimate the maximum time the satellite can go without desaturating its momentum wheels, one can simply divide the capacity of the momentum wheels by the torques present on the satellite:

$$time\,[\text{s}] = \frac{capacity\,[\text{Nms}]}{torques\,[\text{Nm}]}$$

This gives the time between saturating the momentum wheels. Note however, that this is the case when all the torques are added. In reality, some will be working in other, sometimes counteracting, directions.

Fuel needed

The amount of fuel needed can be calculated by:

$$mass = \frac{torque/arm}{g_0 \cdot I_{sp}} \cdot (lifetime)$$

In this, $mass$ is the amount of fuel needed for the attitude control, $torque$ is the total torque present on the satellite estimated earlier in this appendix, arm is the arm of the thrusters, which is taken to be 1 m, g_0 is the gravitational acceleration, I_{sp} is the specific impulse of the fuel and lifetime is 10 years, given in seconds. The specific impulse is determined by thruster and fuel choice and can be seen as fuel efficiency.

E Data rates

For the sizing of the telemetry, tracking & command and the command & data handling subsystems, it is necessary to know the rate with which data will be generated on board of the satellite. Next to this, it is important to know the amount of data that eventually has to be distributed to the end users.

Therefore in this appendix, two specific data rates will be quantified: that of the laser altimetry measurements and the housekeeping data.

E.1 Laser altimetry data

The amount of data generated in one second by taking laser altimetry measurements is computed using the following equation:

$$D = n_l \cdot f_p \cdot q \cdot n_s \cdot O \tag{E.1}$$

where n_l is the number of lasers, f_p the pulse repetition rate in Hz, q the quantization level of the signal in bits, n_s the number of samples per pulse, and O the overhead factor.

For POLESat, three separate categories of measurements are distinguished, because of their different characteristics. There are measurements over ice, land & water.

As discussed in paragraph 10.2, the photon counters in POLESat will be sensitive to two different wavelengths, 1064 nm and 532 nm. Since the applications of these wavelengths are different, also the requirements for the sampling will not be the same.

1064 nm will be sampled at 2 GHz (7.5 cm range bins) / 16-bit , while 532 nm will be sampled at 500 MHz (30 cm range bins) / 8-bit. The 16 bit is sufficient to maximize the data extracted from the incoming photons (maximum photons $\approx 80,000$ (table 10.5), with a photon-to-electron conversion efficiency of roughly 0.5 results in $\approx 40,000$ electrons in minimally 8 bins of 8 ns requires more than 12 bit A/D conversion).

Measurements over ice

Over ice, all 5 lasers of POLESat will be operating with a pulse repetition rate of 75 Hz. Of each returned waveform at 1064 nm, 1000 samples will be stored; for 532 nm, this is 250 samples per waveform (analogous to ICESat). It is expected that the overhead for measurements over ice will be about 10% (based on ICESat data rate [48]). In the end, this results in a data rate over ice of:

$$D_{ice} = 5 \cdot 75 \cdot \left(16 \cdot 1000 + 8 \cdot 250\right) \cdot 1.1 = 7.425 \text{ Mbps}$$

Measurements over water

When flying over water, the lasers of POLESat are set at a pulse repetition rate of 40 Hz. Of the returned waveform at 1064 nm, 400 samples will be stored, and at 532 nm, 100

samples will be stored. The overhead for measurements over water is expected to be 25%.

This results in a data rate of:

$$D_{water} = 5 \cdot 40 \cdot \left(16 \cdot 400 + 8 \cdot 100\right) \cdot 1.25 = 1.602\,\text{Mbps}$$

Measurements over land

Over land, the laser settings of POLESat will be the same as over water. However, the amount of samples stored and the overhead will be different, namely the same as for the measurements over ice.

This results in a data rate over land of:

$$D_{land} = 5 \cdot 40 \cdot \left(16 \cdot 1000 + 8 \cdot 100\right) \cdot 1.25 = 3.960\,\text{Mbps}$$

To estimate the total average data rate, it is assumed 50% of the measurements will be taken over water, 25% over land and 25% over ice (analogous to ICESat Brenner et al. [14]). This gives a total average data rate of:

Next to the reflected waveforms, also the transmitted laser pulse has to be stored. With a 6 ns sample time, this results in 216 bits of additional data per pulse. Since this is negligible compared to the total average data rate, the TT&C and C&DH subsystem will be sized using a data rate of 3.7 Mbps.

E.2 Housekeeping data

Amount of data generated in bits:

$$D = n \cdot q \cdot f_s \cdot t \tag{E.2}$$

with n the number of monitored parameters, q the quantization level in bits, f_s the sampling frequency and t the monitoring time.

500 parameters monitored Sampling frequency 1/30 Hz 8-bit Monitoring time of 1 day

Glossary

A/D converter Analog to digital converter.

Ablation removal of material from the surface by vaporization.

Acidification the process whereby air pollution is converted into acid substances.

Along-track distance: The distance between two adjacent footprints along a ground track.

Across-track distance: The distance between the footprints perpendicular to the ground track.

Albedo the extent to which an object, the earth, diffusely reflects light.

Along-track distance: The distance between to adjacent footprints along the ground track.

Apogee: The point in an orbit farthest from the Earth.

Altimetry the science of measuring elevations.

Apogee the point farthest from the earth in the orbit.

Arctic the region around the Earth's North Pole.

Atmosphere transmittance The ease at which radiation propagates through the atmosphere.

Avalanche photodiodes Extremely sensitive detectors of light, These detectors multiply the signal produced by incident light by as much as 10^8.

Average bulk density The average density of the total amount of material

Beam quality The total set of parameters that define the quality of the beam.

Bipropellant Propellant that consist of a fuel and an oxidizer.

Body mounted solar panel A solar panel that is mounted on the body of the satellite.

Campaign time The elapsed time after which the satellite will follow the same ground track; the time of one measuring campaign.

Contact time The time that there is contact with the ground station.

Cryosphere the portions of the Earth.s surface where water is in solid form.

Decommissioning The process of putting the satellite out of service at the end of life.

Defraction The bending of (light-) waves around the edge of an obstacle.

Degree-day models A model which gives the average temperature for the location.

ΔV **budget** The velocity change requirements for various propulsive tasks.

Desaturation The return to normal operation after the APD has been saturated.

Detector bandwidth The difference between the upper and lower frequencies that can be detected by the detector.

Dimers A chemical entity consisting of two subunits held together by intramolecular forces.

Disturbing torque The unwanted forces that disturb the attitude of the satellite.

Divergence The deviation of a laser beam from a perfectly straight line.

Dopant An impurity element added to a crystal to alter the optical properties.

Downlink data rate The rate a which data can be transmitted to the ground station.

Dry mass The total mass of the satellite without propellant.

Dusk-down orbit A special sun-synchronized orbit that will never be in an eclipse of the earth.

Eclipse The state of a satellite when an object obscures the satellite from sunlight.

End-pumped The pump energy is applied to the crystal along with the beam direction. This required that the laser diodes are placed close to the laser beam.

Effective detector diameter: The diameter of the surface of the detector that is used to collect photons.

Effective operational coefficient: The total time in which measurements are performed divided by the total lifetime.

Effective operational coefficient The time when measurements are done divided by the total lifetime.

Effective detector diameter The diameter that is needed if the full area is used to collect photons.

Elevation angle The angle of the measured terrain with the horizontal plane.

Ephemeris A table giving the coordinates of a celestial body at a number of specific times during a given period.

Exited state The quantum-electric high energy state of a molecule or ion.

Exhaust velocity The velocity at which the exhaust gasses will leave the thruster.

Faraday isolator A device that rotates the polarization of light. When polarizing the light on both sides the light can only travel in one direction.

Flash lamp A flashing lamp that is used in laser pumping.

Focal length The distance between the lens and the focal point.

Folded cavity An optical cavity consisting of more than 2 mirrors.

Footprint The area illuminated by a single laser beam.

Frequency doubler A crystal that absorbs light and creates light at twice the frequency.

Full waveform measurements A measurement method where the full detected return signal is stored.

Fusion isostasy The equilibrium between the gravitational forces and the earth crust forces that will compress the snow to ice.

Gain medium The material where the stimulated emission takes place. An Nd:YAG crystal is the gain medium used in the laser for POLESat.

Gain-switching A way to create a pulsed system by switching the pump energy on and off.

Geiger mode The mode of an APD operates slightly below the threshold voltage.

Geolocation accuracy See horizontal accuracy.

Global warming The increase in the average temperature of the Earth's near-surface air.

Ground segment The total communications satellite system which is situated on the earth.

Horizontal accuracy The accuracy of the location of the elevation measurements.

Housekeeping data Data about the status of the satelite.

Hybrid propellant Propellant consisting of a solid and liquid propellant component.

Hydrology The study of the movement, distribution, and quality of water throughout the earth.

Index of refraction A measure for how much the speed of light is reduced while traveling through a material.

Inclination The angle between the satellite orbital plane and the plane containing the Earth?s orbit around the sun.

Intracavity losses The losses inside the cavity caused by the Q-factor.

Isostatic rebound the rise of land masses that were depressed by the huge weight of ice sheets during the last glacial period.

Laser ranging determining the distance to a reflective object.

Louvers thermally activated shutters that regulate the thermal- environment during spaceflight.

Mass balance The change in the total mass of the land ice and snow on Antarctic and Greenland.

Marine biota the plant and animal life in the oceans.

Mode-locking A way to create a pulsed system by allowing only 1 pulse to resonate in the optical cavity.

Monocoque A structure in which the skin absorbs all or most of the stresses to which the body is subjected.

Monopropellants Propellant consisting of a single component.

Natural frequencies frequency at which a free system vibrates.

Optical amplification The amplification of a light by means of stimulated emission

Optical cavity Also called optical resonator. Place between the 2 or more main mirrors where the light is amplified by stimulated emission in the gain medium.

Optical efficiency The amount of energy that is transmitted though the optical elements like lenses.

Optical modulator The unit used in active pulse generation that controls the transmittance of light.

Orbit time The time to complete one orbit.

Perigee The point nearest the earth's center in the orbit.

Phase array antenna A group of antennas in which the effective radiation pattern is reinforced in a desired direction and suppressed in undesired directions.

Photon counter A photo detector that is so sensitive that it allows detecting of a single photon.

Piezo actuator A highly accurate actuator that reacts on an electrical current through its material.

PIN diodes a diode with a wide region between a p-type semiconductor and an n-type semiconductor regions.

Population inversion A state where more members of a material are in an exited state than in the ground state.

Polar region The regions near the geographic poles.

Pulse duration The length of a pulse expressed in nanometers.

Pulse energy The energy of one pulse.

Pumping Supplying energy to the gain medium.

Quantization level A particular subrange for a quantized wave.

Quasi-collimated Near parallel light rays.

Q-switching A way to create a pulsed system by regulating the loss-factor inside the cavity.

Range window The length of the waveform that is transmitted to the earth.

Repetition rate The amount of pulses per second.

Resonator The setup of the optical cavity. See optical cavity.

Sample rate The number of samples per second that will be taken of the full waveform.

Saturation The condition of being saturated.

Scale height The distance over which a certain quantity decreases by a factor equal to the natural logarithm.

Side-pumped The pump energy is applied to the crystal perpendicular to the beam direction.

Signal-to-noise ratio The ratio of a signal power to the noise power corrupting the signal.

Single elevation measurements A measurement method where only return signals containing at least a certain amount of energy are recorded

Slant range The line-of-sight distance between two points.

Slant range accuracy The accuracy in the direction of the slant range. For nadir pointing measurements it is the same as vertical accuracy.

Solid state mass memory A memory type that uses no moving components.

Specific impulse The impulse per unit of propellant.

Spontaneous emission The emission of light when an electron spontaneously falls from the exited state to the ground state.

Standing wave A wave that remains in a constant position.

Star tracker A device used for determining the attitude of the satellite by determining the direction of the stars.

Stimulated emission The emission of light when a photon triggers the transformation from the exited state to the ground state.

Sun-synchronous orbit An orbit in which the satellite's orbital plane is at a fixed orientation to the sun.

Tectonics The study of the earth's structural features.

Turnable The possibility to vary the wavelength of the laser beam.

Vertical accuracy The accuracy in vertical direction of the elevation measurements.

Bibliography

[1] ACAL, cited 28-05-2008. URL http://www.acaltechnology.com/datasheets/Radiatron/guide.pdf.

[2] Ball Aerospace, cited 26-05-2008. URL http://www.ballaerospace.com.

[3] R. S. Afzal, A. W. Yu, J. L. Dallas, A. Melak, Lukemire A. T., L. Ramos-Izqueirdo, and W. Mamakos. The geoscience laser altimeter system (glas) laser transmitter. *IEEE Journal of selected topics in quantum electronics*, 13(3), 2007.

[4] B. N. Agrawal. *Design of Geosynchronous Spacecraft*. Prentice Hall, 1986.

[5] AIAA. URL http://pdf.aiaa.org/preview/CDReadyMSPOP06_1317/PV2006_5806.pdf.

[6] B.A.C. Ambrosius. *Space systems engineering and technology I part 2 (AE1-801)*. 2003.

[7] O.A. Anisimov, D.G. Vaughan, T.V. Callaghan, C. Furgal, H. Marchant, T.D. Prowse, H. Vilhjálmsson, and J.E. Walsh. Polar regions (arctic and antarctic). In *Climate Change 2007: Impacts, Adaptation and Vulnerability. Contribution of Working Group II to the Fourth Assessment Report of the Intergovernmental Panel on Climate Change*, chapter 15, pages 653–685. Cambridge University Press, 2007.

[8] Astrium, 2008 [cited 26-05-2008]. URL http://www.astrium.eads.net.

[9] S Aycu and B. Celik. *Structural Material Selection and Processing for Low Earth Orbit Spacecraft Regarding Atomic Oxygen Effect*.

[10] S. Bae and B. E. Schutz. Precision attitude determination. Technical report, Center for Space Research, The University of Texas at Austin, 2002. GLAS Algorithm Theoretical Basis Document Version 2.2.

[11] V. Barantsevich and V. Shabalkin. Heat pipes for thermal control of iss solar battery drive. *Applied Thermal Engineering*, 23(9):1119–1123, 2003. doi: 10.1016/S1359-4311(03)00041-3.

[12] A. R. Boehm. Vertical probability of cloud free line of sight(pcflos) given the mean and standard deviation of sky cover. *unpublished USAF ETAC Probability and Statistics Memo*, 1980.

[13] Boeing, 2008 [cited 25-04-2008]. URL http://www.boeing.com.

[14] A. C. Brenner, H. J. Zwally, C. R. Bentley, B. M. Csatho, D. J. Harding, M. A. Hofton, J. B. Minster, LeeAnne Roberts, J. L. Saba, R. H. Thomas, and D. Yi. Glas algorithm theoretical basis document 4.1, 2003.

[15] Broad Reach Engineering, 2008 [cited 26-05-2008]. URL http://www.broadreachengineering.com.

[16] D. Budikova. Albedo., 2008. Encyclopedia of Earth.

[17] S. H. Byun. *Satellite Orbit Determination Using GPS Carrier Phase in Pure Kinematic Mode*. PhD thesis, The University of Texas, Austin, December 1998.

[18] Colloquium, 2008 [cited 26-05-2008]. URL http://www.colloquium.fr.

[19] Continuum. URL www.continuumlasers.com.

[20] Earth Observing System Data and Information System. URL http://nasadaacs.eos.nasa.gov.

[21] Deutsches Zentrum fur Luft- und Raumfahrt, 2008 [cited 26-05-2008]. URL http://atmos.caf.dlr.de/projects/scops/orbit_analysis/orbit_analysis_actual.html.

[22] F. Dugue, F. Roux, B. Bonafos, J. Y. Billard, and D. H. Fruman. Development of a micro pump for hydrazine propulsion systems. 2001. AIAA-2001-3831-664.

[23] EaglePicher. URL http://www.eaglepicher.com,[cited26-05-08].

[24] A. Einstein. Zur quantentheorie der strahlung. *Physikalische Zeitschrift*, XVIII(121), 1917.

[25] EMCORE. Btj triple-junction high efficiency solar cells for space applications, cited 20-05-2008. URL http://www.emcore.com/assets/photovoltaics/Emcore_BTJ_DS_May_07.pdf.

[26] Renewable energy world. URL http://www.renewableenergyworld.com/read/news/story?id=49483,

[27] European Space Agency, 2008 [cited 25-04-2008]. URL http://www.esa.int.

[28] European Space Agency, 2008 [cited 26-05-2008]. URL http://www.esa.int/esaMI/Operations/SEM8YCSMTWE_0.html.

[29] L. Fiorani. Laser altimeter for a microsatellite. *Journal of Optoelectronics and Advanced Materials*, 2(2), 2000.

[30] P. Fortescue and J. Stark, editors. *Spacecraft Systems Engineering*. John Wiley & Sons, 1995.

[31] P. A. Franken, A. E. Hill, C. W. Peters, and G. Weinreich. Generation of optical harmonics. *Phys. Rev. Lett.*, 7(4):118–119, Aug 1961. doi: 10.1103/PhysRevLett.7.118.

[32] C. S. Gardner. Ranging performance of satellite laser altimeters. *IEEE Transactions on Geoscience and Remote Sensing*, 30(5), 1992.

[33] General Dynamics Advanced Information Systems, 2008 [cited 26-05-2008]. URL http://www.gd-ais.com/Capabilities/offerings/space/datasheets/MMS-BandXCVR.pdf.

[34] Hamamatsu, cited 26-05-2008. URL http://jp.hamamatsu.com.

[35] R. J. Hamann and M. J. L. van Tooren. *Systems Engineering and Technical Management Techniques - Part 1*. Delft University of Techonlogy, Faculty of Aerospace Engineering, 2006.

[36] D. J. Harding, J. L. Bufton, and J. J. Frawley. Satellite laser altimetry of terrestrial topography: Vertical accuracy as a function of surface slope, roughness, and cloud cover. *IEEE Transactions on Geoscience and Remote Sensing*, 32(2), 1994.

[37] Hipparcos. URL http://www.rssd.esa.int,[cited20-05-08].

[38] G. P. Karman, G. S. McDonald, G. H. C. New, and J. P. Woerdman. Laser optics: Fractal modes in unstable resonators. *Nature*, 402(138), 1999. doi: 10.1038/45960.

[39] KSAT. URL http://www.ksat.no.

[40] L-3 Communications Cincinnati Electronics, 2008 [cited 26-05-2008]. URL http://www.cmccinci.com/pdfs/t722_approved.pdf.

[41] P. Lemke, J. Ren, R.B. Alley, I. Allison, J. Carrasco, G. Flato, Y. Fujii, G. Kaser, P. Mote, R.H. Thomas, and T. Zhang. Observations changes in snow, ice and frozen ground. In *Climate Change 2007: The Physical Science Basis. Contribution of Working Group I to the Fourth Assessment Report of the Intergovernmental Panel on Climate Change*, chapter 4. Cambridge University Press, 2007.

[42] T. M. Lillesand, R. W. Kiefer, and J. W. Chipman. *Remote sensing and image interpretation*. Wiley, 5th edition, 2003.

[43] Powerlase Limited. URL www.powerlase.com.

[44] Roderik Lindenbergh. Project guide design synthesis exercise, 2008.

[45] Marlow, cited 28-05-2008. URL http://www.marlow.com.

[46] J. S. McFarlane, R. J. Kniffen, and J. Lichatowich. Design and testing of amroc's 250,000 lbf thrust hybrid motor, 1993. AIAA 93-2551.

[47] NASA, 2008 [cited 25-04-2008]. URL http://www.nasa.gov.

[48] NASA Goddard Space Flight Center. Icesat, cited 16-04-2008. URL http://icesat.gsfc.nasa.gov.

[49] NASA Goddard Space Flight Center, 2008 [cited 26-05-2008]. URL http://eo1.gsfc.nasa.gov/new/validationReport/Technology/Documents/Summaries/04-XPAA_Re

[50] National Space Agency of Ukraine, 2008 [cited 25-04-2008]. URL http://www.nkau.gov.ua.

[51] R. Noomen, Q. P. Chu, and A. Kamp. *Space systems engineering and technology III (AE3-803)*. 2nd edition, 2007.

[52] Noren, cited 28-05-2008. URL http://www.norenproducts.com.

[53] National Oceanic and Atmospheric Administration. URL http://www.noaa.gov.

[54] BFI OPTiLAS. URL www.bfioptilas.com. Private correspondence.

[55] Orbital. URL http://www.orbital.com/NewsInfo/Publications/Thermal_Louvers_Brochure.pdf.

[56] Dr. R. Paschotta. An open access encyclopedia for photonics and laser technology. URL www.rp-photonics.com/encyclopedia.html[cited26-05-08].

[57] Dr. T. Phillips, cited 26-05-2008. URL http://science.nasa.gov. Science at NASA.

[58] Earth Observing Principal Investigato Portal. URL http://eopi.esa.int.

[59] F. Remy and M. Frezzotti. Antarctica ice sheet mass balance. *C. R. Geoscience*, 338: 1084–1097, 2006.

[60] Cosine Research. URL www.cosine.nl. Private correspondence.

[61] Eric Rignot and Robert H. Thomas. Mass balance of polar ice sheets. *Science*, 297: 1502–1506. doi: 10.1126/science.1073888.

[62] H. J. Rim, G. W. Davis, and B. E. Schutz. Dynamic orbit determination for the eos laser altimeter satellite (eos alt/glas) using gps measurements. *J. Astron. Sci*, 44(3): 409–424, 1996.

[63] A. W. Smith. *Elements of Physics*. McGraw-Hill Book Company, Inc., 5th edition, 1948.

[64] Spectrolab. URL http://www.spectrolab.com/DataSheets/Panel/panels.pdf.

[65] M. A. Stephen, J. L. Dallas, and R. S. Afzal. Multi-billion shot, high-fluence exposure of cr:yag passive q-switch, 1997.

[66] Surrey Satellite Technology, 2008 [cited 26-05-2008]. URL http://www.sstl.co.uk/documents/SSTL_S_Band_Quadrifiliar_Antenna_1.pdf.

[67] B. D. Tapley. Statistical orbit determination theory. *Advances in Dynamical Astronomy*, pages 396–425, 1973.

[68] M. J. Weber. *Handbook of Lasers*. CRC Press, 2001.

[69] E. Weisstein. Spherical cap, cited 28-05-2008. URL http://mathworld.wolfram.com/SphericalCap.html.

[70] J. R. Wertz and W. J. Larson, editors. *Space Mission Analysis and Design*. Microcosm Press, 1999.

[71] D. J. Wingham, A. J. Ridout, R. Scharroo, R. J. Arthern, and C. K. Shum. Antarctic elevation change from 1992 to 1996. *Science*, 282(5488):456–458, 1998. doi: 10.1126/science.282.5388.456.

[72] S. Wu, T. P. Yunck, and C. L. Thornton. Reduced-dynamic thechnique for precise orbit determination of low earth satellite. *Proc. AAS/AIAA Astrodynamics Specialist*

Conference, August 1987.

[73] T. P. Yunck and S. C. Wu. Non-dynamic decimeter tracking of earth satellites using the global positioning system. *AIAA 24th Aerospace Sciences Meeting*, 1986.

[74] B. T. C. Zandbergen. Space engineering & technology (couse notes), part a2, 2004.

[75] B. T. C. Zandbergen. Tu delft space systems engineering sis-pages, cited 26-05-2008. URL `www.sse.lr.tudelft.nl`.

[76] B. T. C. Zandbergen. Some typical hybrid propellant rocket motor, 1995. M-680.

[77] H. J. Zwally, B. Schutz, W. Abdalatic, J. Abshirea, A. Bentley, J. Brenner, J. Deziof, D. Hancock, D. Hardinga, T. Herring, B. Minster, K. Quinn, S. Palm, J. Spinhirne, and R. Thomas. Icesat's laser measurements of polar ice, atmosphere, ocean and land. *Journal of Geodynamics*, 34:405–445, 2002.